Available online at www.sciencedirect.com
ScienceDirect
Physics Reports 432 (2006) 43–113
PHYSICS REPORTS
www.elsevier.com/locate/physrep

Nuclear clusters and nuclear molecules

W. von Oertzen[a,b], Martin Freer[c,*], Yoshiko Kanada-En'yo[d]

[a] *Hahn-Meitner-Institut GmbH, Glienicker Street 100, 14109 Berlin, Germany*
[b] *Fachbereich Physik, Freie Universität, Berlin*
[c] *School of Physics and Astronomy, University of Birmingham, Birmingham B15 2TT, UK*
[d] *Institute for Theoretical Physics, Kyoto University, Kyoto 606-8502, Japan*

Accepted 7 July 2006

editor: G. E. Brown

Abstract

Clustering has long been known to be influential in the structure of ground and excited states of $N = Z$ nuclei. States close to the decay thresholds are of particular interest, as clustering becomes dominant. Recent studies of loosely bound light neutron-rich nuclei have focused attention on structures based on clusters and additional valence neutrons, which give rise to covalent molecular binding effects. These nuclear molecules appear only at the extremes of deformation, in the deformed shell model they are referred to as super- and hyper-deformed. The beryllium isotopes provide the first examples of such states in nuclear physics. Further nuclear molecules consisting of unequal cores and also with three centres can be considered. These arise in the isotopes of neon and carbon, respectively. Molecular states in intrinsically asymmetric configurations give rise to parity (inversion) doublets. Examples of recent experiments demonstrating the molecular structure of the rotational bands in beryllium isotopes are presented. Further experimental evidence for bands as parity doublets in nuclei with valence neutrons in molecular orbits is also analysed. Work on chain states (nuclear polymers) in the carbon isotopes is discussed. These are the first examples of hyper-deformed structures in nuclei with an axis ratio of 3:1. Future perspectives are outlined based on a threshold diagram for covalent nuclear molecules with clusters bound via neutrons in covalent molecular configurations.

PACS: 24.10.−i; 25.70.Bc

Keywords: Nuclear clusters; Molecular binding; Valence neutrons; Nuclear molecules

Contents

* Corresponding author.
E-mail address: m.freer@bham.ac.uk (M. Freer).

0370-1573/$ - see front matter © 2006 Elsevier B.V. All rights reserved.
doi:10.1016/j.physrep.2006.07.001

1. Introduction

1.1. Nuclear clusters in $N = Z$ nuclei

The subject of clustering transcends many areas of science, from clusters of galaxies to clusters of micro-organisms, and in each instance there is some evolutionary advantage. In nuclear physics, clusterisation enhances, in certain circumstances, the binding energy of the system. The concept has a history of more than 40 years when detailed studies started, but is actually one of the oldest models of the nucleus, since the α-cluster model was developed even before the discovery of the neutron [292–295]. However, after this discovery, the single-particle description of nuclei based on the concept of a mean field for all nucleons became the prime focus.

The last 30 years have seen the discovery of complex cluster structures composed of alpha particles in what are called α-conjugate nuclei, that is nuclei with $N = Z$, which have an even, and equal, number of protons and neutrons [105]. In general, this precipitation of the nuclear liquid drop into more weakly interacting strongly bound droplets reveals highly symmetric structures, and the preponderance of α-clusters is due to their high stability. The binding energy per nucleon

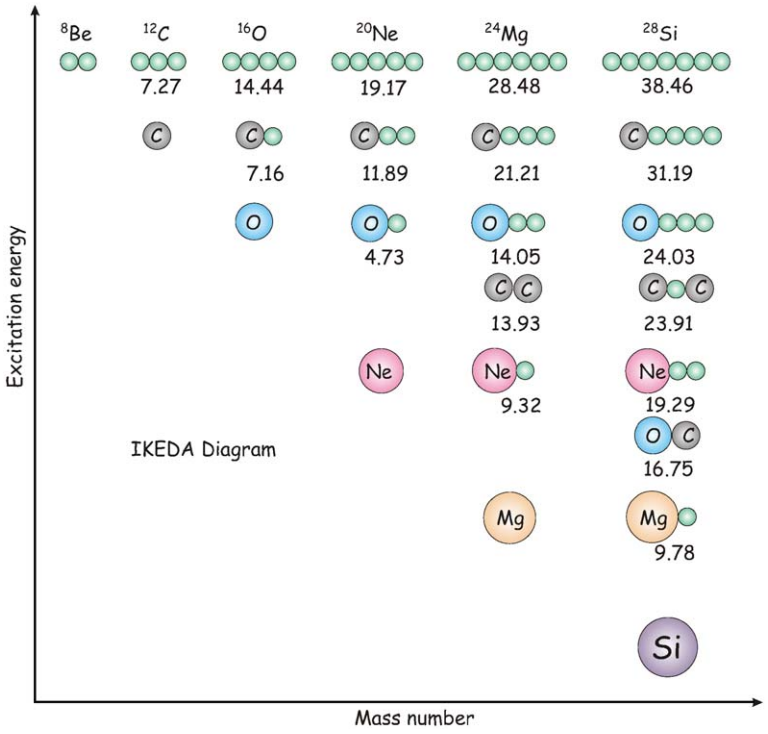

Fig. 1. The Ikeda threshold diagram for nuclei with α-clustering. Cluster structures are predicted to appear close to the associated decay thresholds. These energies needed for the decomposition of the normal nucleus into the structures are indicated in MeV, adapted from [144].

of the α-particle is significantly larger than in all other neighbouring light nuclei, and the first excited state of the ^{4}He resides at 20.21 MeV. Together with a strong, and repulsive α–α interaction, arising due to the Pauli exclusion principle [90,251], α-cluster states are rather robust against the collapse into more compact shell model-like configurations. This realization led to a strong revival of the α-particle model in the 1960s [132,262,297,298] with the use of the resonating group method [295,298]. States in nuclei based on α-particles and other strongly bound sub-structures with $N = Z$ (e.g. ^{16}O) are typically not found in ground states, but are observed as excited states close to the decay thresholds into clusters, as was suggested in 1968 by Ikeda. The Ikeda diagram [144,136] is shown in Fig. 1, this links the energy required to liberate the cluster constituents to the excitation energy at which the cluster structures prevail in the host nucleus. The clear prediction, which is borne out experimentally, is that cluster structures are mainly found close to cluster decay thresholds.

The formation of clusters is a fundamental aspect of nuclear many-body dynamics, which must exist simultaneously with the formation of a mean-field. Under the assumption of spherical symmetry this gives rise to the nuclear shell structure. Importantly, clustering gives rise to states in light nuclei which are not reproduced by the shell model. The nuclear shell model does, however, play an important role in the emergence of nuclear clusters, and also in the description of special deformed nuclear shapes, which are stabilised by the quantal effects of the many-body system, namely the deformed shell gaps (as opposed to the spherical shell gaps).

This connection is illustrated by the behaviour of the energy levels in the deformed harmonic oscillator [46], shown in Fig. 2. The numbers in the circles correspond to the number of nucleons, which can be placed into the crossing points of orbits. At zero deformation there is the familiar sequence of magic numbers which would be associated with spherical shell closures, and the associated degeneracies. At a deformation of the potential, where the ratios of the axes are 2:1, these same magic degeneracies reappear, but are repeated twice. This establishes an explicit link between deformed shell closures and clustering. As an example, at a deformation of 2:1 the occupancy by both protons and neutrons of the levels labelled by the degeneracies $2 + 2 + 6 = 10$ would correspond to the deformed ^{20}Ne nucleus. The degeneracies $2 + 6 = 8$ are associated with the formation of ^{16}O and thus an ^{16}O+α cluster $(8 + 2)$ structure

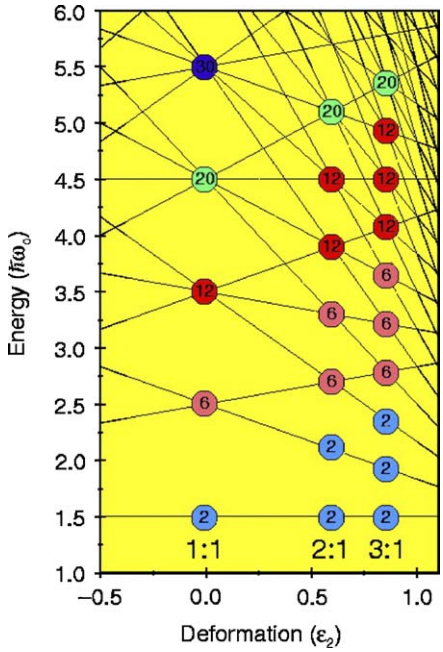

Fig. 2. Energy levels of the deformed axially symmetric harmonic oscillator as a function of the quadrupole deformation (oblate and prolate, i.e. negative and positive values of ε_2, respectively). Degeneracies appear due to crossings of orbits at certain ratios of the length of the long axis (the symmetry axis) to the short perpendicular axis. The regions of high degeneracy define a shell closure also for deformed shapes [109].

Table 1
The constituents for the nucleon magic numbers N in nuclei with super- and hyper-deformed prolate shapes

Deformed	spherical constituents	
N	Superdeformation, dimers	
4	$2+2$	α–α
10	$8+2$	^{16}O–α
16	$8+8$	^{16}O–^{16}O
28	$8+20$	^{16}O–^{40}Ca
N	Hyperdeformation, chains	
6	$2+2+2$	α–α–α
12	$2+8+2$	α–^{16}O–α
24	$8+8+8$	^{16}O–^{16}O–^{16}O
36	$8+20+8$	^{16}O–^{40}Ca–^{16}O
48	$20+8+20$	^{40}Ca–^{16}O–^{40}Ca
60	$20+20+20$	^{40}Ca–^{40}Ca–^{40}Ca
N	Oblate nuclei, pancakes	
8	6+2	^{12}C–α
12	6+6	^{12}C–^{12}C
18	12+6	^{24}Mg–^{12}C
24	12+12	^{24}Mg–^{24}Mg

Also shown are those corresponding to oblate deformations with no oscillator quanta perpendicular to the plane of deformation and with axial asymmetry, from Rae [238].

would be predicted for ^{20}Ne. This concept, fundamental for the understanding of the appearance of clustering within the nucleus, has been discussed before in detail [3,54,214,215,238] (see also Section 2.2). In particular the work of Rae was seminal in crystallising the discussion. To illustrate this point, we show in Table 1 the compilation made by Rae [238], following an examination of the properties of the deformed harmonic oscillator as shown in Fig. 2.

We see that the deformed magic structures with special stability (and corresponding magic numbers) are expected for particular combinations of spherical (shell-model) clusters. For example, for super-deformed structures (2:1) the magic numbers have a decomposition into two magic numbers, of two spherical clusters, e.g. ^{20}Ne$\equiv$ (^{16}O + α). Thus, one would expect clusterisation not only to appear at a particular excitation energy (the Ikeda picture), but also at a specific deformation. These structures give rise to not only rotational bands, but also to exotic vibrational modes, e.g. the butterfly mode described for the ^{24}Mg+^{24}Mg scattering resonances [302,273] and also those in the ^{28}Si+^{28}Si system [219].

In the present review, it will become evident that additional valence neutrons do not destroy these structures, instead interesting nuclear structures described by molecular concepts will emerge.

An extension of the above discussion will show, that the intrinsically reflection symmetric states with hyper-deformation (3:1) are related to cluster structures consisting of three clusters. In going to larger deformations and placing particles in the orbits in which the oscillator quanta are only along the deformation direction, longer α-chain states are produced. For example, the linear 3α configuration corresponds to the filling of the three lowest levels at 3:1 labelled with degeneracy numbers 2 in Fig. 2 (see also Fig. 8).

Cluster structures with intrinsically reflection asymmetric shapes will consist of clusters of different size and magic numbers, for example in the ^{20}Ne nucleus. They are then related to octupole shapes [3,54,134]. The octupole deformations give rise to the observation of rotational bands with parity inversion doublets [46,54].

1.2. Clustering in neutron-rich nuclei

The interest in nuclear clustering has been pushed strongly due to the study of neutron-rich and of exotic weakly-bound nuclei. This is a field which has attracted worldwide attention, because the weakly-bound nuclear systems exhibit unique features related to the quantal properties of the many body systems, like halos [165] and clustering.

More explicitly, the strong clustering in weakly-bound systems can give rise to two-centre and multi-centre nuclear configurations, whose structures can be described by the concepts of molecular physics. Valence neutrons can exist in molecular orbitals, their role becomes analogous to that of electrons in covalent bonds in atomic molecules. In the nuclear case, these covalent neutrons stabilize the unstable multi-cluster states. The form of the covalent orbits for p-states is illustrated in Fig. 3. The figure shows the result of combining two orientations of the p-orbits, which in the atomic case would be found in the covalent binding of oxygen or carbon atoms. One linear combination, with the single particle orbits aligned perpendicular to the separation axis (a), gives rise to a π-type bonding orbit (b). The other alignment, illustrated in (d), gives rise to the σ-bonding orbit (e). The other arrangements, (c) and (f), give anti-bonding configurations.

These concepts can also be used to describe the exchange of valence neutrons between cluster cores on the nuclear scale. For example, ^{9}Be may be considered to be composed of two α-particles and a valence neutron, forming, at larger $\alpha + \alpha$ separations ^{5}He nuclei, where the neutron resides in a $p_{3/2}$-orbit(see Section 3.3). The linear combinations of two such orbits give rise to nuclear molecular π- and σ-bonds in ^{9}Be [283]. It should be noted, however, that unlike in atomic systems, in nuclei no "ionic" molecular binding effect can occur (with valence neutrons of different binding energies at the asymptotic centres).

The structures based on such nuclear multi-centre configurations are difficult to obtain in the shell model approach (even with an extremely expanded basis). On the other hand, they are very well reproduced by a "model independent" approach, Antisymmetrized Molecular Dynamics (AMD, see in particular [172,176], and Section 5.4). These calculations actually illustrate the origin of the molecular cluster structure: the nuclear forces are saturated in spin–isospin space in the α-clusters and in other $N = Z$ nuclei, the remaining interactions are weak and give rise to unique quantal structures for the weakly bound nucleons.

A qualitative argument can be used to illustrate the relative strength of the molecular interaction between the cluster constituents in multi-cluster structures and of the strength of the mean field: only in a strongly deformed weakly bound system can the quantal (molecular) binding effects compete with the mean field aspect of nuclear forces, because the latter are saturated within the $N = Z$ clusters.

A new threshold diagram is required, in order to describe the structure of non-alpha conjugate nuclei, i.e. those with valence neutrons, which reside in covalent orbits. Following the arguments summarised in Table 1, covalent molecular structures should be built mainly from α and ^{16}O components. The states close to the thresholds for the decomposition

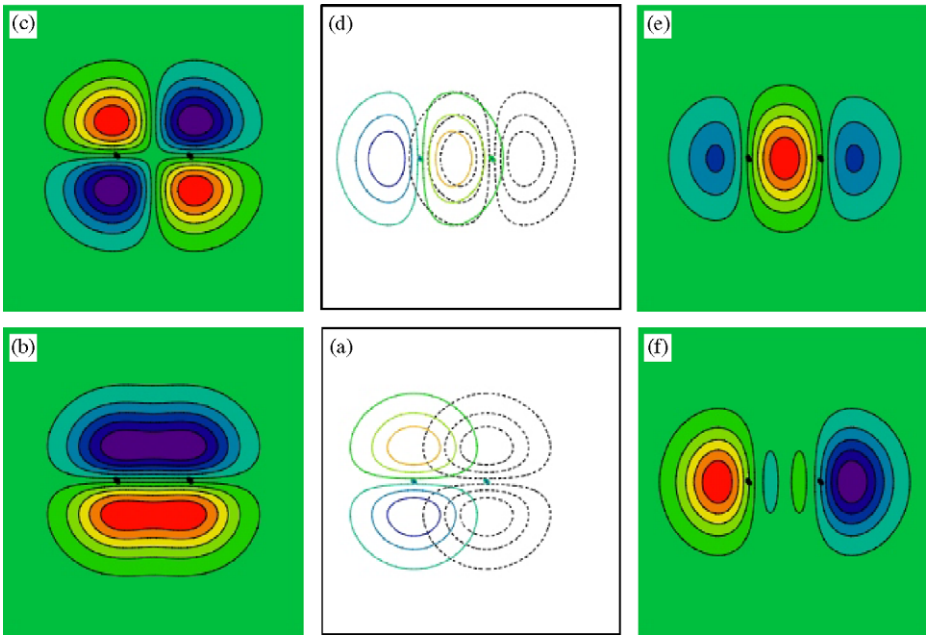

Fig. 3. Molecular wave-functions for two centres constructed from harmonic oscillator wave functions with $(n_x, n_y, n_z) = (1, 0, 0)$ and $(0, 0, 1)$ orbits, equivalent to p-states. Here the z-direction is aligned with the separation axis of the two centres indicated by the black dots. (a) shows the overlap of the two individual wave functions. Diagrams (b) and (c) the result of forming linear combinations: (b) corresponds to the binding π-state, and (c) to the anti-binding state. Diagram (d) shows the overlap of the two (0,0,1) orbits, forming the σ-configurations, and (e) and (f) the two linear combinations, from [109].

into clusters and valence neutrons are expected to be bound by the covalent neutrons. This extended Ikeda-diagram appears in Fig. 4, it shows some of the combinations for which covalently bound shape-isomeric structures are expected. The relevant threshold energies for the decomposition into the constituents [282,285] are given. Many of the structures that appear in this figure will be considered in the present review.

This review concentrates on recent work on the structure of excited states in light nuclei related to molecular structures consisting of clusters and valence nucleons. It is organised as follows. In Section 2 we give a historical introduction. In Section 3 the important question of the nucleus–nucleus potentials is addressed, the potentials have special properties for strongly bound clusters and the presence of valence neutrons gives important effects. We review the status and recent developments for $N = Z$ cluster nuclei in Section 4. Section 5 starts with an examination of the different theoretical approaches for the $N = Z$ nuclei. Then a brief description of the Bloch–Brink α-cluster model is given and of the models used for the study of the structures including valence particles, such as the generator coordinate method (GCM), the AMD-approach, and the molecular orbital (MO) theories. We review the experimental evidence for molecular structures in nuclei, first for beryllium isotopes in Section 6. This is extended to three centre systems in carbon isotopes in Section 7 and in Section 8. Section 9 presents perspectives for future research in weakly bound exotic nuclei.

2. Clusters and valence nucleons in light nuclei

In this Section some basic principles of molecular concepts in nuclear physics are shown.

2.1. The first nuclear molecules—a brief history

The late 1920s simultaneously saw the beginning of a quantum mechanical description of the nucleus together with the birth of the nuclear clustering concept. The existence of preformed α-particles within the nucleus and the known stability of this sub-unit inspired ideas that α-clustering might be the favoured state of nuclei [118]. The merits of this description were discussed by Bethe and Bacher in the first in a series of three monumental reviews of the state of

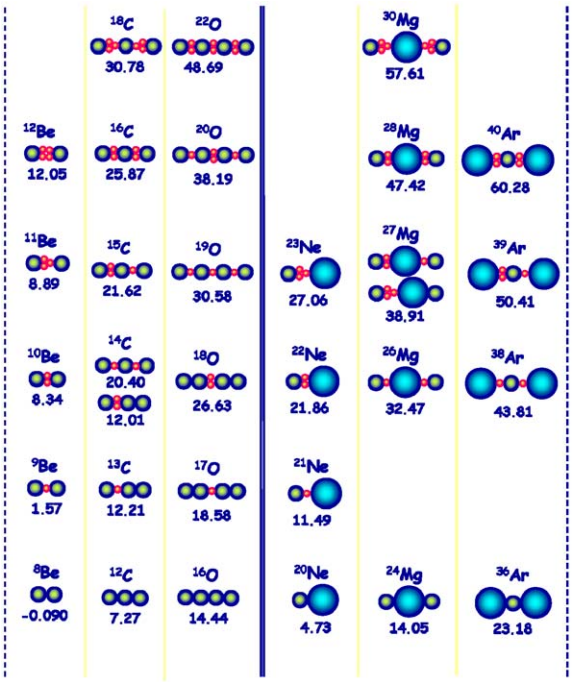

Fig. 4. Extended threshold diagram (as in Fig. 1) for states in nuclei. Some molecular structures with clusters and covalent valence neutrons are shown. Only α-particles and ^{16}O- nuclei are used. The schematic shapes are given with the threshold energies for the decomposition into the constituents.

nuclear physics in the late 1930s [35]. Four premises for the possible existence of the α-clustering were considered relevant; (i) the high binding energy per nucleon of the α-particle, (ii) the failure of the Hartree approximation, in which the individual nucleons moved in the mean potential of all the other nuclear constituents, to reproduce the α-particle binding energy, (iii) light nuclei such as ^{8}Be, ^{12}C, ^{16}O, etc., were known to have much higher binding energies than their neighbours, and (iv) the observed α-decay of heavy radioactive nuclei. Following earlier work by Heisenberg on the exchange forces acting between two α-particles, and the notion of a van der Waals force, Bethe and Bacher notionally constructed the nature of the interaction potential between the α-particles. It was concluded that the interaction was such so as to produce a "trough" at some separation (see Fig. 5 and 12), and the consequence of such an interaction potential would be to produce a ^{12}C nucleus with a equilateral triangular arrangement and for ^{16}O a tetrahedral structure. Further, the change in binding energy from ^{8}Be to ^{12}C, and from ^{12}C to ^{16}O was observed to be consistent with the formation of two, three and six α–α bonds, respectively.

Following the work of Bethe et al. [35], Hafstad and Teller [123] developed a description of $A = 4n$ saturated nuclei. The term saturated was derived from Heisenberg's [126] observation that for this group of nuclei the binding energy of a nucleus is proportional to the number of constituents. To obtain such a condition they developed an α–α interaction potential which was repulsive at short and long ranges (due to the repulsive exchange forces and the Coulomb potential, respectively), and attractive at intermediate distances due to the "van der Waals" or polarisation forces. Such a description produced good agreement with the binding energies of the so-called saturated nuclei. The α-particles are placed in a geometrical model in a close packing configuration, which determines the number of bonds. They predicted that after ^{16}O the number of new bonds that are formed increases by three for each α-particle, again, as was suggested by Bethe and Bacher [35]. These binding energy systematics are shown in Fig. 5, together with the α–α interaction potential used. Note, in the case of ^{28}Si there is an addition of four, rather than three, bonds, due to the fact that the next optimum location for the α-particle results in an oblate structure which has four nearest neighbours with which to form bonds.

In a remarkable example of insight Hafstad and Teller [123] extended their rather simple, yet successful, description of cluster-like nuclei to $(4n + 1)$ type systems, e.g. ^{9}Be, ^{13}C and ^{17}O. Their ideas were based upon the structure of the ^{5}He nucleus in which the last neutron was in a p-orbit. The binding energy of ^{5}He with respect to the neutron and

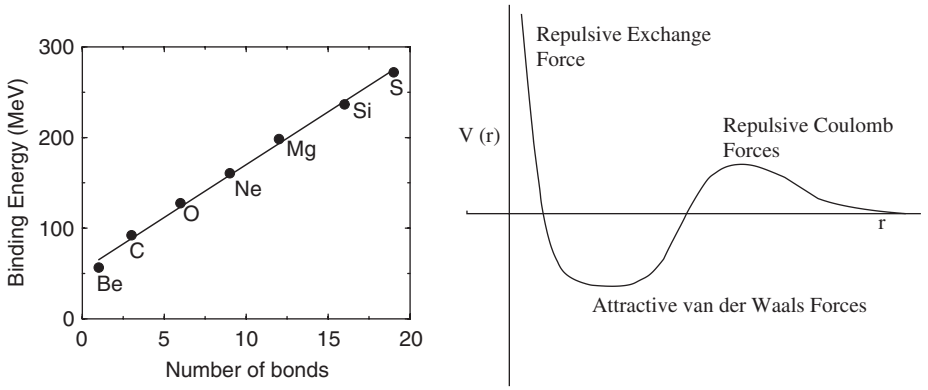

Fig. 5. Left: The binding energy systematics leading to the α-cluster model used by Hafstad and Teller [123]. The plot shows the change in binding energy versus the number of bonds in an alpha-particle model. For example, ^{8}Be has 1 bond, ^{12}C–3, ^{16}O–6, ^{20}Ne–9, etc., see text. Right: the α–α interaction potential used in Ref. [123], see also Fig. 12.

α-particle was defined to be B. Importantly, the neutron was assumed to interact strongly with the α-particle at short distances only. The wave functions of the neutron associated with each α-particle were designated $\psi_{1,2}$. The two-centre wave functions for the system, ^{9}Be, are obtained by linear combinations of the single centre states (see also the more detailed discussion in Section 3.3). The average energy of the neutron was thus computed according to

$$\overline{E}(\psi_1+\psi_2)=\frac{\int(\psi_1+\psi_2)H(\psi_1+\psi_2)\,\mathrm{d}\tau}{\int(\psi_1+\psi_2)^2\,\mathrm{d}\tau}, \tag{1}$$

where $H=(V_1+V_2+T)$, and $V_{1,2}$ are the interaction potentials of the neutron with each α-particle and T is its kinetic energy operator. On expansion three types of terms result, one has the form $\int\psi_1(V_1+T)\psi_1\,\mathrm{d}\tau$ which is equal to the binding of the neutron in ^{5}He (B), terms of the form $\int\psi_1(V_2)\psi_1\,\mathrm{d}\tau=R$, which correspond to the additional potential energy of the neutron near the first α-particle due to the presence of the second. Finally there are the exchange terms $\int\psi_1H\psi_2\,\mathrm{d}\tau=Q$. Setting $\int\psi_1\psi_2\,\mathrm{d}\tau=S$, the average energy of the neutron became

$$\overline{E}(\psi_1+\psi_2)=\frac{B+R+Q}{1+S}, \tag{2}$$

for $S\simeq 0$ the average energy reduces to

$$\overline{E}(\psi_1+\psi_2)=B+R+Q. \tag{3}$$

The systematics of the binding energies of the neutron-excess cluster nuclei were thus obtained as

$$\begin{aligned}
&^{5}\mathrm{He}-(^{4}\mathrm{He}+n)=B,\\
&^{9}\mathrm{Be}-(^{8}\mathrm{Be}+n)=B+(R+Q),\\
&^{13}\mathrm{C}-(^{12}\mathrm{C}+n)=B+2(R+Q),\\
&^{17}\mathrm{O}-(^{16}\mathrm{O}+n)>B+3(R+Q).
\end{aligned} \tag{4}$$

The more general formulation is known as the Hückel method for molecular orbits, see Section 2.4. These systematics agreed remarkably well with the available experimental data. Thus, not only had Hafstad and Teller developed the ingredients of a successful α-cluster model, they had also provided the framework for the extension to neutron-rich nuclei with the formulation of a molecular state in which the neutron is exchanged between the two α-particles. Since the 1930s the ideas underpinning the appearance of clustering have evolved considerably. In the following discussion we explore the underlying link between the mean-field and clustering and illustrate the emergence of molecular characteristics.

2.2. Clustering and deformed shells

We resume the discussion of the relationship between the shell model and the cluster model. This is done on the basis of the harmonic oscillator (HO), which has long been the basis of many calculations of the properties of nuclei. With refinements, which include $l.s$ and l^2 terms, the nuclear shell structure is reproduced as are many of the ground-state spins and parities. Most relevant for systems described here is the deformed harmonic oscillator important in the deformed shell model, or the Nilsson model [218].

Fig. 2 showed the energy level scheme of the deformed harmonic oscillator as function of deformation. The large degree of degeneracy present in the spherical oscillator is lost as the potential is deformed. This decrease in degeneracy reduces the number of correlated particles and thus the stability of the system. However, at a deformation represented by the axis ratio 2:1, and similarly for 3:1, etc., the degeneracy returns providing enhanced stability. Thus, at the deformed shell closures quasi-stable structures appear. Fig. 2 also illustrates a further feature, important for clustering predictions. At 2:1 the degeneracies of the spherical oscillator are repeated twice (i.e. 2, 2, 6, 6, 12, 12,. .) and at 3:1 three times, a pattern which is repeated for each order of deformation. This fact was already mentioned in the introduction, where it was shown that the degeneracy pattern may be interpreted in terms of clusterisation (Table 1). A deformation with the axis ratios 2:1 corresponds to degeneracy sequences with the cluster combinations ^{4}He+^{4}He, ^{4}He+^{16}O and ^{16}O+^{16}O. This observation was formulated more mathematically by Nazarewicz and Dobaczewski [215]. They demonstrated, using group theory, that for deformations with axis ratios n:1, there was a decomposition into n groups. Thus, it is possible to view the deformed harmonic oscillator at a deformation with the ratio 2:1, as consisting of two degenerate harmonic oscillator potentials. Similarly for deformations corresponding to axis ratios of 3:1, three identical potentials are superimposed.

By the addition of a microscopically derived shell correction term to a liquid drop energy, a measure of the potential energy of the nucleus can be determined as a function of deformation. This scheme is called the Nilsson–Strutinsky (NS) method [47,239,240]. It describes a multitude of physical phenomena, in particular the famous cases of fission isomers which originate due to secondary minima in the fission barrier. In light nuclear systems, the NS calculations performed by Leander and Larsson [191] exemplify the role of the deformed shell closure in $N = Z$ nuclei. This study found a series of deformed secondary minima for nuclei such as ^{24}Mg. The same approach was used by Ragnarsson, Nilsson and Sheline [239,240] to predict a whole series of new magic numbers which coincide with a variety of cluster sub-structures. The underlying link between cluster structure and the deformed HO is a strong indication for the existence of clustering in the deformed minima.

The connection between the deformed shell model and cluster model was made explicit by Fulton and Rae [113], where the structures found within the Bloch–Brink α-cluster model [51,201] were compared with those found in the NS calculations of ^{24}Mg, this is shown in Fig. 6. It was found that the detailed predictions for the shapes of the stable deformed configurations were identical in the two models.

The separation of the cluster-like components within the deformed HO at a deformation of 2:1 can be performed within the framework of the double-centre oscillator or the two-centre shell model [88]. Fig. 7 shows the solution of the Schrödinger equation for two potentials as a function of their separation using the two-centre oscillator framework. This description allows the evolution of the quantum numbers from separate clusters to a fused system to be traced. In essence the wave functions of the fused system correspond to two linear combinations $\psi_\pm$,

$$\psi_\pm = \frac{1}{\sqrt{2}}\left(\psi_1 \pm \psi_2\right), \tag{5}$$

where $\psi_{1,2}$ are the wave functions corresponding to the two separated potentials. The two linear combinations produce symmetric and asymmetric states. Harvey [125] encapsulated the evolution of quantum numbers in the Harvey prescription: (i) the number of quanta n_z along the collision axis, which defines the z-direction, are conserved or can be increased due to the collision energy, (ii) excitations of particles or clusters into orbits perpendicular (x- and y-axes) to this common axis are forbidden to first order. Thus,

$$N_+ = 2n_z \quad \text{and } N_- = 2n_z + 1, \tag{6}$$

$N_\pm$ is the total number of oscillator quanta in the fused system and, n_z is the number of z-quanta along the common axis which is defined by the relative motion. This conserves the number of nodes along the axis of separation in the original

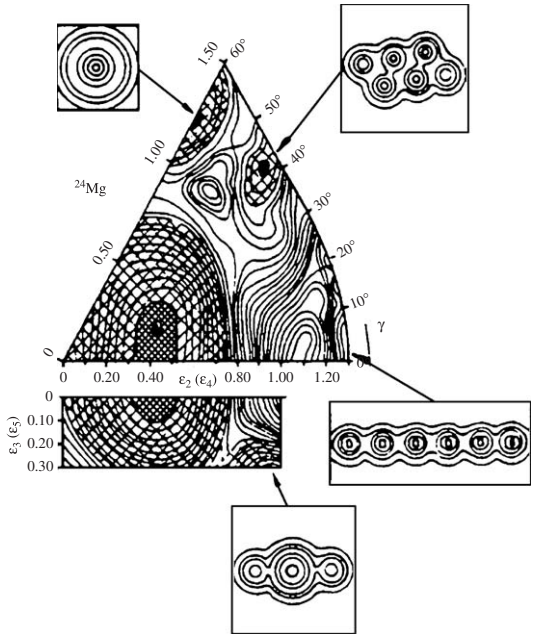

Fig. 6. Nilsson–Strutinsky and α-cluster model calculations for ^{24}Mg [191,113]. The potential energy is shown as a contour plot for the deformation parameters ε_2 and γ. Minima are found at particular deformations. For some of the potential minima the shapes obtained with the α-cluster model are indicated. The lower part shows the potential energy for the extension to octupole shapes with the parameter ε_3.

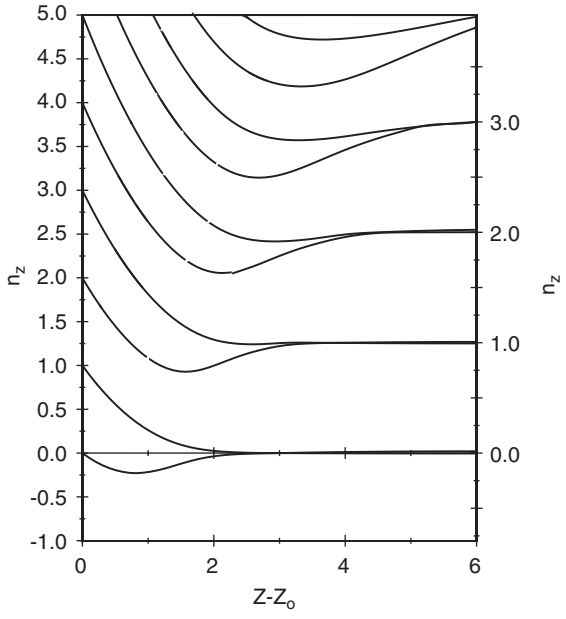

Fig. 7. Energy levels in a double centre oscillator. The energies of the orbits are plotted for different n_z quantum numbers as a function of the separation $(Z - Z_0)$ of the two oscillator potentials. For large separations the associated n_z quantum numbers in the two potentials are degenerate. The degeneracy is lifted when the two potentials overlap giving $n_{z-\text{total}} = 2n_z, 2n_z + 1$. The two-centre levels which result from the fusion of the two oscillator potentials possess an energy given by $\hbar\omega_o(1.5 + n_x + n_y + n_z)$, from [103].

wave functions for the symmetric case (ψ_+) and introduces an additional node for the asymmetric wave function (ψ_-). This may readily be extended to an arbitrary number of clusters (or potentials) fused along a single axis, i.e. for one-dimensional structures [103,105].

This extension of the deformed harmonic oscillator permits the decay properties of a predetermined cluster state to be described. The population of ^{12}C+^{16}O and ^{16}O+^{16}O cluster states in inelastic scattering and α-transfer reactions has been successfully described employing this approach [34,105]. Similarly, for the formation of chain states in nuclear reactions, where particular orbits must be populated, the Harvey rules have to be considered. These rules are equivalent to the fractional parentage rules in multi-nucleon transfer reactions. The deformation and the orientation of the target nucleus must allow the population of the strongly deformed configurations. It should be noted that the correspondence found by Harvey are exactly those contained within the SU3 description explored by Nazarewicz and Dobaczewski [215]. The algebraic features of the SU3 are also at the basis of the RGM- models for molecular resonances and the work of Hess et al. [127].

2.3. Valence nucleons and nuclear molecules

The deformed harmonic oscillator (DHO) framework also provides a useful starting point for the description of nuclear molecules with valence neutrons.

For example, starting with the simplest two-centre system ^{8}Be, composed of two α-particles, we have a deformation of 2:1, and in the DHO the orbits occupied by the quartets (2p+2n) are $(n_\perp, n_z) = (0,0)$ and (0,1). Here $n_\perp$ is the number of oscillator quanta on both the x and y axes and n_z is the number of quanta along z-axis (the deformation or separation axis). A valence neutron can then occupy the (1,0) or (0,2) orbits. The wave-functions of these orbits have a strong overlap with those shown earlier in Figs. 3b and e, respectively. In other words these two DHO orbits contain molecular properties. In the Nilsson picture they correspond to orbits which have K-quantum numbers (projection of the angular momentum onto the deformation axis) $K^\pi = 3/2^-$ and $K^\pi = 1/2^+$, respectively. This gives rise to molecular states in ^{9}Be with spin and parity $3/2^-$ and $1/2^+$, respectively and their rotational excitations. This prediction is experimentally well confirmed [283] (see the discussion in Section 6.1.1).

To illustrate these points Fig. 8 once more shows the diagram of the deformed harmonic oscillator with the orbits for different K-quantum numbers. The orbits with maximum number of quanta on the Z-axis gain energy if the system becomes more elongated. The figure illustrates the location of different "molecular" valence particle orbits for the prolate systems, namely the orbits perpendicular to the z-axis, which serve as π-orbitals with their densities outside of the z-axis. The intersections labelled P_2, P_3, P_4 show the location of these π-orbitals for the multi-α chain states. It should be noted that the molecular orbitals with π-character extend to all deformations where nucleons in the clusters have all of the quanta along the z-axis. The next available orbit above the population of the additional α-cluster state is that with the π-character. Thus, molecular structures with delocalised π-neutrons will play an important role in all linear chain systems.

Clearly, the molecular orbits should be formed from linear combinations of those based on the α-particles at each cluster centre. Thus, the ideas developed in terms of the two-centre shell model, or the double-centred oscillator, are useful in developing molecular wave functions. A related approach is the method designed for atomic molecules, namely the Hückel method, which may be adapted to nuclei.

2.4. The Hückel method for molecular orbits

The Hückel Method is a general approach to describe the wave functions of valence particles (and their binding effects) in a multi-centre system. Wave functions of molecular orbits (ψ) may be expressed as linear combinations of n single-particle nuclear wave functions (χ_n)

$$\psi = C_1\chi_1 + C_2\chi_2 + \cdots + C_n\chi_n, \tag{7}$$

where χ_i are the single-centre orbitals and C_n are the coefficients to be evaluated, which determine the relative contribution of each single orbital. The molecular wave function must satisfy the relation for the energy E and the total Hamiltonian H

$$H\psi = E\psi. \tag{8}$$

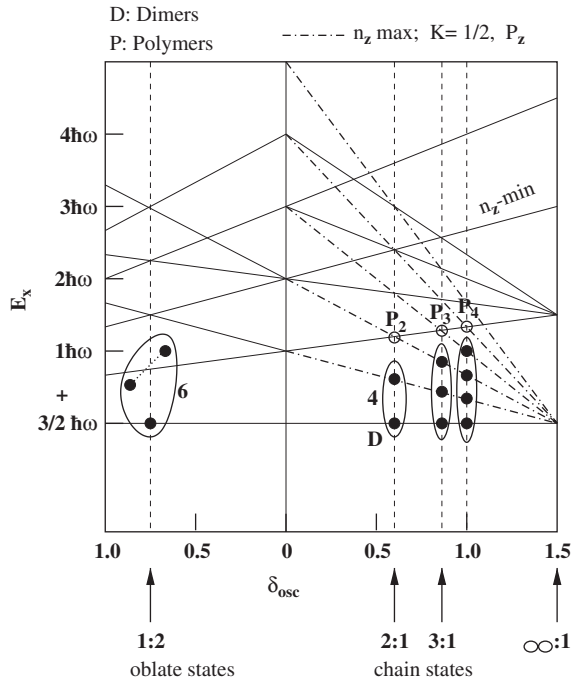

Fig. 8. Energy diagram of orbitals of nucleons in an axially deformed harmonic oscillator, adapted from [46]. The black dots represent the four-fold spin, isospin degenerate population (forming an α-particle). The open dots mark the positions of valence nucleons, they lie on the perpendicular orbitals (x or y). The deformation parameter $\delta_{\rm osc}$ is defined as the ratio of the difference of the oscillator frequencies perpendicular to those along the z-axis to their weighted sum.

For the two-centre system the energy E is obtained using a variational method (see also Ref. [95])

$$E = \frac{C_1^2 H_{11} + 2C_1 C_2 H_{12} + C_2^2 H_{22}}{C_1^2 + 2C_1 C_2 S_{12} + C_2^2}, \tag{9}$$

where the notation $\int \chi_i^* H \chi_j \, \mathrm{d}\tau = H_{ij}$ and $\int \chi_i^* \chi_j \, \mathrm{d}\tau = S_{ij}$ has been used. This is analogous to the analysis performed by Hafstad and Teller [123]. The final wave functions are determined by the coefficients C_1 and C_2. The solutions for the values of E are found from the secular determinant

$$\begin{vmatrix} H_{11} - E & H_{12} - ES_{12} \\ H_{12} - ES_{12} & H_{22} - E \end{vmatrix} = 0.$$

Using symmetry arguments for equal cores (like in the case of ^{9}Be) we define $H_{11} = H_{22} = \alpha$). The value of H_{12}, the resonance integral, is set to β if the two clusters are neighbouring, and to zero if they are not (in longer chains). This latter condition is often used for more complex systems with many centres and restricts the neutron exchange to be with nearest neighbours only. Furthermore, the simplifying approximation is that the wave functions will have "zero overlap", i.e. the non-orthogonality term of the wave functions, S_{12}, is set to zero. The secular determinant, subject to these conditions, then becomes

$$\begin{vmatrix} \alpha - E & \beta \\ \beta & \alpha - E \end{vmatrix} = 0.$$

We will use $(\alpha - E)/\beta = x$, in the specific case we have the molecular wave-functions

$$\psi = \frac{\chi_1 \pm \chi_2}{\sqrt{2}}. \tag{10}$$

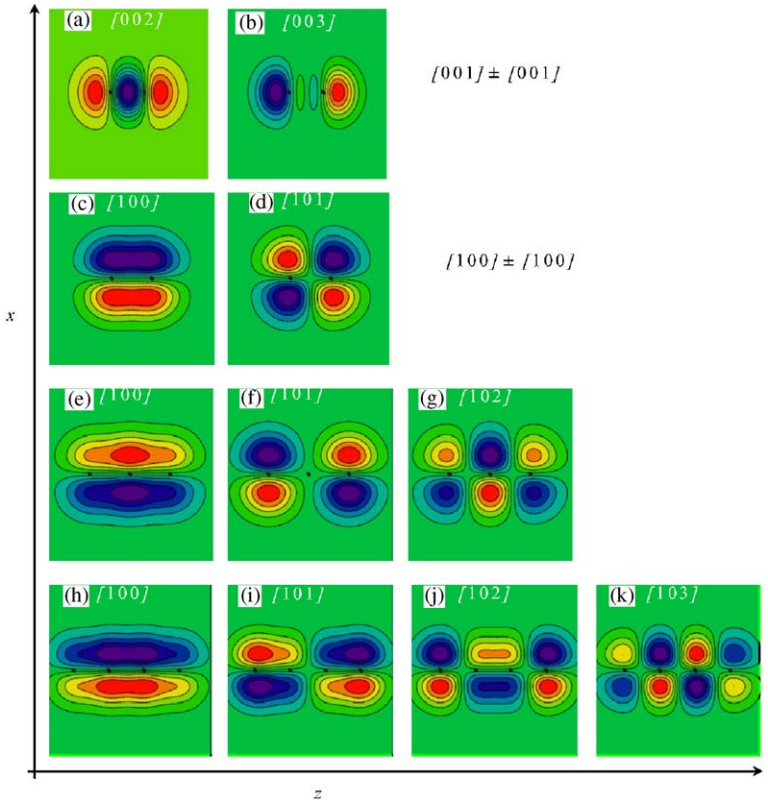

Fig. 9. Contour plots of the densities for valence neutrons in chain-like α-particle configurations for up to four-centre systems using the Hückel-method. In the panels (a) and (b) the linear combinations corresponding to $[n_x, n_y, n_z] = [0, 0, 1]$ HO wave functions (for two centres), with σ-type bonds are shown. In all of the other plots for two-,three- and four-centres, the [1, 0, 0] orbit is used for the valence particle, which generates π-configurations. The labels on each panel refer to the HO-orbit classification indicating a significant overlap with the molecular orbit, see Ref. [203].

Following this approach with the harmonic oscillator potential ($V = \frac{1}{2}m\omega^2$) the molecular orbits of the valence neutron in ^{9}Be can be modelled in an analytical form (see Ref. [203]).

This process can be repeated for more complex nuclei. For example, the secular determinants for the prolate and linear arrangement of three α-particles of ^{12}C. In oblate and triangular configurations these are, respectively:

$$\begin{vmatrix} x & 1 & 0 \\ 1 & x & 1 \\ 0 & 1 & x \end{vmatrix} = 0 \quad \text{and} \quad \begin{vmatrix} x & 1 & 1 \\ 1 & x & 1 \\ 1 & 1 & x \end{vmatrix} = 0.$$

The roots of the polynomial solution of the secular determinant give the relative energies between the molecular orbits in terms of the parameter β.

Fig. 9 shows result for the density contours for σ and π configurations for a two-centre system (part (a) and (b)). Further the π-bonding states in three- and four-centres using the Hückel approach are illustrated. As stated earlier, the π-orbit gives density distributions which are concentrated outside of the axis of the linear α-chain configurations. The π-orbits shown in parts (c), (e) and (h) of Fig. 9 correspond to the points P_2, P_3 and P_4 in Fig. 8. From the Hückel approach it follows, as noted earlier, that the π-type orbit gives the lowest energy for all of the linear chain systems and is likely to play a significant role in their stabilisation.

3. Cluster collisions and molecular potentials

3.1. Nucleus–nucleus potentials, relation to threshold diagrams

There is a strong relationship between clustering, molecular resonances and the properties of the nucleus–nucleus potentials. In the Hauser–Feshbach (HF) picture, with a binary channel consisting of two clusters, the formation or decay of resonances is governed by the real and imaginary parts of the optical potential. The imaginary part is responsible for the width or the life time of the cluster resonances. In part this was realized in the early stages of heavy-ion scattering by Feshbach [94], see also Ref. [120]. In the early work mainly shallow potentials have been adopted in order to obtain resonant behaviour. In addition, the observation of resonant molecular structure at the thresholds can be related to a small imaginary part. The latter is mainly observed for systems consisting of strongly bound clusters. It is these cluster–cluster potentials which then give rise to the molecular configurations with additional valence particles. In this way, molecular characteristics of the optical model potentials play an essential role in the description of the (cluster + n + cluster) systems.

The aim is to describe both bound and resonant states in the same potential. Such work has been pursued for systems involving α-particles by Michel et al. in Ref. [206], where in particular the $\alpha+^{16}$O system is discussed, an example with particularly rigid clusters. In the original Ikeda diagram the ^{12}C nucleus was included. The experience of the last decades has shown [254] that systems consisting of fragments with large deformations (and thus strongly excited 2^+ states), give rise to a particularly complicated splitting of the resonant structures (see Refs. [91,143]). Thus, ^{12}C may not be treated as an inert cluster.

In the work on molecular resonances in nucleus–nucleus collisions at low energies with identical bosons (^{12}C+^{12}C and ^{16}O+^{16}O) mainly shallow "molecular potentials" have been used to describe the "resonant" structures observed in the excitation functions. As stated, for the imaginary potential surface transparency was required, which is well accounted for by the model of number of open channels (NOC) by Haas and Abe [122]. The strongly-bound clusters giving the smallest NOC. This model was further developed and applied to the decay of various binary decays [31,32]. The centrifugal potential for larger angular momenta gives a repulsive effect at smaller distances, and effective potentials with a pocket result.

This approach is contrasted by the more recent work based on the double folding model. When applied to the scattering of ^{4}He and of ^{16}O nuclei, it gave very deep real potentials [179–181,217]. The deepness is a mean field effect, which is due to the strong spacial overlap of all the nucleons at smaller distances. Deep potentials combined with a small absorption allow the observation of rainbow scattering, which is very prominent in α-particle scattering. This phenomenon is generally observed for combinations of strongly bound clusters [179–181,217], for which all reaction Q-values are very negative, giving a weak imaginary potential.

Rainbow scattering allows the determination of the potentials at small distances, and thus in principle ítś study is of primary importance for the determination of nucleus–nucleus potentials. We repeat here the basic facts of rainbow scattering [48,164,289]. The rainbow structure appears if the real nuclear potential is strong enough, i.e. refractive, in order to deflect particles into "negative angles", which are on the opposite side of the Coulomb trajectories. A maximum "negative" deflection (rainbow) angle, θ_R, occurs for intermediate impact parameters. Such trajectories are shown in Fig. 10. In the region of the rainbow angle several partial waves contribute to the same angular region and a particular

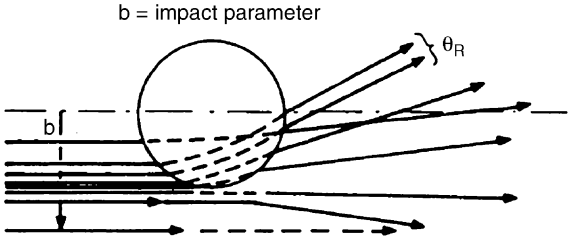

Fig. 10. The trajectories for ^{16}O+^{16}O scattering at $E_{lab} = 350$ MeV [286] as a function of impact parameter b. For large values of b, deflection to "positive" angles occurs. The scattering to "negative" angles for small values of b is shown. The maximum negative angle corresponds to the rainbow angle θ_R, see also Fig. 11.

oscillating interference structure due to contributions from the inner region appears. These patterns are referred to as Airy-structures [48,181].

More recent analysis of the elastic scattering of ^{4}He and ^{16}O projectiles on nuclei was based on the more advanced double folding model. In this approach very deep potentials are obtained, which are able to describe all details of the differential cross sections at many energies [179–181,217] and over a large angular range covering many orders of magnitude. This self-consistent double-folding model uses an effective density dependent nucleon–nucleon interaction adjusted to the properties of nuclear matter [177–180]. This gives a potential which is very deep in accordance with the model independent analysis of the experimental results. For the ^{16}O+^{16}O system the elastic scattering has only recently been studied in more detail [217,181], and the phenomenon of rainbow scattering [48,164,256,286,289] has been observed at energies of 10–70 MeV/*u*. These studies allowed the determination of the nucleus–nucleus potential over a large range of the inter-nuclear distances. Some of the data are shown in Fig. 11, where the evolution of the refractive structure at several energies is illustrated. The primary rainbow angle appears at 55° for 350 MeV incident energy, for lower energies it moves outside the observable angular region, however, the next order Airy-structure moves into the region observed in the experiment (below 90°). These correspondingly higher order maxima and minima are referred to as 2nd and 3rd-order Airy-structures, respectively. They appear inside the "lighted" region and move through 90° towards larger angles with decreasing energies [217]. This feature creates strongly oscillating excitation functions, which have been measured extensively at $\theta_{cm} = 90°$. In contrast to this, the strong regular maxima and minima in these data were formerly interpreted as resonant molecular structures [91,254].

The self-consistent double-folding model appears to be valid down to rather low energies, where the Pauli principle would inhibit the penetration of the two clusters. A repulsion in the potential energies has been proposed to result [255]. However, the data can be described with the deep potentials down to energies of 5 MeV/nucleon. This validity of the approach can be understood because the effective relative momentum of nucleons in the overlap region remains quite large for the deep potentials. This effect of self consistency strongly reduces the effect of the Pauli principle, as described by Subotin et al. [255]. The use of the deep potentials is discussed for ^{16}O+^{16}O by Kondo et al. in [184,221,255] and for α-scattering in Ref. [206]. For these potentials the wave-function of relative motion must have a sufficient number of nodes to give wave functions consistent with the Pauli principle.

The deep potentials have many bound states which are not physically relevant, and are not allowed by the Pauli principle. This problem was solved by D. Baye [28] with a procedure called the super-symmetric transformation of the deep mean-field potential to a phase-equivalent shallow potential. In these transformations the unphysical bound states are removed and finally a potential results which typically is shallow and shows repulsion at small distances. The resulting potentials can be considered to be of molecular type. For the two most relevant cases, the interaction of two α-particles (^{8}Be) and α+^{16}O (^{20}Ne), phase-equivalent local potentials have been produced [206]. The result is a potential with a shallow attractive part and a strong repulsion at small distances. These are shown in Fig. 12. For the α–α potential the empirical molecular potential created by Ali and Bodmer [10] to describe ^{8}Be (dashed curves), is seen to coincide well with the super-symmetric local potential. Similarly, in the case of the (α+^{16}O) system, the elastic scattering as well as the bound states of ^{20}Ne have been successfully described with the shallow phase-equivalent potential by Michel et al. [206].

For the earlier systematic work on resonances (e.g. ^{16}O+^{16}O) a remarkable conclusion concerning the structures observed in excitation functions can be drawn: the gross structures in the cross sections at 90° at the lower energies, and previously discussed with shallow potentials as "molecular" resonances [91], can now also be explained by strongly attractive potentials. They are explained by rainbow scattering with the passage through $\theta_{cm} = 90°$ of the Airy-minima and -maxima of the higher order rainbow structure [48].

For the lowest energies there is still the concept of super-deformed (molecular) states in ^{32}S, consisting of two ^{16}O-nuclei which has been described by Ohkubo and Yamashita [222] with the deep potential model, and also by Kimura and Horiuchi [182] with the AMD method. Actually, the local potentials between clusters, which are repulsive at small distances and otherwise weakly attractive, are needed for nuclei with additional neutrons in order to build covalently bound nuclear cluster structures which are discussed below.

3.2. The nucleon exchange potential, elastic transfer

Scattering of two nuclei consisting of two clusters and valence nucleons have played an important role in the development of the molecular orbital model of nucleons. In the scattering systems with two nuclei differing only by

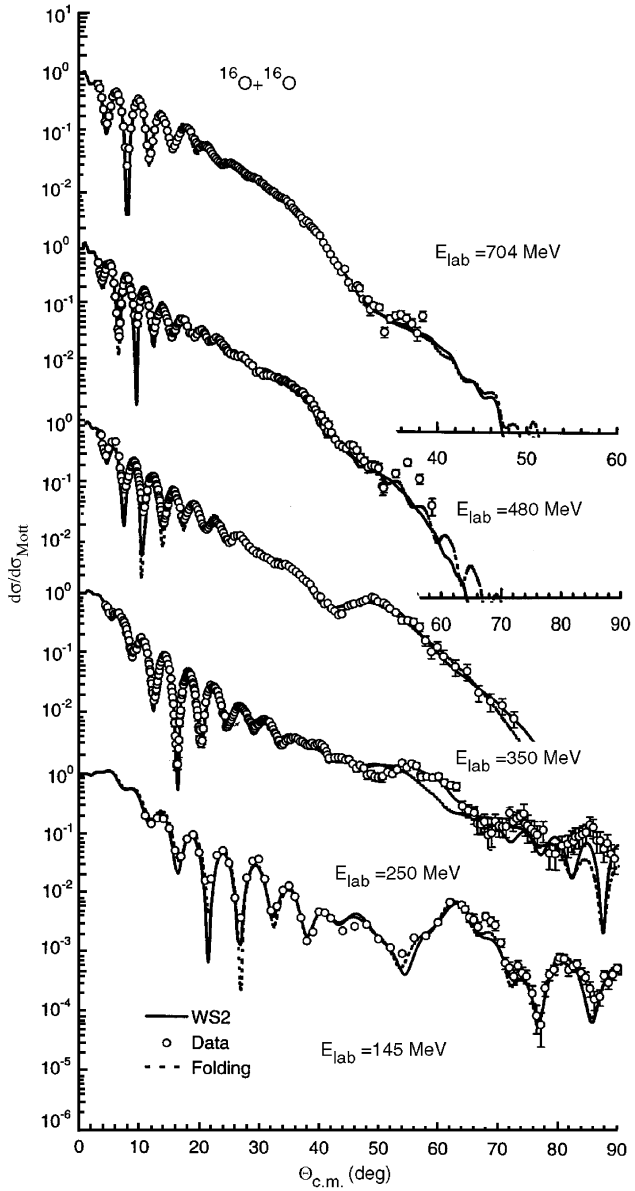

Fig. 11. Differential cross sections of $^{16}O+^{16}O$ elastic scattering divided by the Mott-scattering cross section. The primary rainbow maximum is observed for $E_{lab} = 350$ MeV at an angle $\theta_R = 50°$; at $E_{lab} = 480$ MeV it is at 35°; at lower energies it moves to larger angles, beyond 90°, outside the observation region. The strong maximum observed at $E_{lab} = 145$ MeV belongs to a higher order Airy-structure, from Refs. [181,256].

one or a few valence nucleons (or holes), a pronounced effect due to the exchange of the nucleons between two identical cores is observed, also called the elastic and inelastic transfer [277–279]. The amplitudes of the two processes, elastic scattering $f_{el}(\theta)$ and the exchange amplitude $f_{tr}(\pi - \theta)$ for the transfer of the valence particle, e.g. from the projectile to the target, are added coherently. Due to the coherent superposition of the two amplitudes a pronounced interference structure is observed in the intermediate angular range in the angular distributions. At higher energy the transfer process is concentrated at small angles at the appropriate grazing angle, located at θ_{gr}, thus it can be clearly observed with a maximum located at $\theta = (\pi - \theta_{gr})$ in the elastic channel. Because the projectile and target nuclei are interchanged in this process, a backward rise in the elastic channel is observed. This is illustrated for the elastic scattering of $^{37}Cl+^{36}S$ in Fig. 18 in Section 3.4 which shows a peak at $\theta_{CM} = 130° = 180° - \theta_{gr}$ due to the proton transfer.

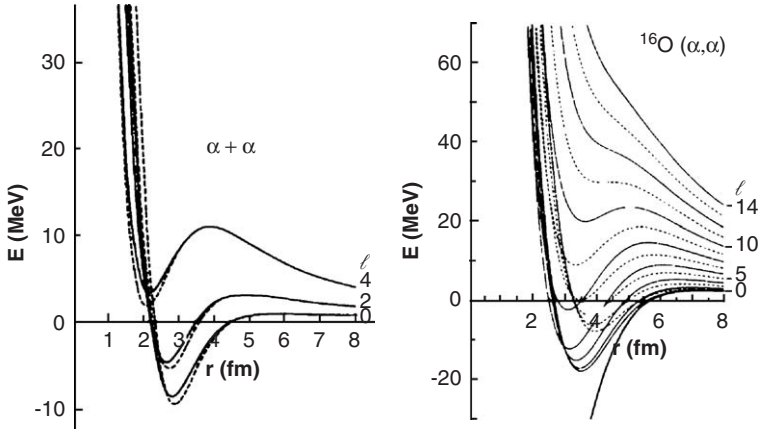

Fig. 12. Two examples of molecular local potentials for the α–α interaction, i.e. for ^{8}Be, and for the α-^{16}O system, forming ^{20}Ne. Different partial waves are shown. Figure adapted from Ref. [206].

In the optical potential the effect of nucleon exchange can be described by the antisymmetrisation of the whole system, which gives rise to a parity dependent nucleus–nucleus potential [26,27,277–279]. For the description of such scattering systems the two-centre harmonic oscillator model and the GCM have been pursued by Baye and coworkers [4,26,27]. On the other hand, the approach based on the molecular orbital method for the valence particles has been developed by Imanishi and von Oertzen [147,277–280]. This was extended later [148] to the method of rotating molecular orbitals (RMO). The valence particle transfer between nuclei has also been treated in the two-centre shell model by Park et al. [229] and a review of their method can be found in Ref. [265].

The parity dependence of the nucleus–nucleus potential can also be obtained in the coupled reaction channels approach in which various channels corresponding to the exchange of nucleons are included. In this approach, again via the introduction of local and phase equivalent potentials, the dependence on parity and on angular momentum appears. In using such potentials for the cluster–cluster interaction the analysis of the elastic channel can directly predict the occurrence of parity-split bands in nuclei with a particular cluster structure as discussed by Baye [27].

3.3. Nuclear molecular orbitals and the two-centre shell model

We come back to a more detailed discussion of the wave functions of two-centre systems. The two-centre state with one valence particle, mentioned in Section 2.1, is a classical example treated in quantum mechanics. The text books on physical chemistry contain the details for these approaches, where the cores (the atomic nuclei) and the valence particles (electrons) are treated without antisymmetrisation in their region of overlap. The method in atomic physics is called the linear combination of atomic orbitals (LCAO), which has also been used in nuclear physics as the linear combination of nuclear orbitals (LCNO) for valence neutrons [277,279,148]. This method was applied to the structure of ^{8}Be, ^{9}Be and $^{12-13}$C, corresponding to the exchange of neutrons and α-particles, respectively [1,223]. The microscopic approach for the nuclear structure, using the LCNO, was extended and applied by Itagaki et al. [150,152,153] to neutron-rich nuclei to describe dimers, chain structures (in carbon), and triaxial deformation. In all approaches a decision has to be made about the number of configurations, which will be mixed together. The success in the description of the rotational bands, and the spin values where they terminate, may thus vary from model to model.

The beryllium isotopes, as a starting point for the first nuclear covalent molecule, give us the occasion to define some basic facts. We need to inspect the structure of the single centre, the ^{5}He nucleus, which as the basic building block contains the (^{4}He + neutron) interactions $V_{n,\alpha_i}(\mathbf{r}_{n\alpha_i})$ for the covalent neutron. We use coordinates as shown in Fig. 13.

The total Hamiltonian, $H_{\rm tot}$, can be written as follows:

$$H_{\rm tot} = T(\mathbf{R}) + T(\mathbf{r}_n) + H_{\alpha_1} + H_{\alpha_2} + V_{\alpha_1,\alpha_2}(\mathbf{R}) + V_{n,\alpha_1}(\mathbf{r}_{n\alpha_1}) + V_{n,\alpha_2}(\mathbf{r}_{n\alpha_2}). \tag{11}$$

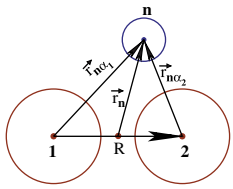

Fig. 13. The coordinates for the two-centre orbitals of neutrons as described in the text.

If we use as the coordinates (Fig. 13) the vector from the centre of the molecule $\mathbf{r}_n$, and the distance between the cores $\mathbf{R}$, we obtain for the individual coordinates for the neutron from the centres α_i

$$(\mathbf{r}_n - \mathbf{R}/2) = \mathbf{r}_{n\alpha_1}, \quad \text{or}$$

$$\mathbf{r}_n = (\mathbf{r}_{n\alpha_1} - \mathbf{R}/2) = (\mathbf{r}_{n\alpha_2} + \mathbf{R}/2). \tag{12}$$

The single-centre shell model states $\phi^K_{n,l_1}(\mathbf{r}_{n\alpha_1})$ of the sub-systems ^{5}He$(p_{3/2})$, are used to construct the molecular wave function by a linear combination of the nucleonic orbitals, for example for ^{9}Be states. Because of the axial symmetry the projections of the spin K are introduced, K being the projection of the neutron angular momentum onto the axis defined by the two clusters. The linear combinations contain the sign p connected to the parity Π (and the g/u property, as explained below):

$$\Phi^{K,\Pi}_{\mathrm{LCNO}}(\mathbf{R}, \mathbf{r}_n) = N(R)\frac{1}{\sqrt{(1+\delta^{K,p}(\mathbf{R}))}}\left[C_1\psi_{\alpha_1}\psi_{\alpha_2}\phi^K_{n,l_1}(\mathbf{r}_{n\alpha_1}) + (-)^p C_2\psi_{\alpha_1}\psi_{\alpha_2}\phi^K_{n,l_2}(\mathbf{r}_{n\alpha_2})\right]. \tag{13}$$

The molecular wave function must be invariant under the exchange of the two identical cores, the phase $(-)^p$ defines the gerade g, (positive sign) and ungerade u, (negative sign) property. Only for two equal centres and the same single particle wave functions the parity π, and the property of invariance defined by g and u are related.

The parity operation for the neutron wave-function is simply defined by

$$\mathbf{r}_n \to -\mathbf{r}_n \tag{14}$$

Using Eq. (13) for the two-centre wave-function, we realize that the total parity Π in the LCNO wave function is related to the g and u property by

$$\Pi = (-)^p(-)^l. \tag{15}$$

Into this relation, Eq. (15), the parity of the individual single-centre wave functions enters via the $(-)^l$ sign. This is borne out in the plot of the molecular orbitals in the correlation diagram shown in Fig. 15.

The amplitudes C_1 and C_2 will give a measure of the sharing of the neutron between the two asymptotic wave functions, e.g. the two ^{5}He$(p_{3/2})$ states. For identical cores these amplitudes are identical. In the more general case, with two different centres, with different binding energies and quantum numbers, or for the same centres with different single particle states, the molecular wave function has different properties. Because of the intrinsic reflection asymmetry the wave function has no well defined parity. The two amplitudes C_i will become very different and an additional parity projection is needed. In this case the valence particle may concentrate at one centre and we could obtain ionic binding as in atomic physics, however, because the neutron carries no charge, this situation has no molecular binding properties in nuclear physics.

The overlap of the single particle states determines the non-orthogonality, $\delta^{K,p}(\mathbf{R})$, and it depends on the distance $\mathbf{R}$.

$$\delta^{K,p}(\mathbf{R}, \theta) = (-)^p \int \phi^{*K}_{p3/2}(\mathbf{r}_{n\alpha})\phi^K_{p3/2}(\mathbf{r}_{n\alpha} - \mathbf{R})\,\mathrm{d}\mathbf{r}. \tag{16}$$

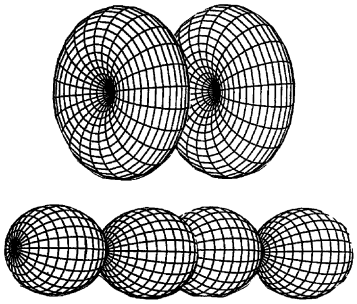

Fig. 14. Illustration of the spacial overlap of two p-shell orbits corresponding to $m = 1$, for π (upper part) and, to $m = 0$, for σ (lower part) molecular orbitals, respectively [283].

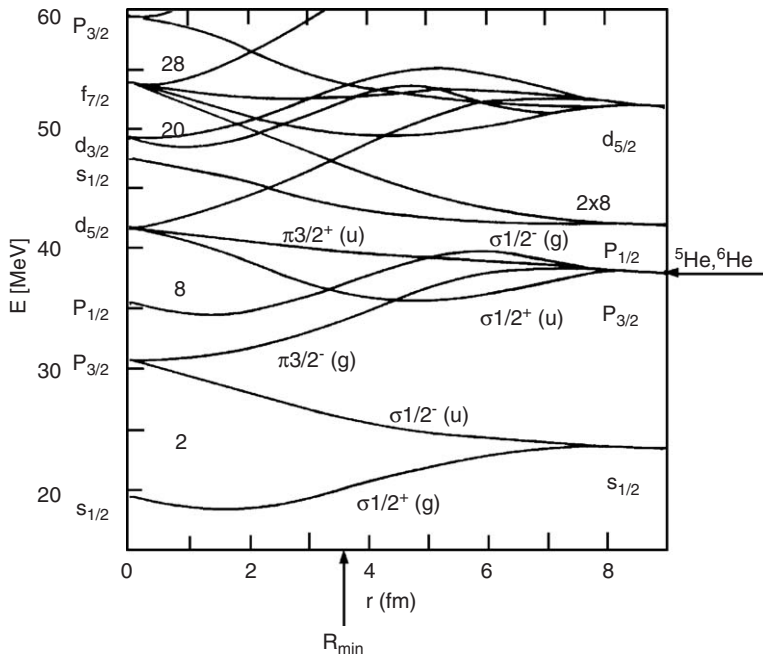

Fig. 15. The correlation diagram of molecular orbitals for a two-centre system [283]. The position of the asymptotic p-shell orbits in ^{5}He at large distances, forming π and σ molecular orbitals is indicated. At $R_{\min}$, the α–α potential attains its minimum. The quantum numbers (K, parity and the related gerade and ungerade (g and u) property) for the various two-centre orbits are shown.

Actually, the integral with the wave functions of Eq. (16), folded with the interactions V_{n,α_i} is known as the exchange energy $\Delta E^K(\mathbf{R})$. For equal amplitudes, C_i, a maximum binding energy $\Delta E^K(\mathbf{R})$ is obtained (see Ref. [95]).

As in atomic physics, where the spin–orbit interaction is, however, weak, we introduce the projection of the orbital angular momentum l of the single centre wave functions $\phi_l^K(p_{3/2})$ of the valence nucleon and we use the names introduced in molecular physics as σ for $m = 0$ and π for $m = 1$. The spatial structure of the two possible configurations, σ and π, for a p-orbit ($l = 1$ for the case of $^{9-10}$Be) are shown in Fig. 14.

The diagonalisation of all interactions in Eq. (11) without the kinetic energy term leads to the correlation diagram for molecular states classified by their symmetries and K-quantum numbers, as shown in Fig. 15. This method has been pursued in ion–atom collisions and for nuclear reactions in the approach of Park et al. [229]. In the latter case the kinetic energy operator creates, due to the finite mass of the valence particle and the non-locality of the coordinates, couplings (separated into rotational and radial motion) between the relative motion of the two fragments and the internal degrees of freedom. These couplings produce two kinds of effects: the rotational (Coriolis) coupling, giving rise to

K-mixing, and the radial couplings responsible for the transitions between individual channels, which are eigenstates of the two-centre system.

These correlation diagrams (Fig. 15) are a common tool in atomic molecules and atom–ion collisions [128]. For the axial symmetry the quantum numbers are conserved for all distances and merge close to the united nucleus limit at small distances into the quantum numbers of the Nilsson model. This conservation of quantum numbers is also reflected in the "Harvey rules", discussed before. It comes thus as no surprise that the behaviour of the lowest orbits in correlation diagram in Fig. 15 is the same for atomic and nuclear cases. In both cases the $\sigma K = 1/2(u)$ orbital, which gains energy with decreasing distance at the beginning of the energy splitting at large distances, crosses the $\pi K = 3/2(g)$ orbit and then has to move up to the deformed Nilsson orbit, the $K = 1/2$ orbital of the $d_{5/2}$-shell. We note further that for the $p_{1/2}$-shell the orbit with the negative parity has the lower energy due to the relation given in Eq. (15). This sign of the splitting for the p-shell has been confirmed in the study of the exchange of the neutron in the parity dependence of the potentials in $^{13}C+^{12}C$ scattering [38,279].

The complete description of the mean field behaviour of such a two cluster nuclear system must take full account of the distribution of the neutrons and protons. This is described by the two-centre shell model (TCSM) approach, which was implemented 30 years ago [247]. The diagram shown in Fig. 15 is a solution of the Schrödinger equation for single nucleons as a function of the separation of two shell model potentials. Placing nucleons into these orbitals one has to include the residual (pairing) interaction, which will change the two-centre system, once several valence nucleons are introduced.

The ordering of the energy levels at a separation distance of the two potentials of ~ 3.5 fm, as indicated in Fig. 15, is reflected in the level scheme of ^{9}Be. The rotational band structure in ^{9}Be and the structure of other beryllium isotopes (see Section 6.1.1) can be described completely as two-centre configurations.

3.4. Hybridisation and Coriolis couplings

Two important features of molecular physics appear in the elastic scattering of two nuclei with valence particles, including the elastic transfer of the valence particle. Features, which are also important in the rotational bands of nuclei and for the covalently bound systems discussed below:

(i) the hybridisation of valence particle orbitals [37,147,230,281] and,
(ii) the Coriolis coupling between states of different K-quantum numbers in the rotating frame [46,148].

The first effect, the hybridisation, is well known in physical chemistry, it introduces a dynamical mixing of single shell orbitals of different parity, like the s-orbit and the p-orbit in molecules with carbon atoms, as introduced by Pauling [230]. This gives rise to the distorted orbitals, the hybridized bonds which are responsible for binding in carbon polymers.

In nuclear physics again the vicinity of the s-orbit and the p-orbit is observed in light nuclei, for example in carbon isotopes [148,280]. Most conspicuous is the case of ^{13}C. The hybridisation effect is illustrated in Fig. 16 for the $p_{1/2}$-orbit (^{13}C-ground state) mixed with the opposite parity $s_{1/2}$-and $d_{5/2}$-orbits. The top part of the figure shows schematically that this gives rise to a destructive and constructive addition of densities, depending on the sign of the mixing along the axis. In the scattering of ^{13}C nuclei with ^{12}C, the elastic scattering associated with the $p_{1/2}$-, and the inelastic channels with the $s_{1/2}$- and the $d_{5/2}$-states, respectively, in ^{13}C have been measured as function of incident energy and analysed by Imanishi [147]. In this analysis [148,149] using the RMO-model, with the incorporation of the elastic transfer, the inelastic excitation and the "inelastic transfer", referring to the neutron transfer to the ground state and the excited states, is enhanced due to the hybridisation effect. This is seen because the probability of finding the valence particle between the two centres is increased.

Fig. 16 shows the effect of hybridisation on the two-centre valence particle density for a chosen channel spin and parity. The figure also shows the effect of the neutron exchange and hybridisation on the total potential. At large distances (10.5 fm) the overlaps of the undistorted single particle wave functions are seen. With decreasing distance and with larger overlap the distortion sets in, creating a strong increase of the density of the valence neutron on the axis between the two centres. Because of the additional binding energy the latter shows a lower barrier if compared to the case without valence neutron. The resulting distortion of the density of the valence particle along the line connecting the two centres is known to give rise to enhanced binding in atomic systems and can play also the same role in nuclear

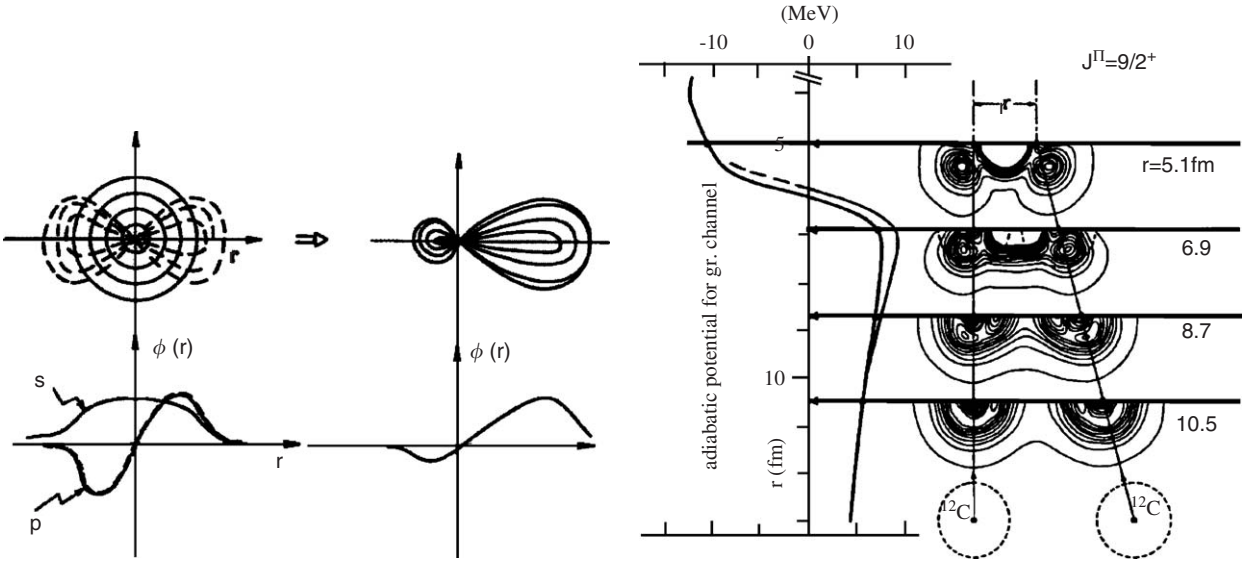

Fig. 16. Left part: schematic illustration (adapted from Ref. [230]) of the hybridisation effect: the distortion of valence orbits due to configuration mixing of states with different parity (*s*- and *p*-orbits). Right part: the potential between two ^{12}C-nuclei with (and without—the higher of the two potentials) the presence of the valence neutron. The states of ^{13}C with $p_{1/2}$, $s_{1/2}$ and $d_{5/2}$ are incorporated in the mixing calculations. The contour plots show the evolution of the densities of the valence neutron in the two-centre state, in the energetically lowest configuration as function of the distance between the two ^{12}C-centres. The densities are shown for a specific total channel spin and parity, corresponding to a grazing collision. There a strong enhancement of the density and of the transfer probability is observed [149].

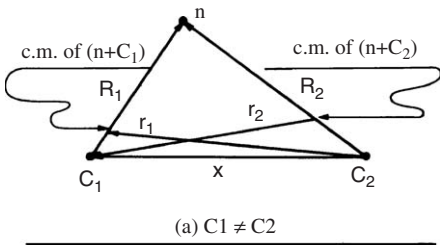

Fig. 17. The "non-local" coordinates for the exchange of a valence particle with finite mass. Two asymptotic channels, with the possible channel coordinates r_1 or r_2, can be used [149].

systems. This result can also be understood in the usual coupled reaction channels (CRC) approach as arising from the combined coherent action of the transfer and inelastic interactions (see Ref. [281]).

The second effect, the Coriolis coupling, is a well known problem for rotating nuclei, but is particularly strong for valence particles in a two-centre system. It arises from the coupling of the individual angular momentum of the valence particle with the collective motion of the core. It introduces in rotational bands a mixing of states with different *K*-quantum numbers. More specifically, it causes, for rotational bands with $K = 1/2$, a peculiar Coriolis decoupling effect, a coupling between states with $\Delta K = 1$. This leads to a staggering in the energy sequence of states in the bands (see Fig. 22, as well as Fig. 26 and Fig. 28). In order to understand this we must examine the interactions. The single-particle potentials at the two centres give rise to the bound states. But at the same time these interactions, $V_{\mathrm{n,C}}(\mathbf{R}_i)$, are responsible for the transfer from one core to the other and for the single particle excitation within one mass partition. If the coordinates, shown in Fig. 17 are used to describe the collision process, then the finite range effect due to the finite mass of the valence nucleon becomes important. This arises as for the different mass splits two different asymptotic coordinates have to be chosen, which show the non-locality. The molecular wave functions $\Phi^K_{\mathrm{LCNO}}(\mathbf{R}_1, r_1)$ of the valence particle *n*, are obtained by the LCNO-approach. In the RMO calculation a channel wave function of

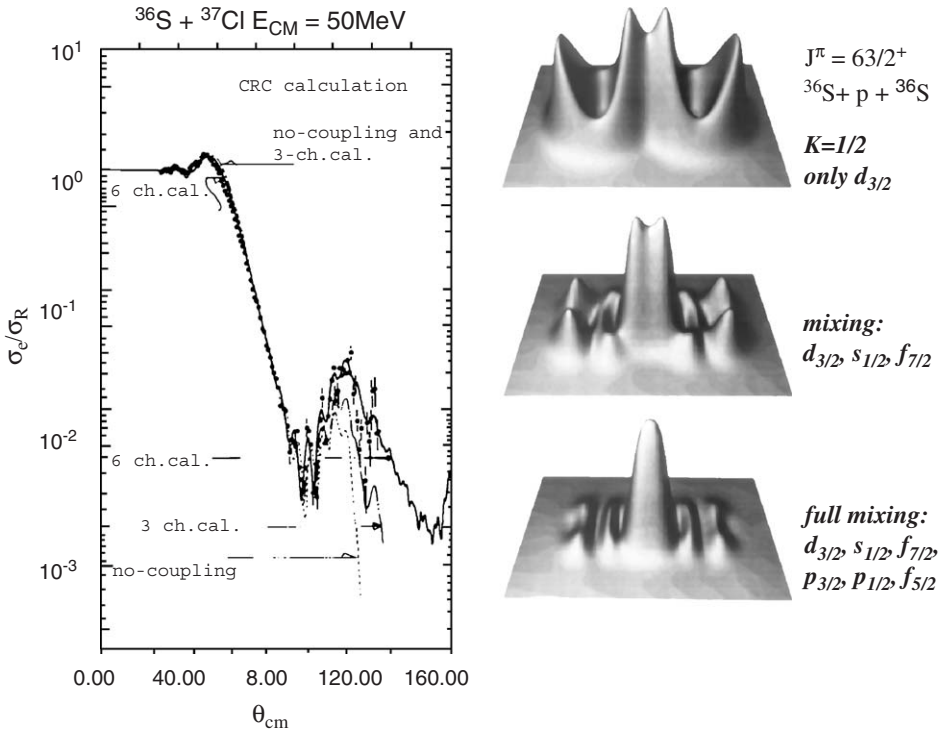

Fig. 18. Left: Angular distributions of the elastic scattering of ^{37}Cl+^{36}S showing the elastic transfer of a proton as a maximum at back angles. Note that the elastic transfer corresponds to the transfer of the proton between the ^{36}S cores leading to the ground states in both final state nuclei, and thus a process indistinguishable from elastic scattering. The different CRC calculations show the increasing effect with the inclusion of more excited single particle states of ^{37}Cl. These shell model orbits are cited on the lower part of the figure. The rise of the proton transfer cross section at $\theta = 125°$ is enhanced due to the increased valence particle density (configuration mixing). Right: Calculations for the intrinsic density distribution of the valence proton, illustrating the effects due to configuration mixing of states with different parity (hybridisation). The overlap of two pure $d_{3/2}$-valence orbits (upper part) changes with the stepwise inclusion of the couplings with the higher shells ($s_{1/2}$, $f_{7/2}$, etc.) creating a distortion as seen in Fig. 16, from [37,281].

good total spin and parity is created by using the two-centre wave functions $\Phi^K_{\mathrm{LCNO}}(\mathbf{R}_1, r_1)$, and the two signs of the signature, s, will appear,

$$\Psi_1^{J,K,\Pi}(\mathbf{R}_1, r_1) = N(R)\left[D^J_{MK}(\mathbf{X})\Phi^K_{\mathrm{LCNO},1}(\mathbf{R}_1, r_1) + (-)^s D^J_{M,-K}(\mathbf{X})\Phi^K_{\mathrm{LCNO},1}(\mathbf{R}_1, r_1)\right]. \tag{17}$$

As mentioned previously, in the diagonalisation of interactions in Eq. (11) using the states of Eq. (17), the kinetic energy operator creates due to the finite mass of the valence particle and the non-locality of the coordinates, rotational and radial couplings.

The rotational Coriolis coupling gives rise to K-mixing, and the radial couplings induce the transitions between individual channels, which are eigenstates of the two-centre system. In the RMO-approach of Imanishi and von Oertzen the diagonalisation for the two-centre wave-functions is done including the Coriolis coupling, and the concept of RMO with mixed orbitals is obtained. With this approach specific features of the intrinsic molecular states, namely their distorted intrinsic density distributions (see e.g. Figs. 16 and 18) can be obtained. The radial couplings remain, they become particularly strong at avoided crossings of two levels with the same quantum numbers, but belonging to different asymptotic states. The transitions connected to these avoided crossings are known as Landau–Zener transitions [148,149,190]. Resonant behaviour in the population of single particle states was initially claimed in the reaction ^{17}O+^{13}C in Ref. [64] to be due to the Landau–Zener effect. Complete quantum mechanical models showed that such sharp resonances are not possible due non-local effects. Thus subsequent experimental work [101] by the same group corrected this result and showed that the experimental resonances were due to a target contaminant. Subsequent

theoretical work showed that due to the quantal effects sharp structures due to Landau–Zener transitions can indeed not be expected. The general expectation of smooth structures as function of energy is explained in Refs. [148,149].

The intrinsic density distribution with hybridisation obtained in the RMO-approach has been shown for the case of $^{13}C+^{12}C$ in Fig. 16. In the following example this effect is illustrated directly with the single-particle states of a valence proton in ^{37}Cl. In this case the (*sd*)- and the (*fp*)-shells are involved, which will be the basis for mixed-parity orbitals. Their population was observed in the scattering of $^{37}Cl+^{36}S$, studied by Bilwes et al. [37,281]. The proton transfer and the inelastic transfer and the inelastic scattering populate the single particle states in ^{37}Cl. With the difference of one proton the role of the cores is exchanged in the transfer process. The product of the transfer is again $^{36}S+^{37}Cl$, giving rise to a pronounced backward rise in the angular distribution of the "elastic" scattering. Thus the differential cross section for ^{37}Cl scattering contains the elastic transfer of the proton producing the ^{36}S nucleus as a backward rise at angles $\theta(^{37}Cl) = 180° - \theta(^{36}S)$.

In order to describe the dynamical effects in such a system there are two ways to obtain the differential cross section in a CRC analysis:

(a) The first is the "standard" CRC-approach using the appropriate eigenstates of the separated nuclei in the system $^{37}Cl+^{36}S$, with known spectroscopic properties for the valence proton in the single-particle states in ^{37}Cl (six channels up to 6 MeV excitation energy as indicated in Fig. 18).

(b) In the second approach the RMO basis is used and the same single particle states, creating intrinsic two-centre states, classified by total spin and parity. The intrinsic states in this case are two-centre states as mixed linear combinations of the valence nucleon orbitals in the single particle states of ^{37}Cl. The hybridisation of the ground state and the excited states in ^{37}Cl via transfer and inelastic excitations leads to an enhanced proton transfer probability in the ground state, see Fig. 18. The enhanced proton transfer cross section is only reproduced if all channels (in particular the *fp*-shell) are included in the calculation. In the second part of the figure the density distributions of the valence proton are shown for the two-centre scattering states with different degrees of mixing. This example corresponds to partial waves of a grazing collision which is characterised by a total spin $J = 63/2^+$ and channel quantum number $K = 1/2$. The figure shows the result of the RMO-calculation with different numbers of single particle states included. For the complete 6-channel calculation the differential cross section is strongly enhanced. This can be understood with the increased density of the valence proton between the two centres induced due to mixing of orbitals differing in parity. The detailed study of this system [37,281] showed that the data can only be reproduced if the mixing of all six individual orbits of the proton in excited states of ^{37}Cl is included. The same distinct non-linear effect of the mixing interactions is also observed in the CRC-calculations [281]. There it is also due to the combined action of inelastic transitions and the transfer interactions.

4. Cluster states for $N = Z$, recent results

There has been an enormous effort devoted to exploring and understanding the appearance of clustering in $N = Z$ systems, much of the experimental work probing quasi-molecular resonances via the collision of two clusters [49,91,120]. These studies suggest that two-body cluster structures exist in a broad variety of systems extending to $^{28}Si+^{28}Si$ [219]. These resonances were most prominently observed in the $^{12}C+^{12}C$ system [11,49,52,53,91] where their energies coincided with the Coulomb barrier, and were thus called "Barrier-top" resonances. Their widths were of the order of a few hundred keV which indicated a nuclear complex which lived for an appreciable amount of time, and which could not be explained in terms of the influence of the compound nucleus [91]. Recently some progress has been in understanding the multi-cluster nature of light nuclei, in particular there has been some work on the possible existence of α-chain states nuclei. There has also been a concerted effort to provide a much greater insight into the resonances in one particular system, ^{24}Mg, namely $^{12}C+^{12}C$, by performing a comprehensive series of measurements over a wide variety of decay channels and also to the extremes of centre-of-mass energies. Here, we record a few of the developments made in these areas.

4.1. Chain states

The focus of cluster studies of α-conjugate nuclei has been two fold, as reviewed in [105,114,305], (i) the search for exotic α-particle complexes and, (ii) studies of large di-cluster structures within light nuclei. Renewed interest

in exotic linear α-particle chain configurations was sparked by the study of the $^{12}C(^{12}C, 6\alpha)$ reaction by Wuosmaa et al. [303], where a resonance-like structure was observed at $E_{cm} = 32.5$ MeV. Initially experimental evidence has been obtained for a 4α-chain state in ^{16}O by Chevallier et al. [61]. Intensive experimental and theoretical investigation ensued [58–60,102,131,157,159,194,236,237,304]. The totality of this effort was to demonstrate that the observed resonance could not be characterised in terms of a linear chain of six α-particles, or as was suggested by Rae et al. a shape eigenstate [236]. Actually a state in which the rotational members are energetically degenerate, owing to the large deformation, cannot be characterised uniquely by a single angular momentum but by shape alone. Rather more mundanely the resonance was found to belong to a sequence of resonances extending to much higher energies (see below).

In fact, there would appear to be a complete absence of chain-like structures in α-particle nuclei, beyond the simplest case ^{8}Be. As an example, the 7.65 MeV state in ^{12}C a 0_2^+ state, (the so-called Hoyle state[142]) has a long association with the 3α-chain [51,261]. However, there exists no clear experimental evidence for the inevitable 2^+ rotational state [105] close to the second 0_2^+, and it is generally accepted that the state possesses a rather different character which has overlaps with an extended α-particle arrangement [92]. Actually, in the study with the microscopic 3α-cluster models such as RGM, GCM, and OCM in 1970s, the 0_2^+ state was regarded as a loosely bound cluster structure [111,112,137,213,271]. Most recently, the state has been identified with an α-particle Bose–Einstein condensate (BEC) [268,115] where all α-particles exists with a relative *S*-state in the centre-of-mass wave function. This feature of a dilute α-particle state close to the nα decay threshold [307] may be a general feature of $A = 4n$ conjugate systems.

The remaining possibility for a chain configuration in the 3α system is that the third 0^+ state in this nucleus at 10.3 MeV possesses such a chain structure, although this state has a width of 3 MeV and exists in an excitation energy region in which there are many overlapping levels. The states in this energy region have recently been studied using *β*-decay at CERN [116]. The states are also observed in inelastic scattering of α-particles by Itoh at RCNP (Osaka) [162]. It would appear that in all likelihood that linear-chain structures do not exist and this is largely due to the instability against the bending mode, in which the chain collapses into a more compact object. Indeed a study of the stability of the 4α chain by Rae [237] found that the 4α chain, as described by two ^{8}Be $(\alpha + \alpha)$ subunits, was unstable against collapse into the more stable kite and tetrahedral cluster arrangements. It should be noted, however, that the measurements of the $^{12}C(\alpha,^{8}Be)^{8}Be$ reaction may be interpreted in terms of a rotational band with the 4α-chain structure [61]. Such an connection still remains to be confirmed. Calculations by Itagaki et al. [152] find a similar result for ^{12}C. It is expected, as in the case of the beryllium isotope, ^{9}Be, that the addition of valence neutrons can stabilize the chain-like structures in the carbon and oxygen isotopes [283]. Experimental evidence for such structures is given in Section 8.3.2. Calculations using the molecular orbital approach appear to demonstrate that for particular mixed orbitals of neutrons (with hybridisation) in ^{14}C and ^{16}C a very distinct stabilisation of the bending mode [152] can be expected. We note that as in molecular science with atoms, that the covalently bound chains can also be stabilised by the centrifugal forces in their rotational bands.

4.2. *Resonant structure in* ^{24}Mg

The subject of resonances in the $^{12}C+^{12}C$ system has a long and complex history, dating back to the early 1960s to the pioneering work of Bromley et al. [11,52,53], an era which is reviewed in [91]. The weight of experimental evidence suggested that resonances observed in reactions of two ^{12}C nuclei close to the Coulomb barrier were well described by a ^{24}Mg structure with a significant overlap with a $^{12}C+^{12}C$ cluster structure [91]. However, despite a significant quantity of data and enormous theoretical input, a clear and definitive explanation of the resonances did not emerge.

The most recent efforts have sought to expand the systematics of the resonances both in terms of decay channels and the centre-of-mass energy. One of the most dramatic observations was made for the 6α decay channel [303]. Driven by this interest in the 6α chain state, new excitation functions and alignment measurements provided some new insights into the nature of the resonance structures in this system at high energies. Fig. 19 shows the excitation function measurements made for the $^{12}C(^{12}C,^{12}C(3^-))^{12}C(3^-)$ reaction [50,58]. The data extend up to excitation energies in ^{24}Mg of $E_x \sim 64$ MeV, a region in which all resonance-like structures would be expected to be extremely broad. Nevertheless, there is evidence for three resonance-like peaks, a sequence, which was shown in reference [50] to terminate at $E_{cm} = 43$ MeV. This behaviour is characteristic of all of the other inelastic channels leading to α-unbound final states, that is to say for any inelastic channel leading to an excitation in ^{12}C at $E_x \geqslant 7.65$ MeV.

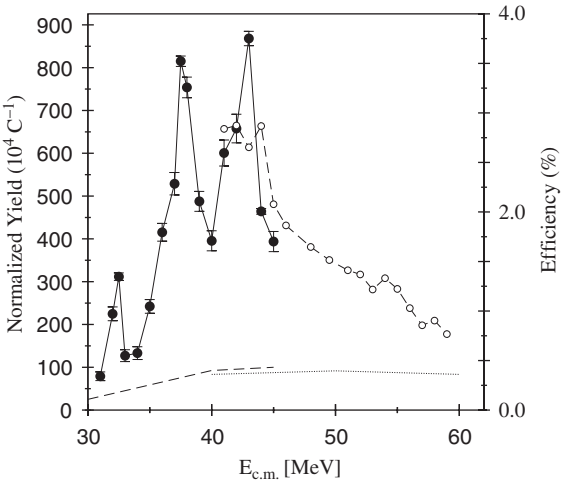

Fig. 19. Yield in the ^{12}C(^{12}C,^{12}C[3$^-$])^{12}C[3$^-$]) reaction as function of centre of mass energy, showing high energy resonances. The corresponding excitation energy range of 44–64 MeV in ^{24}Mg is given, from [50]. The dashed and dotted lines show the detection efficiency with the scale shown on the left side.

The inelastic channels leading to the excitation of particle-bound states had previously been measured by Cormier et al. [67] and also found to terminate at a similar energy. The result of these studies suggest that the resonances which are observed in ^{12}C+^{12}C scattering at energies all the way down to the Coulomb barrier ($E_{cm} \simeq 6$ MeV), and beyond, have an upper limit at excitation energy in ^{24}Mg of 57 MeV. One possible interpretation is that at this energy the structure of ^{24}Mg changes so that the configuration with which the resonances are associated is no longer sustained. Nilsson–Strutinsky (NS) [191,240], α-cluster model (ACM) [201] and Hartree–Fock (HF calculations) [97], all show evidence for quasi-stable cluster-like structures associated with deformed configurations, as shown in Fig. 6. The stability of these structures has been tested within the various models.

Measurements of the angular distributions of the decay α-particles for the ^{12}C(0_1^+)+^{12}C(3$^-$) [306] and ^{12}C(3$^-$)+^{12}C(3$^-$) [60] final states provide information both on the angular momenta associated with the resonance structures and the spin alignments. In both instances, the reactions indicate that there is complete alignment of the ^{12}C(3$^-$) spin with the orbital angular momentum of the two ^{12}C nuclei. Given the proposed triangular cluster symmetry of the ground state of ^{12}C, the 3$^-$ state would then correspond to a rotation in the plane of the triangle. These measurements then indicate the dissociation of a planar (^{12}C+^{12}C)-cluster structure in ^{24}Mg. Calculations suggest that the rotational band associated with this structure should terminate at $J = 20$ to 24 $\hbar$, and the experimental measurement of the spin of the $E_{cm} = 43$ MeV resonance suggests a spin of 22 $\hbar$ [58,60], in close agreement with theory.

The above picture is what is termed the strong coupling picture, in which the structure of the molecular state is strongly linked to the underlying ^{24}Mg cluster configuration. It should be noted that, for example, in the case of the inelastic scattering associated with the ^{12}C$_{gs}$+^{12}C(2$^+$) and ^{12}C(2$^+$)+^{12}C(2$^+$) final states that the broad structures ($\Gamma = 2$–3 MeV) are fragmented into a series of narrow states. This may be understood in terms of the coupling of the broad quasimolecular band—doorway states—to excited states of the scattering system. In the weak coupling picture the doorway states are associated with a pocket in the potential of the scattering system, and thus the two ^{12}C nuclei couple only weakly to ^{24}Mg. Such ideas form the basis of the band-crossing model [2]. In this description the resonances associated with the pocket in the scattering potential couple most strongly with the aligned inelastic molecular band. Such an approach provides a good description of the experimental data [183]. In the preceding discussion, the broad resonances were associated with a secondary minimum in the ^{24}Mg deformed potential, and the alignment is associated with the intrinsic structure, and the decay channels populated would be those with a strong structural link, i.e. ^{12}C(2$^+$) and ^{12}C(3$^-$). The fragmentation is then generated by the coupling to states at smaller deformations just as predicted for the ^{32}S superdeformed case using the AMD framework [182].

Another recent approach to the study of such resonant states in ^{24}Mg, rather than populating them directly, is to use compound nucleus reactions [68,104,106] like ^{12}C(^{16}O,^{24}Mg*)α. One of the significant advantages of this approach

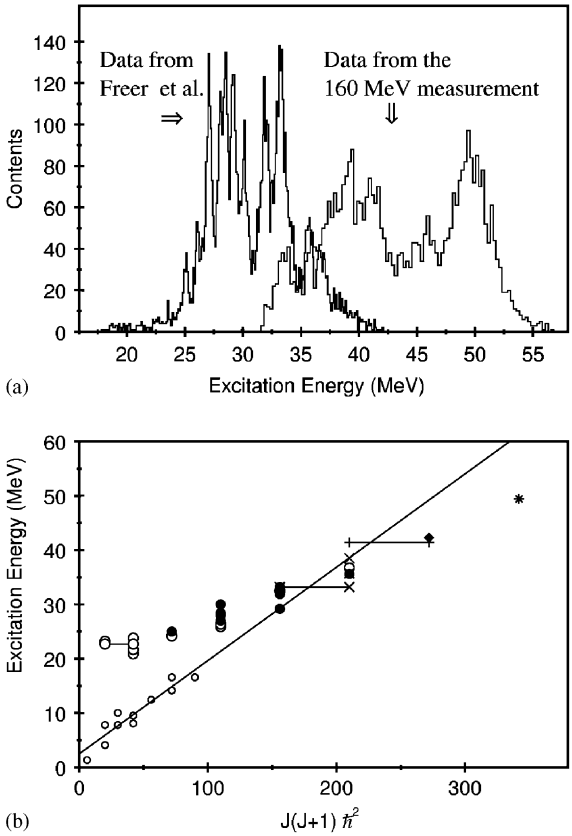

Fig. 20. High energy resonant states in ^{24}Mg observed in the ^{12}C(^{16}O,^{12}C+^{12}C)α reaction. Upper panel: the excitation energy spectrum from two measurements, at beam energies of 160 MeV [205] and 115 MeV ("Freer et al.") [106], respectively. Lower panel: the energy-spin systematics of the ^{12}C+^{12}C cluster resonances (the shallower slope) is compared with those of yrast states (small open circles) in ^{24}Mg. The latter values are extrapolated (solid line) to the cross-over with the cluster band (larger circles).

is that by virtue of the α-emission from the ^{28}Si compound nucleus, a spectrum of ^{24}Mg states are sampled in a single experimental setting. For example, the spectrum of decays of ^{24}Mg excited states sampled using this method [106,205] is shown in Fig. 20. Given the measurement of the angular distributions of the two decay products, a measure of the spins of the excited states is possible. As a consequence, it is possible to chart the systematics of the energies and spins of the states. These, broadly, possess similar characteristics to those found in the inelastic scattering measurements. However, a recent study of this reaction in which excitation energies up to 70 MeV were probed again found a termination of the excited states, but at $E_x = 49.4$ MeV, $J = 18\,\hbar$ [205]. That is to say 7 MeV and four units of spin lower than for the inelastic scattering resonances. The same resonances at lower spins and energies had been earlier observed in a measurement of the ^{12}C(^{20}Ne,^{12}C+^{12}C) α-transfer/breakup reaction [108], leading to the conclusion that the structure of the states possessed a 4p-4h excitation of ^{24}Mg. The prolate deformed shape which appears in the NS, HF and ACM calculations (with an HO configuration $[0]^4$, $[1]^{12}$, $[2]^4$, $[3]^4$) would coincide with these experimental characteristics.

Thus, it is clear that the ^{12}C+^{12}C scattering resonances and cluster structures in the ^{24}Mg nucleus have a direct relation. Similar resonance features have been observed in a large number of other heavier systems [62,63,272], e.g. in compound systems such as ^{28}Si and ^{32}S and heavier. There have been some recent attempts to extend the experimental systematics in these systems using various compound and breakup reactions [20,69,72,73,249,260,270]. We may also mention the phenomenon of anomalous large angle scattering (ALAS) which was related to resonances in $N = Z$ systems, as summarized for heavy ions by Braun–Munzinger in Ref. [49]. However, the new developments in the understanding of the nucleus–nucleus potentials have shown that these phenomena can be understood in terms of the deep potentials from double folding with the proper radial shapes (Woods–Saxon squared if parametrised) as discussed

in Section 3. The rainbow angle at low energies approaches 180° and the large deflection angles gives rise to the ALAS phenomenon. With these potentials the description of the α-particle scattering with ALAS on even $N = Z$ nuclei was possible over the whole angular range and over many energies [22,206].

5. Theoretical approaches, recent developments

5.1. Overview of microscopic cluster models

The microscopic cluster model [132,262,297,298] developed remarkably in the early 1960s with the realization of the resonating group method (RGM) [295]. The evolution of cluster physics in the two subsequent decades was strongly influenced by the RGM, but also new models such as the GCM [51,121,130] and the orthogonality condition method (OCM) [243–245], which were applied to light *p*-shell nuclei (see Refs. in [138]). These three methods are now the traditional microscopic models for the description of the inter-cluster relative motion. The most important aspect of these approaches was the treatment of the Pauli principle among the clusters and the detailed description of inter-cluster motion. The RGM and GCM are fully microscopic, while the OCM is semi-microscopic in the treatment of the Pauli blocking effects. In the RGM the dynamical coordinates of the relative wave function between clusters are treated explicitly. The practical application was limited to few-body cluster systems, because of the complications in separating the internal and relative coordinates with antisymmetrisation.

In order to apply the GCM to the cluster model, Brink adopted the many-centre cluster basis wave function, called also the Bloch–Brink wave function [51]. The Bloch–Brink wave function is written as a Slater determinant and is parameterised by the geometry of the positions of the cluster centres. The GCM calculations were performed with a superposition of the Bloch–Brink wave functions by adopting the relative distance parameters for the positions of cluster centres as the generator coordinates. In principle, the GCM based on the full model space of Bloch–Brink wave functions is equivalent to the RGM [135]. With the GCM approach it became possible to calculate, microscopically, heavy mass systems and also many-cluster systems. For many-body cluster systems, except for two-body systems, the model space of Bloch–Brink wave functions is sometimes truncated. The GCM approach with a truncated model space is rather useful to describe the states by the strong coupling picture (a viewpoint used for overlapping intrinsic states) as the GCM in the Hartree–Fock framework is, while the RGM is directly related to the weak coupling picture (based on clusters with good parity and angular momentum).

Owing to the usefulness of the wave functions, the Bloch–Brink α-cluster model has been widely applied to α-conjugate systems ($Z = N$ nuclei) since the 1960s. For the study of excited states of *sd*-shell nuclei based on the Bloch–Brink α-cluster model, the model space was often truncated within a single Bloch–Brink wave function, and some extended calculations such as unconstrained three-dimensional calculations were performed [24,201]. In addition, the cranking method [235] was applied. Finally, calculations with the variation after projection were performed in Ref. [25].

Following the recent interest in the physics of unstable nuclei, the cluster approaches have been extended and applied to the study of the cluster structure of unstable nuclei. One of the main directions in the study of unstable nuclei are the properties of valence nucleons surrounding one core. Three-body calculations with a core and valence neutrons have been achieved by many groups for the study of neutron halo in nuclei such as ^{6}He and ^{11}Li [14,15,70,71,78,269,274,276]. Baye and Descouvemont have studied cluster features of the Be-isotopes by a GCM approach with Bloch–Brink wave functions involving 2α-particles and valence neutrons. Accurate calculations for many cluster systems (in unstable *p*-shell nuclei) have been performed with the stochastic variational method (SVM) [16,220,275,276].

A cluster model with MO was found to be useful for the description of the cluster structure of neutron-rich Be isotopes [150,248,282,283]. The MO model is based on the picture of independent single particle orbitals MO in the mean field formed by a multi-centre cluster structure. With this model the systematics of cluster structure in Be isotopes with a 2α core and valence nucleons can be explained [283,288]. The explanation of molecular orbitals in the potential model is given in the relation with the two-centre shell model in Section 3.3. Microscopic calculations with the MO model, where the nucleon–nucleon interactions and the antisymmetrisation of nucleons are incorporated, were applied to Be and C isotopes [1,150,152,223,248]. Later the MO picture was extended to deal with the correlation between valence nucleons and the relative motion between clusters by Itagaki [153].

The AMD-approach [166,172,176] is a model which does not rely on the assumption of the existence of cluster cores. Though the model space for an intrinsic state is based on a Slater determinant or on a linear combination of several Slater determinants, one of the advantages of this model is a practical application to general nuclei over a wide mass range. The AMD was extensively used to describe nuclei beyond the $N = Z$ line. These calculations indicate that actually the α-particle is rather robust also in light neutron-rich nuclei.

In contrast to the exact treatment of many-nucleon systems with realistic nuclear interactions, the above-mentioned cluster calculations are regarded as "models", where effective nuclear forces are usually adopted and the model space is often truncated. We should point, here, to the recent remarkable progress of accurate many-body calculations of nuclei beyond few-body systems with realistic nuclear forces [228,300] by Quantum Monte Carlo calculations (QMC) [55,300], which have been performed for nuclei with the mass number $A \leqslant 12$. The density plots of ^{8}Be in [300] indicate that the formation of a 2α-cluster core is actually found also in such realistic calculations. Since these accurate many-body calculations need extensive numerical computation, the calculations of the excited states are still limited to very light nuclei ($A \leqslant 8$) [232].

Some features of the cluster models are given in the following sections and recent theoretical developments with applications to structure studies of unstable nuclei are highlighted.

5.2. Bloch–Brink alpha-cluster model

The Bloch–Brink (BB) model developed by Brink [51] has been applied widely to various calculations of microscopic cluster models because of the handiness of the BB wave-functions. The wave function of the n-body cluster system in the BB-model is expressed as

$$\Psi(\mathbf{S}_1, \ldots, \mathbf{S}_n) = n_0 \mathscr{A}\{\psi(C_1, \mathbf{S}_1), \ldots, \psi(C_n, \mathbf{S}_n)\}, \tag{18}$$

where $\mathscr{A}$ is the antisymmetrisation operator and C_i the ith cluster located at $\mathbf{S}_i$; the wave function is written in terms of HO model wave-functions. The nature of the cluster structures are represented by values of the spatial coordinates in the configuration $\{\mathbf{S}_1, \ldots, \mathbf{S}_n\}$. In order to describe the structure of α-conjugate systems, the BB α-cluster model, where all the clusters, $C_1, \ldots, C_n$ are assumed to be α-clusters, has been used. In the simplest case, a single BB α-cluster or its parity and/or spin projected state is used. In order to avoid the large dimensional variations, a geometric constraint on the coordinates $\{\mathbf{S}_1, \ldots, \mathbf{S}_n\}$ is sometimes imposed. In the last two decades, unconstrained three-dimensional calculations with BB alpha cluster model were performed for *sd*-shell nuclei [24,201,309]. For the study of excited states, the cranking method was applied (cranked BB α-cluster model) by Rae et al. [201,235] to systematically explore the structural properties of α-conjugate nuclei, within the *sd*- and *fp*-shells [308,309], examples of which are shown in Fig. 21. In this figure the density profiles of several nuclei from ^{16}O to ^{44}Ti are shown. Depending on the starting conditions compact states (ground states) or extremely deformed shapes for excited states are obtained, the latter showing strong clustering. The model is able to describe both cases. The stability of chain states [200] was also studied by Merchant and Rae [204].

5.3. Generator coordinate method

The GCM is a microscopic cluster model with antisymmetrisation, where the geometry and the coordinates incorporate the full finite range effects of a three-body or heavier system. The GCM is a general method to describe the collective motion in nuclei. The formalism of the GCM, with a linear combination of BB wave functions, was proposed in Ref. [51] by adopting the cluster centres for the generator coordinates. With the increase of the number of constituent clusters, the dimension of the model space of the basis BB wave function becomes huge. In case of a three (or more)-body system, it is more convenient to truncate the model space to save in computational effort.

The method has been applied to various unstable nuclei by Baye and Descouvemont [29,77–81] for bound and scattering states, the latter particularly for reactions of astrophysical interest. This method provides a good description of the deformed structures of the rotational bands related to the molecular σ- and π-orbitals in ^{9}Be, ^{10}Be and ^{11}Be, even though this model has no explicit molecular orbitals [81]. For the $K = 1/2$ bands (first excited state and ground state in ^{9}Be and ^{11}Be, respectively) the Coriolis decoupling effect, which must be observed in this two-centre structure is well reproduced, see Fig. 22. The ^{9}Be level scheme is reproduced by a mixture of (α+^{5}He) and (^{8}Be + n) configurations.

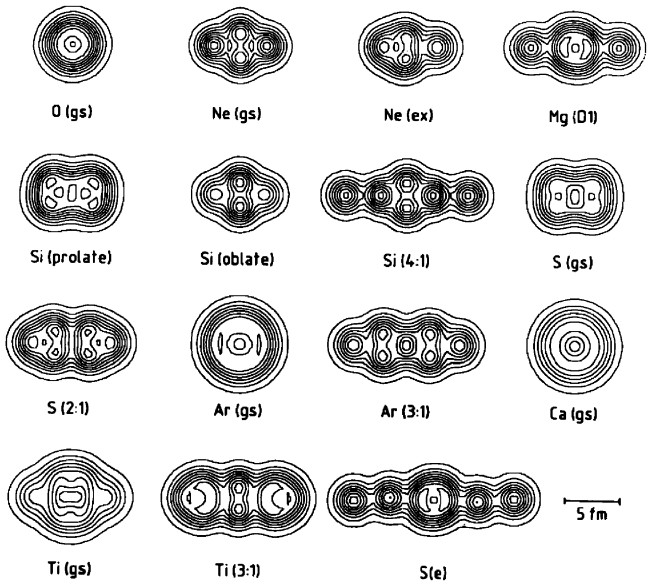

Fig. 21. Alpha-cluster model calculations for three-dimensional structures in nuclei ranging from ^{16}O to ^{44}Ti (from Ref. [308]). The figure depicts density profiles obtained for ground states and for excited states of different shapes, including extreme deformations indicated by their axis ratios (e.g. for Si and Ar).

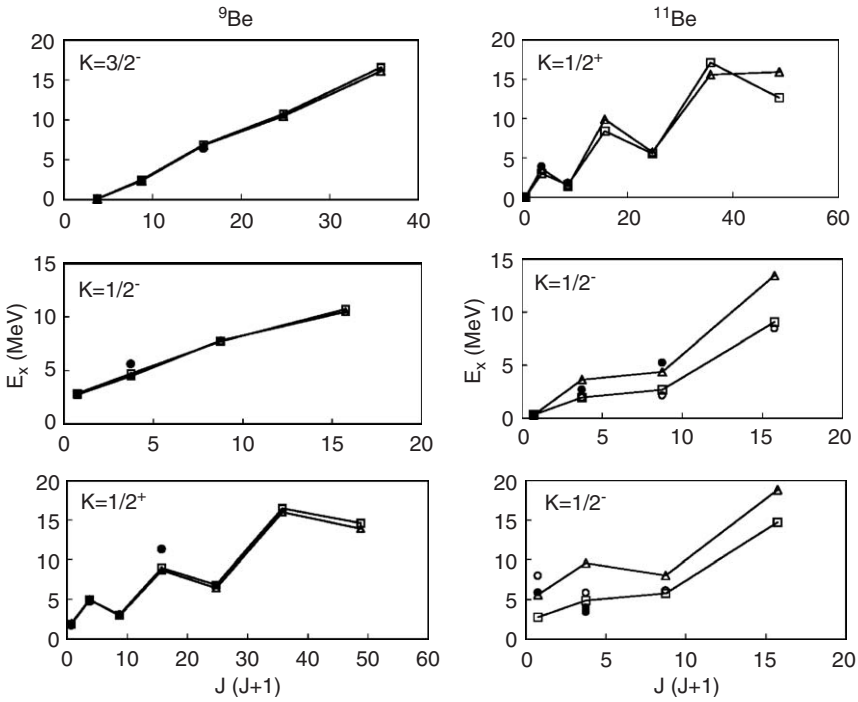

Fig. 22. The systematics of states in ^{9}Be and ^{11}Be forming rotational bands as calculated by Descouvemont et al. [81] using the generator coordinate method (GCM). The $K = 1/2$ bands show the strong Coriolis decoupling effect.

The experimental data are reviewed later in Section 6.1.1. It is important to mention here that the predicted extension of the rotational bands to higher spins awaits experimental confirmation.

The calculations presented in Fig. 22 also show other rotational bands in ^{11}Be. However, the excited $K = 3/2$ band in ^{11}Be (the data are shown later) is not obtained. This latter band should have a very pronounced molecular structure, other calculations, such as AMD [173] or the approach, which uses purely algebraic methods [127], show the molecular behaviour of this band.

Calculations using the GCM method for the $K = 1/2$ bands in ^{19}F and ^{19}Ne again find evidence [86] for the extreme Coriolis decoupling effect in multi-cluster systems. The success of this model strongly depends on the number of single-particle states used as a basis. Descouvemont and Baye [80] have also applied the GCM with coupled-channel calculations to the study of ^{12}Be, where a combination of the ^{6}He+^{6}He and ^{8}He + α channels is used. Their approach has the advantage of the explicit description of the relative inter-cluster motion, which is important to describe the excited states of weakly coupled two-body cluster systems.

Similarly, the work of Arai et al. [17,18] is based on a microscopic multi-cluster model, which is equivalent to the RGM-method, but also closely related to the GCM. Using the R-matrix approach, the molecular structures in ^{9}Be and ^{10}Be are well described, and the structure of the rotational bands in this work can also be related to the deformed shell model.

It should be recalled, in the present context, that clustering appears in two limits: (i) the strong coupling limit; as described by the Bloch–Brink method, where the clustering is described by the intrinsic structure of the composite system, (ii) the weak coupling limit; in which cluster or molecular structures result from the dynamics of the interaction.

5.4. Antisymmetrized molecular dynamics

The already mentioned AMD-method of Kanada-En'yo, Horiuchi and co-workers [139,166–170,175], which is similar to the Bloch–Brink α-cluster model, is based completely on single nucleons. It has been used extensively to describe multi-nucleon systems with $N = Z$, but in particular to nuclei beyond the $N = Z$ line. This method is very useful in describing ground and excited states of stable and unstable nuclei, in particular structures which are not easily obtained in usual shell model approaches. The model reproduces many of the experimental properties of normal nuclei: excitation energies, radii, magnetic dipole moments, electric quadrupole moments and electromagnetic transition probabilities.

The AMD-method was originally developed by Ono et al. for the study of nuclear reactions [224–226]. Later the framework of AMD was extended by Horiuchi and Kanada-En'yo et al., and applied to nuclear structure calculations [84,166–174]. The model has no assumptions regarding the preformation of clusters but is based completely on nucleon wave functions. One of the important characteristics of AMD is the flexibility of the wave function which can represent simultaneously the clustering structures of weakly bound systems as well as more shell-model like structures.

In the first, simplest, version of the AMD [166,167] the energy variation was made after the parity projection while the total-spin projection was done after the variation (variation before projection). In this way the low-lying levels of the lowest bands with positive and negative parities in the isotopes of light nuclei, Li, Be, B and C were described. For the more general study of a wide class of excited states, the AMD approach with the variation after the spin-parity projection (variation after projection) and superposition of the independent Slater determinants was used.

The AMD wave functions are given by a Slater-determinant of wave functions defined as Gaussian wave packets,

$$\Phi_{\mathrm{AMD}}(\mathbf{Z}) = \frac{1}{\sqrt{A!}}\mathscr{A}\{\varphi_1, \varphi_2, \ldots, \varphi_A\}. \tag{19}$$

The wave function is antisymmetrised, and the individual single-particle wave functions φ_i are given by

$$\varphi_i = \phi_{\mathbf{X}_i}\chi_i\tau_i, \tag{20}$$

$$\phi_{\mathbf{X}_i}(\mathbf{r}_j) \propto \exp\left\{-\nu\left(\mathbf{r}_j - \frac{\mathbf{X}_i}{\sqrt{\nu}}\right)^2\right\}, \tag{21}$$

$$\chi_i = \left(\frac{1}{2} + \xi_i\right)\chi_\uparrow + \left(\frac{1}{2} - \xi_i\right)\chi_\downarrow, \tag{22}$$

where χ_i is the intrinsic spin function parameterised by ξ_i, and τ_i is the isospin function which is up (for protons) or down (for neutrons). An AMD wave function is parameterised by the set of complex parameters, like $\mathbf{Z} \equiv \{X_{ni}, \xi_i\}(n=1-3)$ (coordinate space) and $i = 1, -, A$ (particle number). These are the independent variation parameters in the "cooling procedure". In the variational calculations the parity-projected state (or spin-parity projected state) Φ, which minimizes the energy $\mathscr{E}$ of the system, $\mathscr{E} \equiv \langle\Phi|H|\Phi\rangle/\langle\Phi|\Phi\rangle$, is searched for using the method of frictional cooling.

The parity projected eigenstate from a Slater determinant for the total wave function consists of the superpositions with the two signs:

$$\Phi(\mathbf{Z}) = (1 \pm P)\Phi_{\mathrm{AMD}}(\mathbf{Z}), \tag{23}$$

and P is a parity projection operator. For the creation of total angular momentum eigenstates, the wave function is represented by a superposition (an integral) of rotated states,

$$\Phi(\mathbf{Z}) = P^{J}_{MK'}\Phi_{\mathrm{AMD}}(\mathbf{Z}) = \int \mathrm{d}\Omega D^{*J}_{MK'}(\Omega)R(\Omega)\Phi_{\mathrm{AMD}}(\mathbf{Z}). \tag{24}$$

In the more advanced version, the energy variation using the wave function $\Phi = P^{J\pm}_{MK'}\Phi_{\mathrm{AMD}}(\mathbf{Z})$ is done after the spin-parity projection with the aforementioned method of frictional cooling [172]. In the AMD, the structures in various cluster channels are expressed by the corresponding configurations and the separation of the Gaussian centres in the coordinate space is varied. The shell-model like structures are also described by using the zero limit for the Gaussian centres. Due to the ab initio nature of the AMD, the approach is model independent, and surprisingly it gives a strong indication of the formation of clusters (examples are given later).

For each spin-parity state, the optimum wave function is obtained by energy variation for the spin-parity eigenstate ($P^{J\pm}_{MK'}\Phi_{\mathrm{AMD}(\mathbf{Z})}$) projected from the single AMD wave function($\Phi_{\mathrm{AMD}}(\mathbf{Z})$). The $\Phi_{\mathrm{AMD}}(\mathbf{Z})$ is regarded as the intrinsic state where the symmetry is spontaneously broken but is restored by the spin-parity projection operator, $P^{J\pm}_{MK'}$. Thus, the intrinsic wave function can be defined by an AMD wave function $\Phi_{\mathrm{AMD}}(\mathbf{Z})$, which is expressed by a single Slater determinant. Therefore, single particle wave function for each nucleon in the intrinsic system can be extracted as done in [84,171]. For the purpose of the present review the density distributions are very important, they can be shown separately for protons and neutrons, and for all nucleons. In the case of additional valence neutrons, the protons represent the densities and configurations of the $N = Z$ clusters, and thus the extra density of the covalent neutrons can easily by identified (see Figs. 29, 36, 52, 53), where the densities in the intrinsic states are shown. Actually, the behaviour of the valence neutrons in the molecular orbitals with the 2α core are clearly seen in the properties of the single particle wave functions of the intrinsic system of Be isotopes [171,175,176].

If we obtain the optimum AMD wave function with developed cluster structure, it is easy to analyse inter-cluster motions. As mentioned before, the AMD wave function can be regarded as an extended BB-model wave function. In a similar way to the BB model, since the centre-of-mass motion of clusters are expressed by Gaussians located at the positions given by linear combinations of X_{ni}, one can define inter-cluster distances by ignoring antisymmetrisation effects and extract inter-cluster wave functions in the AMD framework as explained in Refs. [172,175].

Finally, the choice of the effective nucleon–nucleon interaction should be mentioned. In many instances of AMD calculations, the MV1 force of Ref. [12] is used, which contains the zero-range three-body force as density dependent terms, in addition to the two-body interaction. We also refer to the method of extended fermionic molecular dynamics (FMD) by Feldmeier et al. [93], which is also an ab initio approach, very similar to AMD. In the latest work [216] the interaction is derived from a realistic nucleon–nucleon force such as the "Bonn"-potential [198], which contains a tensor force. This method has been recently applied to the structure of light $N = Z$ nuclei as well as to neutron-rich nuclei. In both approaches the clustering emerges in a model independent way as a dominant feature for many states in light nuclei.

5.5. Clusters of different size

5.5.1. Intrinsically reflection asymmetric shapes

Molecules may consist of two different species, i.e. the two clusters may be of different size, such structures are very common in atomic molecules. In the book of Herzberg [128], the nature of the rotational spectra for such structures is reviewed. The most important aspect is the broken intrinsic reflection symmetry. The system consisting of such

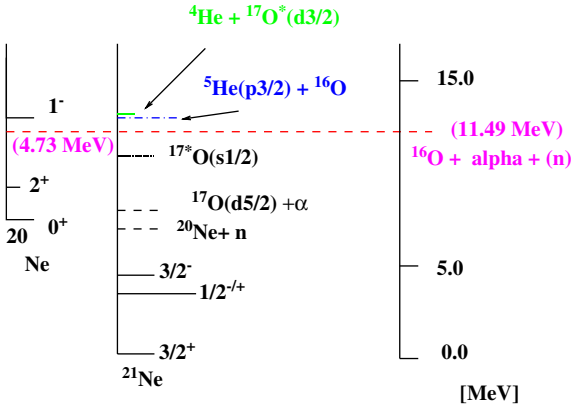

Fig. 23. The thresholds for the decomposition of neon isotopes into the $\alpha + (x\text{neutrons}) + {}^{16}\text{O}$ cluster configurations, the binding energies are aligned to the same level. Note the degeneracy of the $d_{3/2}$ and $p_{3/2}$ resonances in ^{17}O and ^{5}He, respectively, from [285].

an intrinsically asymmetric structure has no defined parity. The parity projection, which is obtained from the linear combinations of two reflected states (see Fig. 25) leads to a splitting (or doubling) of rotational bands. The feature of symmetry breaking has been explored in nuclear physics by Bohr and Mottelson [46], where this phenomenon appears with the odd multipoles of deformation, in particular with the octupole deformation [3,46,54]. Nuclear molecules formed with two different clusters show complicated structures, and their properties of broken symmetry will give rise to a splitting of rotational bands.

The relevance of the intrinsically asymmetric cluster structure of ^{20}Ne was discussed by Horiuchi and Ikeda [134] as the origin of the existence of rotational bands with $K = 0$ as a parity doublet. The circumstances in which bands with K-quantum numbers different from zero appear with both parities for each spin [46,128] is quite remarkable. This is the case of odd mass nuclei and the following section shows that ^{21}Ne provides a perfect example of these conditions [266,285].

5.5.2. *Covalent binding for asymmetric systems*

As noted in Section 3 the system α-^{16}O offers favourable conditions for the formation of molecules. Adding valence neutrons, we expect covalent molecular structures in the isotopes of neon $^{21-22}$Ne. The structure of ^{21}Ne can be discussed in a cluster model with $^{16}\text{O} + \alpha$ and one covalent neutron. For such an asymmetric case we must examine the binding energies of the neutron at the two different clusters. An important feature for molecular physics appears in this system, the properties (binding energies) of the single-particle orbits in the ground states of the neutron at the two centres can be very different as seen in Fig. 23. For the present case we have $^{5}\text{He}(p_{3/2}) + {}^{16}\text{O}$ and the $^{17}\text{O}(d_{5/2}) + \alpha$, as asymptotic configurations at larger separation. For these rather different binding energies, appear: $E_{\text{B}}(^{5}\text{He}) = -890\,\text{keV}$, which is actually a resonance, and the bound state with $E_{\text{B}}(^{17}\text{O}) = +4.14\,\text{MeV}$. This situation of different binding energies would give rise to an "ionic"—configuration with the neutron concentrated at one centre, which can give no binding for valence neutrons. For a sharing with equal amplitudes between the two centres, the binding energies of the valence particle should be equal. A remarkable coincidence occurs for the excited $d_{3/2}$-state in ^{17}O (the $d_{3/2}$-resonance), which lies at 941 keV above the neutron threshold, an energy which is almost degenerate with the $p_{3/2}$ resonance of ^{5}He (at 890 keV) and they overlap strongly due to their large widths. This particular situation is known as the quasi-resonance condition in molecular science, and is essential for the sharing of valence particles with equal amplitudes in covalent structures. Only for this case the quantal strong binding effect can be expected as explained in Ref. [95].

Based on the solutions of the single-centre shell model states of the subsystems $^{5}\text{He}(p_{3/2})$ and $^{17}\text{O}^{*}(d_{3/2})$, and a similar Hamiltonian as in Eq. (11), we can construct LCNO molecular wave functions, with the amplitudes C_i, $i = 1, 2$,

$$\Phi^{K}_{\text{LCNO}}(\mathbf{R}, \mathbf{r}_n) = \frac{N(\mathbf{R})}{\sqrt{(1 + \Delta^{K}(\mathbf{R}))}} \left[C_1 \psi_\alpha \psi^{K}_{^{16}\text{O}} \phi_n(\mathbf{r}_{n\alpha}, p_{3/2}) + (-)^{p} C_2 \psi_\alpha \psi_{^{16}\text{O}} \phi^{K}_{n}(\mathbf{r}_{n^{16}\text{O}}, d_{3/2}) \right]. \tag{25}$$

As before, for the symmetric molecules, we use $\mathbf{R}$ for the distance between the centres of the cores, and for the asymptotic bound states we use the coordinates for the neutron as, $(\mathbf{r}_{n^{16}\text{O}})$ and $(\mathbf{r}_{n\alpha})$. The non-orthogonality $\Delta(\mathbf{R})$

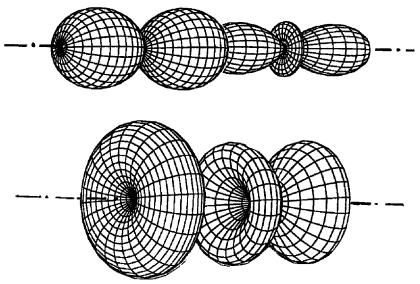

Fig. 24. Illustration of the overlap of the densities of valence neutrons in the (α + n+^{16}O) cluster configuration. The angular parts are shown for $K = 1/2$ (top) and for $K = 3/2$ (bottom), corresponding to $\sigma(m = 0)$ and $\pi(m = 1)$ orbits, respectively, are shown. On the right side is the centre for the $l = 2$, $m = 0$ (top), and for the $l = 2$, $m = 1$ (bottom), wave functions in ^{17}O. The $l = 1$, $m = 0$ (top) and $l = 1$, $m = 1$ (bottom) states in ^{5}He are on the left side, from [285].

is given by the overlap of the single-particle wave functions, with $(\mathbf{r}_{n\alpha} - \mathbf{R}) = \mathbf{r}_{n^{16}\mathrm{O}}$,

$$\Delta^K(\mathbf{R}) = \int \phi^{*K}_{p3/2}(\mathbf{r}_{n\alpha})\phi^K_{d3/2}(\mathbf{r}_{n\alpha} - \mathbf{R})\,\mathrm{d}\mathbf{r}. \tag{26}$$

The wave function in Eq. (25) corresponds to a reflection asymmetric state and no intrinsic parity is defined. As quantum numbers we have the projections on the symmetry axis: of the total angular momenta, K, and of the orbital angular momenta of the valence particle (denoted as in atomic physics by $\sigma(m = 0)$, $\pi(m = 1)$, $\delta(m = 2)$). The σ and π configurations for the present case are shown in Fig. 24. States with total spin I and good total parity Π are constructed by making the linear combinations (two signs (+) and (−) are possible) with the signature $s = (-)^{I+K}$,

$$\Psi^{I,\Pi}_{KM}(\mathbf{R}, r_n) = \left[\Phi^K_{\mathrm{LCNO}}(\mathbf{R}, r_n)D^I_{MK} + (-)^{I+K}\Phi^K_{\mathrm{LCNO}}(\mathbf{R}, r_n)D^I_{M-K}\right]. \tag{27}$$

With this construction we get the peculiar properties of rotational bands as inversion doublets. For $K = 0$ (in ^{20}Ne) the bands have rotational levels with parities which are positive or negative depending on the spin I being even or odd, respectively, called natural parity, namely bands like: 0^+, 1^-, 2^+, 3^-, etc.

The nucleus ^{20}Ne is a well known example of such an asymmetric rotating "top" already discussed above. The positive and negative parities are split in energy, due to a large probability to change between the two reflected configurations. For $K \neq 0$ we will have the case of parity doublets, also discussed by Herzberg in Ref. [128], two rotational bands with both parities for each spin. Again there is the question of the energy splitting, the energies would be degenerate for a rigid intrinsically asymmetric "top". This is the case, if the probability to change from one shape to the other is zero, observed for the odd nucleus ^{21}Ne [285] for $K = 1/2$. For this nucleus we must have two parity split doublets, namely bands for two K-values, $K = 1/2$ and 3/2. The latter represent the two orientations of the single centre orbits with $j = 3/2$. It is very instructive to look into the overlap of the individual wave-functions for these two cases shown in Fig. 24. We observe that for $K = 1/2$ the valence particles are concentrated on the axis (for the σ bond), whereas for $K = 3/2$ (π bond), they are outside of the symmetry axis (Fig. 25).

We can deduce two important conclusions: when the valence neutron remains outside the molecular axis in the case of the $\pi(m = 1)$-configuration, the energy splitting for $K = 3/2$ in ^{21}Ne is expected to be almost the same as for the $K = 0$ doublet in ^{20}Ne (this is shown in Fig. 26). In contrast, in the $\sigma(m = 0)$ configuration of the $K = 1/2$ bands in ^{21}Ne, the valence neutron has a density concentration on the axis between the two centres, thus hindering the exchange of nucleons in the cores. A vanishing of the energy splitting is expected for the case of $K = 1/2$, in accordance with the experimental level scheme, which is summarised in Fig. 26 (the relation to the ^{20}Ne bands is also shown). We note that the molecular $K = 1/2$ bands with the two parities show the strong Coriolis decoupling pattern, whereas another $K_2 = 1/2$ band, related to different structure shows no Coriolis decoupling.

The electromagnetic transitions between the two members of the $K = 3/2$ band which have different parity must be of E1-character. This has been demonstrated [266] in a recent γ-decay study of ^{21}Ne. Note that, in contrast, the corresponding study of transitions between members of the $K = 0^{+,-}$ bands in ^{20}Ne is not possible, because the odd parity states are unbound to α-decay.

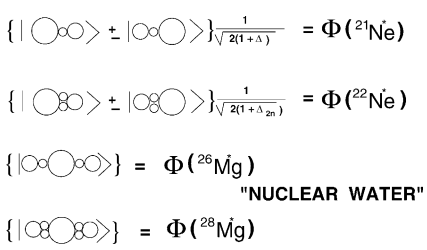

Fig. 25. Scheme for the parity projection in the proposed molecular shape isomers in neon isotopes inn the $\alpha+^{16}\mathrm{O}+X\mathrm{n}$ model. For some isotopes each K-quantum number gives rise to a parity doublet of bands with two signs of the signature. The splitting of the bands will be proportional to the probability to "tunnel" from one configuration to the other, from [285].

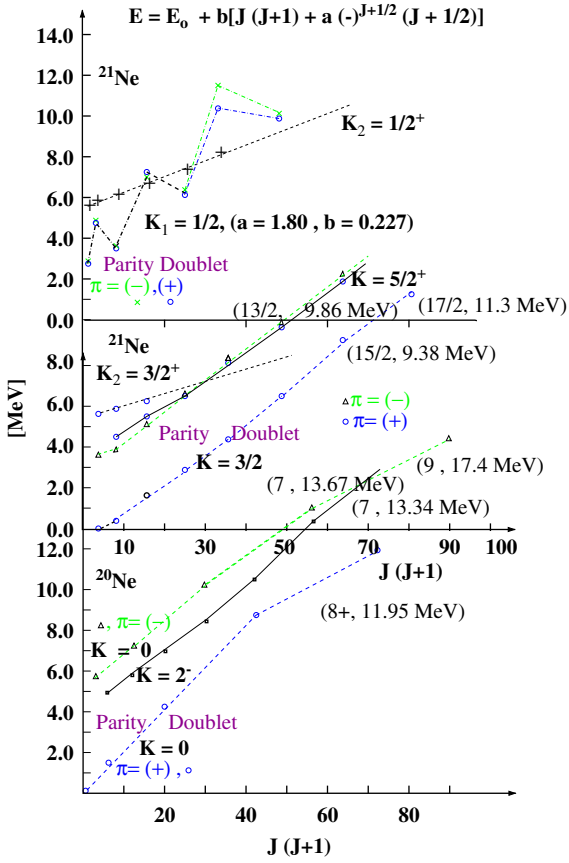

Fig. 26. Rotational bands of ^{20}Ne and ^{21}Ne showing the parity doublet structures, [285]. The energy splitting of the respective $K=0$ and $3/2$ bands in these nuclei is almost the same. However, no splitting is observed for the molecular parity doublet bands with $K=1/2$ in ^{21}Ne, which show strong Coriolis decoupling. The slopes of the shell model bands, with $K_2=1/2^+$ and $3/2^+$ are different.

Data on ^{22}Ne above the cluster decay threshold is sparse, but an experimental approach which has been demonstrated to have considerable merit [119], and is capable of measuring excitation energies, spins, widths and partial widths with great precision, is that of resonant scattering. The study of resonances in the $^{18}\mathrm{O}+\alpha$ system by Rogachev et al. [241] is shown in Fig. 27. The obvious advantage of such a reaction is that resonance cross sections are typically large (~ 100 mb) and it is possible to engineer the target-projectile system such that there is maximal structural overlap with the states of interest. The use of helium targets provides direct access to α-cluster structures. The technique relies on the deceleration of the beam through energy loosing collisions with the target material, in the present example helium gas.

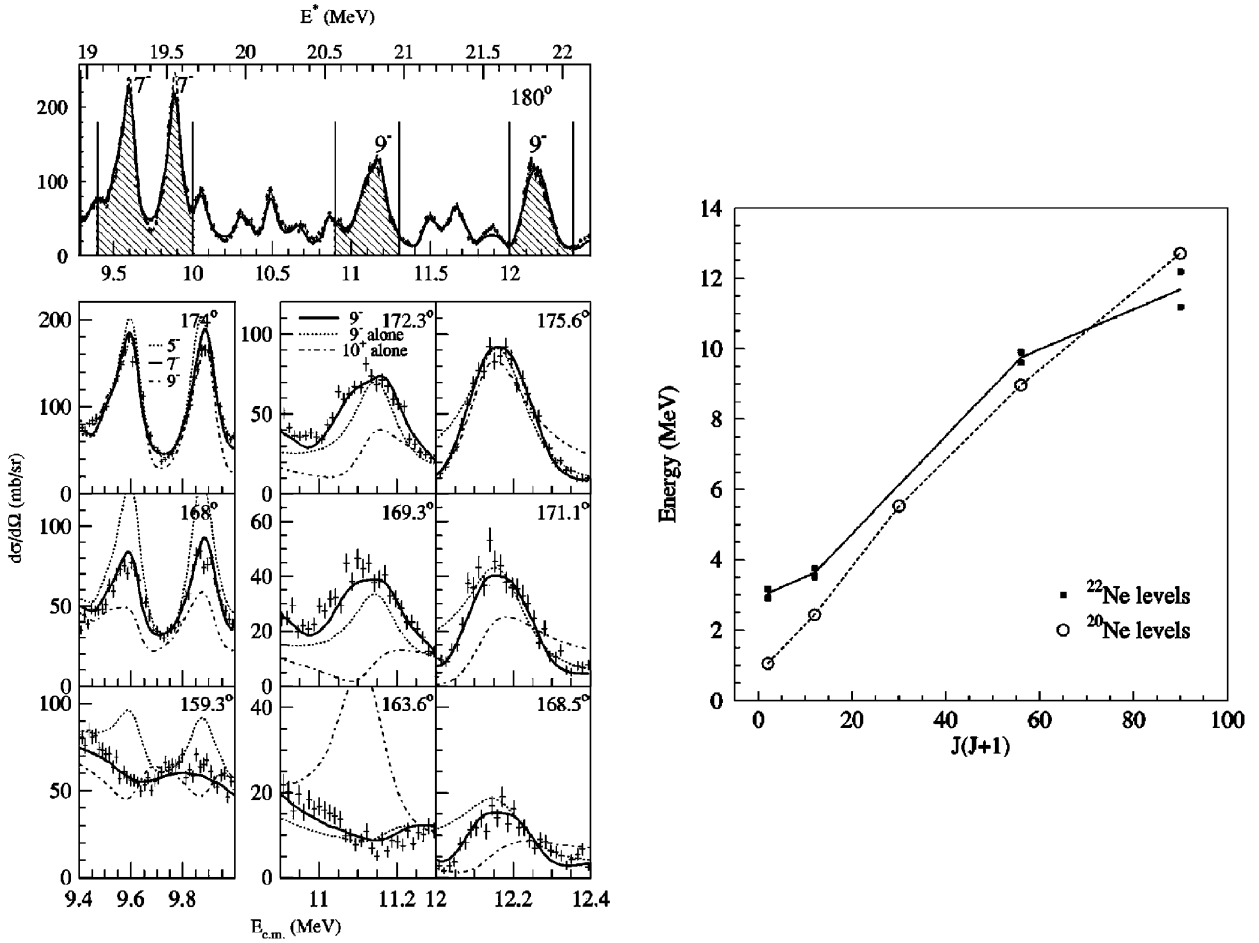

Fig. 27. Excited states of ^{22}Ne, populated in ^{18}O + α scattering. The energy above threshold is given as E_{cm}. *Left hand side*: excitation functions of resonant elastic scattering of at different cm-angles as indicated. *Middle panels*: Details of the upper part with enhanced regions, showing the fits used to determine the spin values as indicated. *Right hand side*: plots of the observed excitation energies as function of spin ($J(J+1)$) for ^{22}Ne compared to corresponding values of ^{20}Ne, from reference [241].

The centre-of-mass energy of the colliding system is thus varied in small increments tracing out an excitation function. Fig. 27 shows the energy spin systematics of the resonances observed in ^{22}Ne obtained using this technique [241]. The systematics of the energies in the bands are compared with those for ^{20}Ne and show a similar rotational trend, but for each rotational level the states are split into two components. This feature may be linked to the molecular exchange of the two neutrons, and has recently been discussed in the context of a cluster model calculation [87].

Based on these findings in particular for ^{21}Ne, but also ^{22}Ne, the occurrence of further intrinsically symmetric and asymmetric shapes for the combinations of $\alpha -$ clusters + neutrons and ^{16}O forming isotopes of Ne and Mg can be predicted. In nuclear physics ^{5}He can play the role of a binding bridge as in chemistry, where H-binding bridges are well known. Some structures are shown in Fig. 25 with their parity projection operation, others were shown in Fig. 4.

6. Experimental results for symmetric two-centre systems

6.1. The structure of beryllium isotopes—complete spectroscopy

The first deformed structure in nuclear physics with an axis ratio of 2:1 is the unbound (by 92 keV) ^{8}Be-nucleus, consisting of two α-particles in an $L = 0$ resonant state. Furthermore, it has been known for more than two decades,

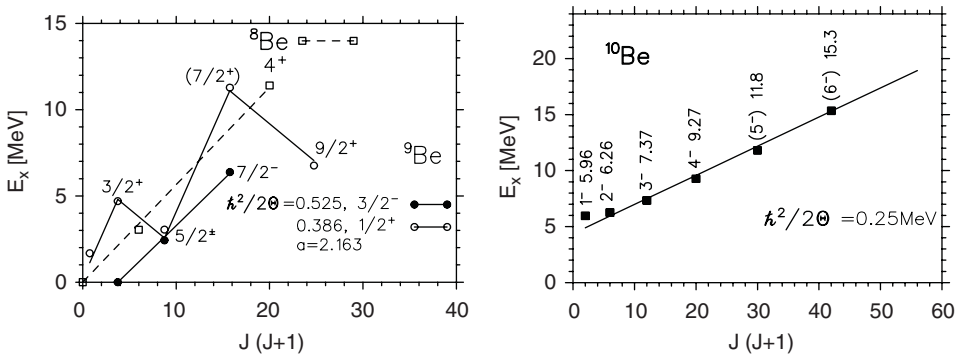

Fig. 28. Rotational bands of ^{8}Be, ^{9}Be (left panel) and ^{10}Be (right panel). The excitation energies are plotted as a function of angular momentum $J(J+1)$. The Coriolis decoupling parameter, a, for the $K=1/2$ band is indicated. From Ref. [41].

that the ground state of the ^{9}Be nucleus can be explained by covalent molecular binding, where two α-particles are bound by the $p_{3/2}$ valence neutron (Fig. 28).

This was determined by molecular orbital models based on the Born–Oppenheimer approximation [98,223,248] where terms in the ratio [(mass of valence particle)/(mass of the core)] are dropped. In 1981, Seya et al. [248] also suggested the existence of the α-cluster cores in neutron-rich Be isotopes bound by neutron molecular orbitals. With modern computing techniques such approximations are not necessary, the most recent calculations are based on the GCM which take full account of all terms in an R-matrix approach [17,18]. The appearance of the two α-cluster cores in neutron-rich Be isotopes has recently been treated in many theoretical studies [80,81,84,150–152,156,166,167,171,173–175,283] as the model case for the nuclear covalent molecules. Actually, these studies suggest that all the low-lying states in neutron-rich Be isotopes can be understood in the molecular orbital picture, where the valence neutrons move in the molecular orbitals around the 2α core.

The experimental level structures of $^{9-12}$Be have been established with a variety of light ion induced single- and multi-nucleon transfer reactions. These experimental results from different sources have been compiled with regard to the aspect of covalent molecular binding, and the corresponding rotational bands were identified in 1996/1997 by von Oertzen [282,283], which at that time was met with great scepticism. The method of molecular orbitals has been applied quite successfully also to ^{10}Be (see the references cited in [283]). The approach used in these studies can be considered to be complete spectroscopy. Using all available experimental data, all the excited states must be grouped either into single-particle states or into rotational bands of the deformed states. For ^{9}Be the deformed shell model is still an alternative useful framework, however, in $^{9-11}$Be the molecular approach gives a complete description of all the states as cluster states. In ^{9}Be there are higher lying states whose spin parity assignment is experimentally still not fixed, however, the number of identified states in this nucleus makes the arrangement into rotational bands quite compelling. As already noted, the $p_{3/2}$ orbit of the valence neutron in the separated fragment channel, in ^{5}He, can give rise to bands with the K-quantum numbers, $K=3/2$ and $1/2$, respectively.

The information on the bands is illustrated in Figs. 28 and 29 for $^{9-10}$Be, and for ^{11}Be in Figs. 30, 32 and 33, respectively. In Fig. 29 the level scheme for ^{10}Be is compared with the results of AMD-calculations. There, the densities of the valence neutrons are shown, they give a striking confirmation of the concept of covalent molecular structure. In the following sections we examine the experimental evidence for such a molecular structure in the beryllium isotopes. We note that the parameterization for the energies $E(J)$ of the rotational bands (including the Coriolis decoupling parameter a: for $K=1/2$ bands) is given by

$$E(J)=\frac{\hbar^2}{2\Theta}[J(J+1)+(-)^{J+1/2}a(J+1/2)], \tag{28}$$

where Θ is the moment of inertia, and J is the angular momentum.

6.1.1. The structure of $^{9-11}$Be

^{9}Be: Inspecting the correlation diagram (Fig. 15) and starting from large distances with the splitting of the molecular orbitals, we note, that close to the minimum of the α–α potential the $K=1/2^{+}-(\sigma)$ orbit crosses the $K=3/2^{-}-(\pi)$

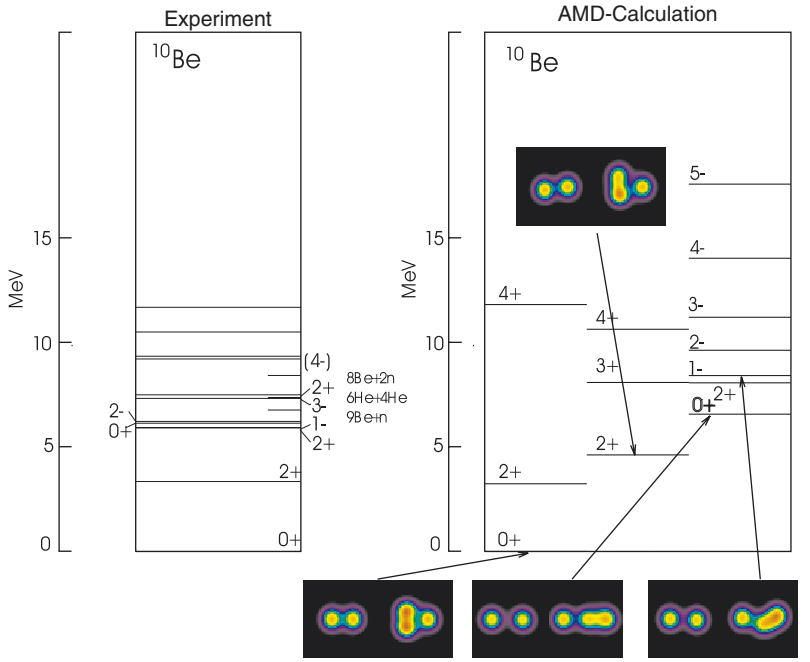

Fig. 29. Left side: experimental level scheme of ^{10}Be, and, Right side: that calculated with the spin parity projected AMD model [170]. The density plots of the intrinsic states are shown in special panels: for protons on the left side of each plot and for neutrons on the right side, respectively. The proton densities represent the positions of the α-particles. The neutron densities show for the ground state a density distribution characteristic of π-binding. The higher lying 0_2^+ state is well reproduced with a larger α–α distance (seen by the density of protons) as compared to the ground state, it shows the σ^2 configuration for the neutrons. The density of the 1^- state shows a mixture of σ–π orbitals with a distorted neutron density.

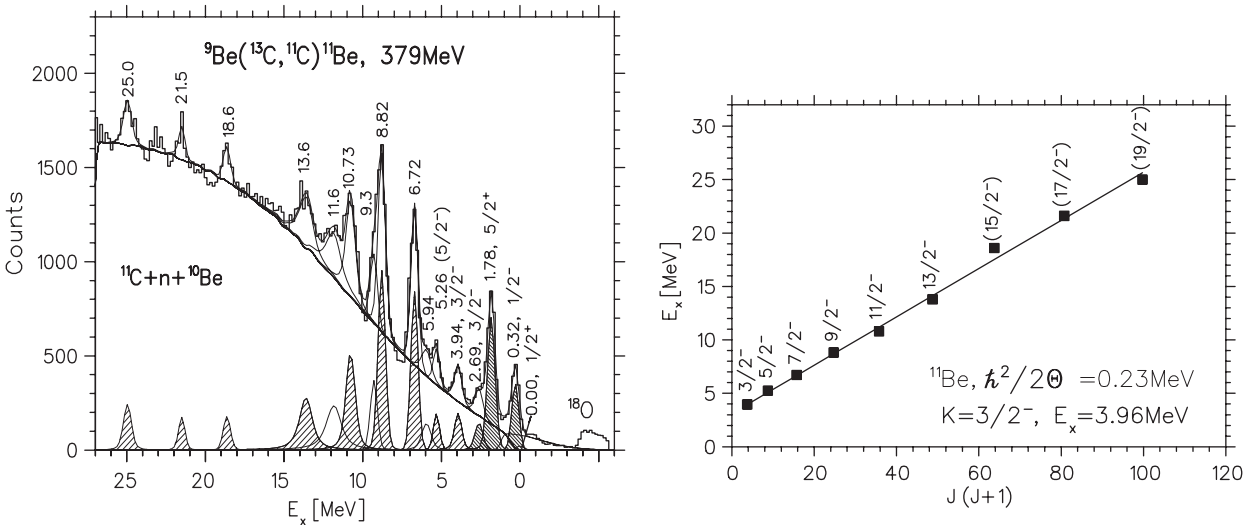

Fig. 30. Left panel: spectrum of the ^{9}Be(^{13}C, ^{11}C) reaction measured at high incident energy. Members of the $K = 3/2^-$ band are strongly populated and are indicated by shading. Right panel: excitation energies of states of the $K = 3/2^-$ band with tentatively assigned spins (for the higher lying states), plotted as function of $J(J + 1)$, from [39,40].

orbit and becomes the lowest state. At even smaller distances the $K = 1/2^+ - (\sigma)$ orbit rises up in energy as it merges into the $K = 1/2$ Nilsson orbit of the deformed united nucleus. The sequence of excited states in ^{9}Be, shown in Fig. 28, is therefore exactly predicted by the two-centre diagram, namely two binding configurations with $J = 3/2^-, 1/2^+$, and their rotational excitations. For the anti-binding states at higher energy with $K = 3/2^+, 1/2^-$, no rotational bands have been identified, because of their expected large widths.

The molecular exchange of a neutron between the α-cores ensures that the intrinsic state is formed, i.e. the clustering appears in the strong coupling limit.

^{10}Be: Again, according to the correlation diagram of Fig. 15, the structure of the states is determined by the evolution of the π and σ orbitals as a function of distance. The ground state of ^{10}Be can be interpreted as a $(\pi)^2$ configuration, whereas the excited 0_2^+ at 6.179 MeV, is associated with the $(\sigma)^2$ configuration, which attains its maximum binding energy at larger core-core distances (see Fig. 29). Similarly for the mixed σ-π-orbit configuration, forming the $K = 1^-$ band, a larger moment of inertia is expected. Indeed, in ^{10}Be with two valence neutrons, all states can completely be explained as rotational excitations of the molecular basis states. The level scheme and the behavior of the two valence neutrons in ^{10}Be have been described also in the MO model [150] and a $(\alpha + \alpha + n + n)$ cluster model calculation [160,161,220].

However, there remain some open problems, particularly regarding the structure of ^{10}Be above the cluster decay threshold. It is known from measurements of proton inelastic scattering that the nucleus is deformed. For example a deformation length of 1.84–1.99 fm is required to describe the 2^+ excitation probability in inelastic scattering with protons [23] (compared to 1.61–2.13 fm for ^{9}Be [124,231,242]), thus it is not unreasonable to assume that there should be a 4^+ member of the ground state band. Similarly, corresponding to the second 0^+ state at 6.179 MeV, a possible 2^+ member of a rotational band is the state at 7.542 MeV, and the 4^+ members of both of these bands would lie in the excitation energy region of 10 to 12 MeV.

The excitation energy spectrum for excited states in ^{10}Be populated using the triton transfer reactions ^{7}Li(^{7}Li, ^{10}Be$^*\rightarrow{}^4$He+^{6}He)α and also the reaction ^{6}Li(^{7}Li, ^{10}Be$^*\rightarrow{}^4$He+^{6}He)^{3}He has been measured at a beam energy of 34 MeV [74]. The result is shown in Fig. 31. This measurement followed on from an earlier one by Soić et al. [252], who had studied the ^{7}Li(^{7}Li, ^{10}Be$^*\rightarrow{}^4$He+^{6}He)α reaction in the region above the α-decay threshold (7.4 MeV). One of the outstanding problems in understanding the structure of ^{10}Be is the determination of the rotational properties. In the measurements of Soić et al. [252] three states could be strongly observed, and a comparison between the ^{4}He+^{6}He and n+^{9}Be decay channels suggested that the 9.64 MeV (2^+) state decayed into both partitions, probably partially suppressed by the Coulomb and centrifugal barriers for the α-decay. On the other hand, the 10.2 MeV state decayed strongly by α-emission and was absent in the neutron decay channel, whilst the opposite was true for the 10.57 MeV state. Taken at face value, this latter information would have indicated that the 10.2 MeV state possessed some cluster content possibly linking it to the 0_2^+ state at 6.179 MeV, and the 10.57 MeV state as the 4^+ member of the ground state band. However, the measurements of Curtis et al. found the 9.6 MeV state to possess a spin and parity of 2^+, the 10.2 MeV peak (10.15 in their measurements) was assigned as $J^\pi = 3^-$. Recent measurements of inelastic scattering of ^{10}Be from a ^{12}C target [5] and neutron transfer [21] on to ^{9}Be found no evidence for the decay of any other states which might be linked to the ground state band. The failure to find 4^+ members of the ground state band (predicted in Refs. [18,81] but not in Ref. [127]) and of the excited band (predicted in all references), remains a puzzle. Measurements of the ^{10}Be(^{14}C, ^{10}Be*)^{14}C [76] and ^{7}Li(^{7}Li, ^{10}Be*) [75] reactions have also been reported. Most recent results by Milin et al. [210], however, suggest a 4^+-state at 10.2 MeV as a member of the second 0_2^+ band. This has been confirmed in measurements of ^{6}He+^{4}He resonant scattering [110].

The study of the rotational systematics of states above the α-decay threshold using breakup reactions provides an insight into structural properties of ^{10}Be. In order to probe the cluster content of the states, measurements of the partial decay widths are essential. Measurements of the α-decay widths [196] of the two 2^+ states at 7.542 and 9.6 MeV suggest that the lower energy state has an enhanced α-decay width compared to that for the 9.6 MeV state. This would suggest that the 0_2^+ band (including the 7.542 MeV state) does indeed possesses a marked cluster structure, in contrast to that of the 9.6 MeV state. The measurement of the α-decay width of the 10.15 MeV (4^+) state [110], clearly demonstrates that the state has an enhanced α-width also. Thus, this would clearly demonstrate that the 6.179 (0^+), 7.542 (2^+) and 10.15 MeV (4^+) states form a rotational band with two σ neutrons.

^{11}Be: For ^{11}Be it was possible to extend the rotational band seen in two-neutron transfer of the (t,p) reaction [6] to higher spins by the use of the ^{9}Be(^{13}C, ^{11}C) reaction at 29 MeV/nucleon measured at HMI-Berlin with the high

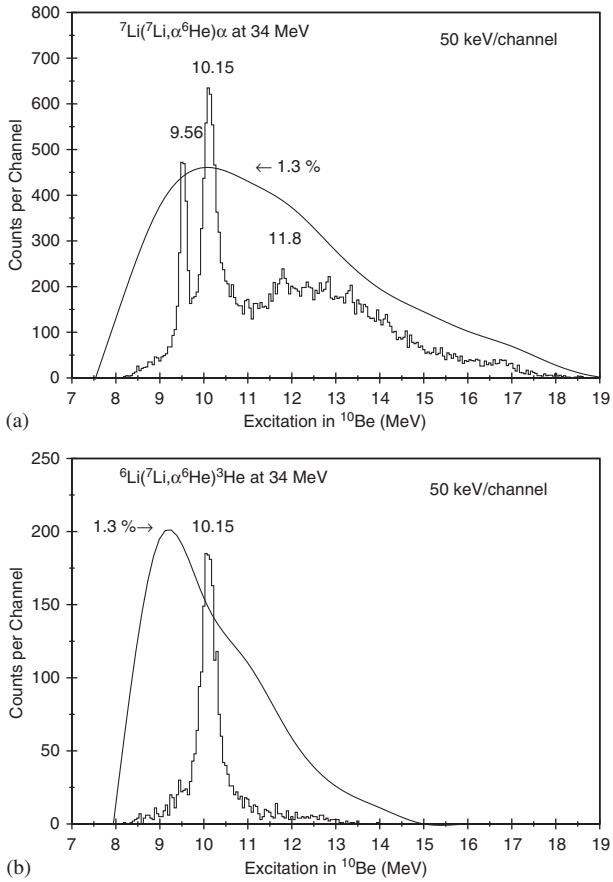

Fig. 31. Excited states in ^{10}Be reconstructed from the invariant mass of the fragments emitted in the cited reactions, (a) ^{7}Li(^{7}Li, ^{10}Be*→^{4}He+^{6}He)α and, (b) in ^{6}Li(^{7}Li, ^{10}Be*→^{4}He+^{6}He)^{3}He, from [74].

resolution magnetic Q3D-spectrometer. Two points are noteworthy in the experimental observations, see Figs. 28, 30 and 32: (i) the large moments of inertia of the excited band in ^{11}Be ($K = 3/2^{-}$) similar to the bands ^{10}Be ($K = 0_2^+$ and 1^-), due to the occupation of the σ-orbit with neutrons; (ii) the very pronounced Coriolis decoupling pattern for the $K = 1/2^+$ band in ^{9}Be, which is also observed with the same strength for the $K = 1/2$ band in ^{11}Be, see [282]. As explained in Sections 3.4 and 5.3, the Coriolis coupling and in particular the decoupling for $K = 1/2$ are characteristic of a strongly deformed molecular structure with two centres. Once again, microscopic cluster calculations of Descouvemont (see Fig. 22) using the GCM-method reproduce this decoupling effect [79,81] (Fig. 33).

Using a large variety of reactions in a systematic study of the structure of beryllium isotopes [39–42,283] rotational bands of ^{9}Be, ^{10}Be and ^{11}Be have been obtained. For the interpretation of the moments of inertia a very large distance between the two α-clusters is needed and these can therefore be characterised as molecular structures of the σ- and π-orbitals. The distinction between valence neutrons and the nucleons in the cores is possible due to their very large difference in binding energies. This is also manifested in Fig. 29, where the density plots were shown together with the level scheme of ^{10}Be. With two neutrons in a π-orbit the "downward" slope of these orbits in the correlation diagram (Fig. 15) favors a smaller distance between the two α-cores for the ground state of ^{10}Be as compared to the excited 0_2^+ which has a less compact shape. The AMD calculations for these distances confirm these expectations as summarised in Fig. 34.

In the AMD calculations the distance between the proton distributions, representing the α-clusters, allows the separation of the α-particles to be determined. Their distance in the ground state is smaller than in the two excited

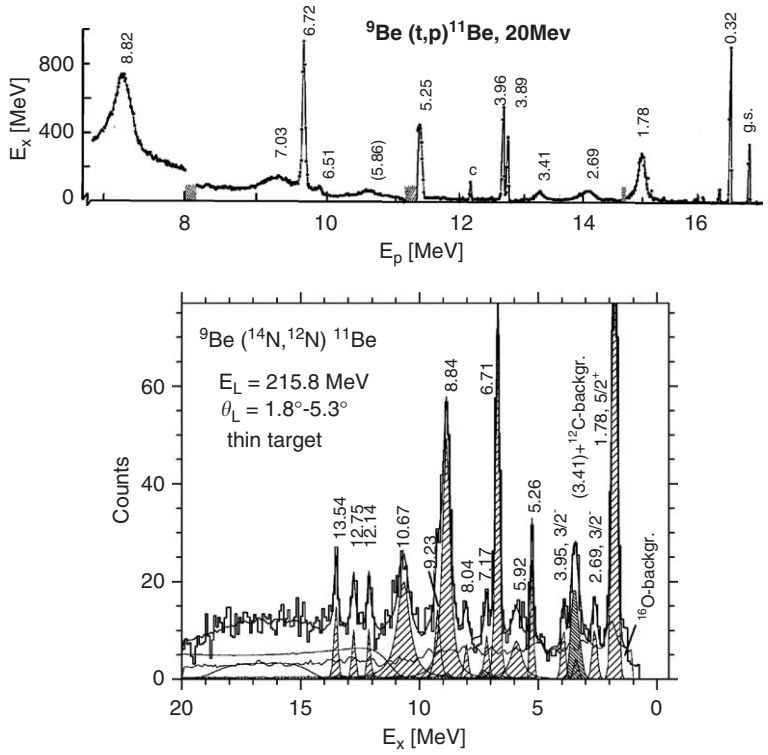

Fig. 32. Population of states in ^{11}Be in two-neutron transfer on ^{9}Be. Upper panel: in ^{9}Be(t,p), from [6]. Lower panel: in the ^{9}Be(^{14}N,^{12}N) reaction [41], (see also Fig. 30). Note the rather small widths of states of the $K = 3/2^-$ band starting at 3.95 MeV, well above the neutron threshold of 0.5 MeV.

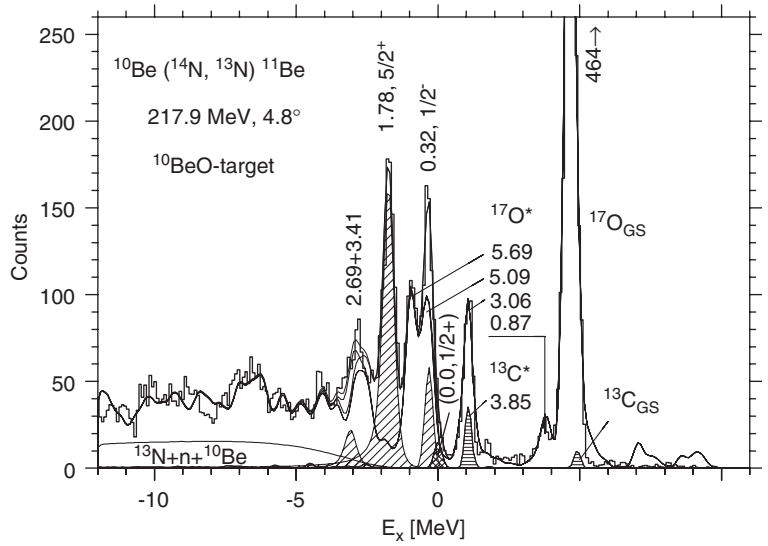

Fig. 33. Excitation of states in ^{11}Be in a one-neutron transfer reaction on ^{10}Be. Note the absence of the states of the $K = 3/2^-$ band, which in contrast is observed very prominently in Figs. 30 and 32, from [41].

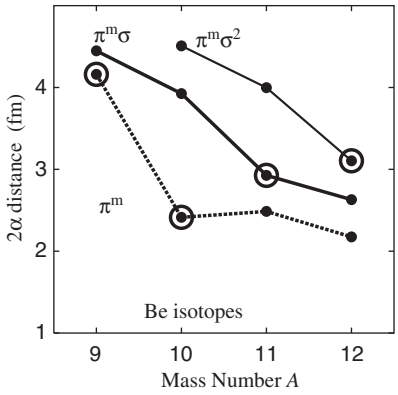

Fig. 34. Evolution of the distance between the two α-particles for states in $^{9-12}$Be as a function of neutron number (from AMD calculations [176]). The three lines connect states with distinct combinations of σ and π-neutrons; the encircled points represent the ground states.

states. The result for the densities provide striking confirmation of the molecular orbital picture. A survey of the structure in beryllium isotopes is given in Fig. 36, where the intrinsic densities before spin and parity projections are shown.

An interesting problem arises within the different model descriptions regarding the band terminations at higher spin. In the work based on the cluster model [81] the rotational bands terminate at higher spins for the $K = 1/2$ and $3/2$ bands in ^{9}Be and ^{11}Be, as compared to the "microscopic algebraic" model of Hess et al. [127], where the Pauli blocking enters for the overlap of the valence nucleons with the nucleons in the α-particles of ^{8}Be. If the 4^+ state in ^{8}Be is interpreted as a cluster state, where the spin comes from the relative motion of well separated clusters, we can indeed with this value reach the higher spin values, namely $11/2^-$ in ^{9}Be, the spin of 7^- in ^{10}Be [11/2 + 5/2)], and the value of $19/2^-$ in ^{11}Be. The latter by the vector addition of the individual spins with $[4 + 3/2 + 2((5/2) = 4)] = 19/2$, but a maximum value of only 17/2 in ^{11}Be is reached in the work of Hess et al. [127]. In the work of Descouvemont [81], the continuation of the $K = 1/2^+$ band in ^{9}Be is extended to spins of $11/2^+$ and $13/2^+$, which are predicted as resonances at 16 MeV and 14 MeV, respectively. Also the $K = 3/2^-$ band in ^{9}Be is calculated to terminate at 13/2 (see Fig. 22). The $K = 1/2^-$ band is also predicted with rather broad states up to higher spins (7/2), but does not exhibit the Coriolis decoupling pattern, as observed in the $K = 1/2^+$ band.

6.1.2. The structure of the isotopes $^{12-14}$Be

The evolution of the shapes (densities of valence particles) of the beryllium isotopes is well illustrated in the systematic AMD calculations (Fig. 36). From these it is found that the distance between the two α-particles decreases with increasing neutron number in the ground states (as shown in Fig. 34). Experimental work on excited states of the heavier isotopes is rather scarce. The binding energies and the thresholds for cluster decay do not decrease although the separation energy of the last neutron decreases. Thus the ^{13}Be nucleus is unbound in its ground state by 2.01 MeV [227]. The ^{14}Be nucleus is bound (a two-neutron Borromean system [199]) and the threshold for the $4n + 2\alpha$ decomposition is 12.1 MeV. Theoretical studies of the $^{12-14}$Be isotopes are mainly in the form of the GCM model of Descouvemont [80] and by Kanada-En'yo et al. using the AMD approach [174,175].

^{12}Be: The ground state of this nucleus is particle stable, the threshold energies for the separation of one neutron (^{11}Be + 1n) are at 3.170 MeV and for two neutrons (^{10}Be + 2n) at 3.673 MeV, this small difference is due to the very small binding in ^{11}Be (of only 0.503 MeV), which also gives some information on the pairing energy. The very high two neutron binding energy in ^{10}Be relative to the value observed in ^{12}Be is explained by a compression of the two α-particles which gives an energy gain for ^{10}Be. However, the repulsive properties of the potential between the two α-particles does not allow a further strong decrease of the α–α distance in ^{12}Be.

Experimental results on excited states of ^{12}Be were first obtained by ^{10}Be(t,p) reactions [9,100], then subsequently by multi-nucleon transfer reactions [42]. States above the cluster decay threshold are also known from several studies with ^{12}Be beams [107,185,246].

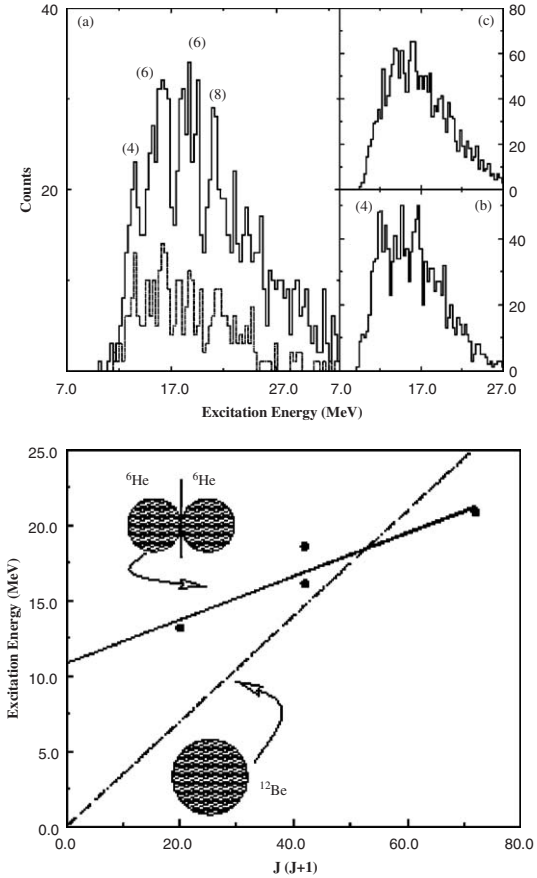

Fig. 35. Excited states of ^{12}Be populated via inelastic scattering using hydrogen and carbon targets. The upper part shows the reconstructed ^{12}Be excitation energy spectra: (a) ^{12}Be→^{6}He+^{6}He for proton plus carbon recoils; (b) ^{12}Be→^{8}He+^{4}He for carbon recoils and (c) ^{12}Be→^{8}He+^{4}He for proton recoils. The dotted histogram in (a) represents ^{6}He+^{6}He decay events identified with carbon recoils. The lower part shows the plot of the moment of inertia for the observed structures from reference [107].

The ^{6}He+^{6}He cluster structure of the nucleus ^{12}Be was studied via inelastic breakup of a ^{12}Be beam produced via the fragmentation at GANIL. The secondary ^{12}Be beam was inelastically scattered at 378 MeV from hydrogen and carbon targets and excited above the ^{6}He+^{6}He decay threshold. The decay products were detected in an array of charged-particle telescopes capable of measurements of the energy, charge, mass and the emission angle of each of the detected decay products. The excitation energy spectrum for the reconstructed coincidences is shown in Fig. 35, and shows a spectrum of states which extends from 12 to 25 MeV [107]. Given the decay channel consists of identical bosons this restricts the observation to states with even spin and natural parity. The angular correlations, although limited in statistics, did appear to show a sequence of states which increased in spin with increasing excitation energy. The energy-spin systematics are shown in Fig. 35b. These indicate the presence of a rotational band whose moment of inertia is consistent with two touching ^{6}He nuclei, and thus possible evidence of such cluster structures in ^{12}Be. More recent studies at RIKEN [246] using a ^{14}Be secondary beam find evidence for a series of states in the nucleus ^{14}Be which decay into ^{6}He+^{8}He, and following the two-neutron removal process the breakup of states in ^{12}Be into two ^{6}He nuclei is observed, which also shows the candidates for the low spin 0^+ and 2^+ states observed in earlier measurements [107].

The second 0_2^+ state in ^{12}Be at 2.24 MeV is very interesting, it is an isomeric state with a lifetime of 50 ns $< \tau <$ 11 μs [250]. In the AMD approach the ground state is considered to be the deformed (molecular) state, which forms a rotational band, and the excited 0_2^+ is considered to be the "shell-model" state. The extreme retardation of the γ-transition is in part related to the large difference in shape of the two 0^+ states. Inspecting the spectra of the ^{10}Be(t,p) reaction [9,100]

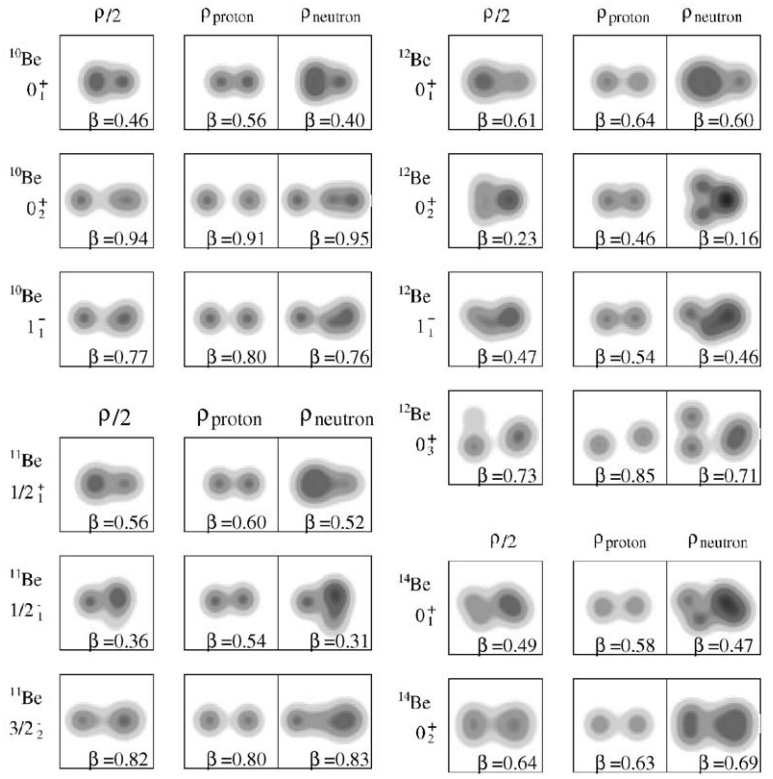

Fig. 36. Density distributions of the intrinsic states of ^{10}Be, ^{11}Be, ^{12}Be, and ^{14}Be obtained by spin-parity projected AMD calculations, from Ref. [176]. The integrated densities of matter, proton and neutron are presented in the left, middle and right panels. The box size is 10 fm.

a very weak peak at 2.235 MeV is observed, which is the excitation energy of the 0^+_2 state. In addition a $K = 1^-$ band was predicted by Kanada-En'yo [175]. This state is now confirmed by the observation of an E1 transition at a very low excitation energy of 2.71 MeV [163]. Another 1^- state predicted by Descouvemont [80] as a member of a $K = 0^-$ band is expected at higher excitation energy. From the AMD calculations it is shown that the 0^+_1, 0^+_2 and 1^-_1 have very different intrinsic shapes formed by neutrons in different covalent orbits (see Fig. 36).

^{13}Be: This nucleus is unbound [227] in its ground state, which is expected to have a $s_{1/2}$ configuration, but it has not been clearly identified. The excitation energy spectrum was obtained for the first time in the double charge exchange [227] reaction ^{13}C(^{14}C,^{14}O)^{13}Be, and a strong resonance was found which is expected to be a $d_{5/2}$ configuration and unbound by 2.01 MeV; the ground state could be a $s_{1/2}$- or a $p_{1/2}$-resonance. Later experiments [33] confirmed the strong resonance at 2.01 MeV, but an additional structure unbound by 0.8 MeV was observed in this spectrum. The latter was assigned as the "ground state" with a tentative $p_{1/2}$ assignment. A measurement of the ^{10}Be(^{14}C,^{12}Be) reaction [76] failed to find any evidence for the break-up of ^{12}Be to ^{6}He+^{6}He due to the rather small cross section for populating the states.

^{14}Be: With the ^{13}Be nucleus being unbound the binding energy of ^{14}Be is only 1.12 MeV for two neutrons. This nucleus is one of the best cases of a two-neutron halo structure (or Borromean nucleus). This is also confirmed by the large value of the measured rms-radius [263,195] of (3.11 ± 038 fm), which is considerably larger than the value for ^{12}Be. Shell model calculations using the neutron–neutron pairing have been performed to reproduce the 2n-binding energy [189]. In such an analysis the structure of ^{13}Be enters directly, and the binding energy is correctly reproduced, if in ^{13}Be the lowest state is an unbound $p_{1/2}$ state at 0.3 MeV. Rather relevant to the present discussion is the recent theoretical study of $^{13-14}$Be [264], which shows that the core, here ^{12}Be, must be deformed in order to explain the structure and binding energies.

Break-up measurements of ^{14}Be, following inelastic excitation of the ^{14}Be projectile, into ^{6}He+^{8}He again indicate that there may exist excited states with cluster and molecular structure above the cluster decay threshold [246].

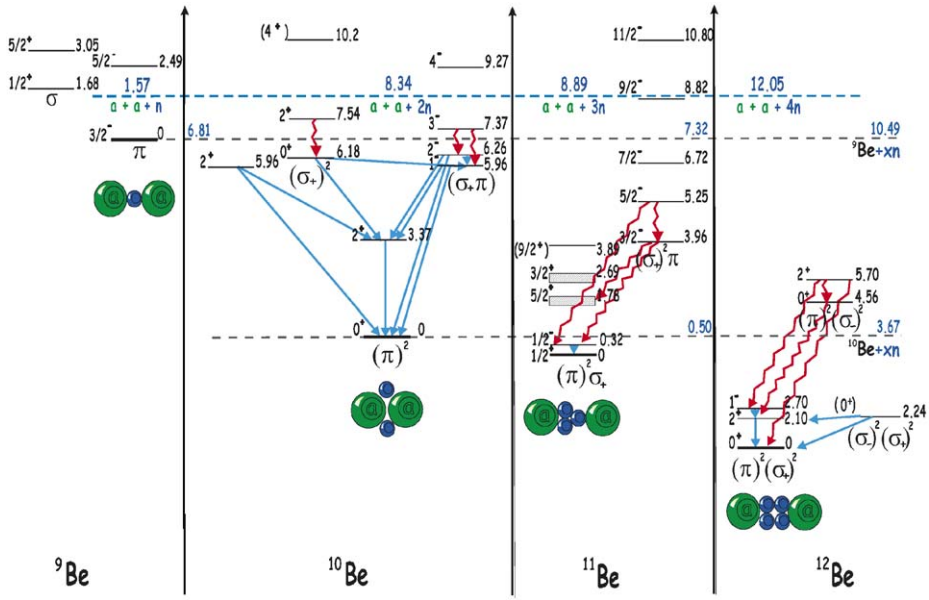

Fig. 37. Structure of states in $^{9-12}$Be with their molecular configurations and proposed γ-transitions. Wavy lines are for transitions across thresholds, straight lines are used to mark observed transitions.

However, the energy-spin systematics of these resonant states remains to be characterised. Using the AMD-approach [174] the structure of excited bands with $K^\pi = 0_2^+$ and with $K^\pi = 2^+$ is predicted to be due to a clustering with ^{8}He+^{6}He (Fig. 36). The same substructure is predicted in ^{15}B. We may thus expect interesting rotational bands in these nuclei.

6.2. *Electromagnetic decay properties in beryllium isotopes*

Electromagnetic transition probabilities contain direct information on the intrinsic structure of nuclear states. In many theoretical models the quadrupole deformation and the electromagnetic decay properties of the beryllium isotopes have been calculated. However, in many of these isotopes, and other light nuclei, the particle thresholds are rather low. Hence, only a few particle stable states can be found, for which electromagnetic decays can be studied, thus direct observations of γ-decays are scarce. In the future, in many of the cases the electromagnetic excitation via electron scattering can be measured. However, these studies will have to wait until electron scattering can be performed in colliding beam experiments as those planned for the new radioactive beam facilities at GSI, Darmstadt, (Germany) or RIKEN (Japan).

There are a few γ-decay studies of the beryllium isotopes which give very important information on the structure of the exited states. In Fig. 37 we present an overview of the structure of the isotopes $^{9-12}$Be with the γ-transitions observed or, alternatively, their unobserved branches (marked by wavy lines), which may be considered in future experiments.

Some of the observed and predicted γ-decay properties are compiled in Table 2. There are a few unique observations, which are directly connected to the molecular structure of the levels in the Be-isotopes. Most noteworthy are the long life times of the excited "isomeric" 0^+ states in ^{10}Be and in ^{12}Be. In the case of ^{10}Be, the 0_2^+ state (which is the band head of a very deformed band with two covalent neutrons in a (σ)-orbit), has the rather long life time of 1.1 ps as compared to the expected femtoseconds for intra-band transitions. This fact is explained by the large rearrangements needed in order to switch from a $(\sigma)^2$ configuration to a $(\pi)^2$ configuration in the lower lying states. Similarly, the even more extremely long life time of > 50 ns observed for the 0_2^+ state in ^{12}Be can be explained by its molecular orbital configuration. In this case a rearrangement of the four valence neutrons is needed for the transition, from (π^4) into $(\pi^2\sigma^2)$, again with a larger change in deformation. The different structure of the 0_1^+ and 0_2^+ states in ^{12}Be is clearly seen in the AMD calculations of Kanada-En'yo and Horiuchi [175] and the density profiles as shown in Fig. 36.

Table 2
Known and predicted γ-ray decays and transition probabilities in the isotopes ^{10,11,12}Be

	E_γ [MeV]	$B(\lambda_i)$	τ_γ	$J\pi_i$	$J\pi_f$	Γ_γ [eV]	$\Gamma_{\rm tot}$ [eV]	$\Gamma_\gamma/\Gamma_{\rm tot}$	λ_i
^{10}Be	3.367	(10.5 ± 1.2)	$(180^{+}_{-}17)$fs	2^+_1	0^+_1(g.s)	$(3.66^{+}_{-}0.73) \times 10^{-3}$		1	E2
	2.811	(3.3 ± 2.0)	$(1.1\text{ps}^{+0.4}_{-0.3})$	0^+_2	2^+_1	$(4.6^{+}_{-}2.8) \times 10^{-4}$	6×10^{-4}	0.77	E2
	0.219	$(1.3 \pm 0.6) \times 10^{-2}$	4.6ps	0^+_2	1^-_1	$(1.4^{+}_{-}0.5) \times 10^{-4}$	6×10^{-4}	0.23	E1
	1.363*	35.72[a]	4.88ps	2^+_3	0^+_2	1.4×10^{-4}	$6.3.10^3$	2.1×10^{-8}	E2
	1.413*	11.2[b]	12.9ps	3^-_1	1^-_1	5.1×10^{-5}	15.7×10^3	3×10^{-9}	E2
^{11}Be	1.29*	37[c]/–		$5/2^-_2$	$3/2^-_3$				E2/M1
	3.64*	2[c]	640fs	$3/2^-_3$	$1/2^-_1$	1.0×10^{-3}	15×10^3	6.4×10^{-8}	E2
^{12}Be	2×10*	14.0[d]	1.43ps	2^+_1	0^+_1 (g.s)	4.6×10^{-4}			E2
	0.90*	8.0[d]	170ps	2^+_3	0^+_2	3.3×10^{-6}			E2
	0.90*	38.2[e]	36ps	2^+_3	0^+_2	1.8×10^{-5}			E2

Branching ratios ($\Gamma_\gamma/\Gamma_{\rm tot}$) are from the lifetimes using standard formulae for the transition probabilities, and $\Gamma = \hbar/\tau$, where Γ_γ and $\Gamma_{\rm tot}$ are the γ-ray and total widths of the levels, respectively, τ is the mean lifetime. $J\pi_{\rm i}$ and $J\pi_{\rm f}$ are the spins and parities of the initial and final states for a transition of multipolarity λL.
'*', The entries correspond to theoretical $B(\lambda L)$ values. The theoretical $B(\lambda L)$ are taken from Refs. as indicated: (*a*) [150]; (*b*) [166]; (*c*) [173]; (*d*) [175]; and (*e*) [80].

The odd isotopes have very few or no bound excited states. For ^{9}Be the electromagnetic transition probabilities between low-lying states and the ground state have been measured by inelastic electron scattering. The relevant decay width is for example, for the $5/2^-_1$ (2.43 MeV)$\rightarrow$ $3/2^-_1$ (g.s.) transition, $\Gamma_\gamma = (8.9 \pm 1.0) \times 10^{-2}$ eV. This would give a branching ratio of $\Gamma_\gamma/\Gamma_{\rm tot} \sim 10^{-4}$, which interestingly would be in reach with the current Ge-detector-array facilities [30].

We may also speculate regarding the transition rates in ^{11}Be: for the $5/2^-_2$(5.25 MeV) $\rightarrow$ $3/2^-_3$(3.96 MeV), $E_\gamma =$ 1.29 MeV ($E2$) transition, the states are the first two members of the $K = 3/2$ band which should have very large $E2$-transition rates, as in the case of ^{10}Be.

For the $3/2^-_3$(3.96 MeV) $\rightarrow$ $1/2^-_1$(0.32 MeV), $E_\gamma = 3.64$ MeV ($E2$), transition, the total width [7] of the 3.96 MeV state is rather small (15 ± 5 keV). Since the AMD-calculations [173] predict that the $B(E2)$ value for this transition should not be small ($2\text{e}^2\text{fm}^4$), it is conceivable that the branching ratio for γ-ray emission could be detected.

Finally, we comment on selected transition probabilities in the even Be isotopes:

Transitions in ^{10}Be involving the $K = 1^-$ band: The transition 3^-_1(7.37 MeV) $\rightarrow$ 2^-_1(6.236 MeV), $E_\gamma = 1.108$ MeV, ($M1$), is from an unbound state but should have a large $B(M1)$ value, since both the initial and final states belong to the same rotational band. However, the theoretical models for ^{10}Be have not yet predicted an exact number. For the 3^-_1(7.37 MeV) $\rightarrow$ 1^-_1(5.958 MeV), $E_\gamma = 1.413$ MeV, ($E2$), transition Kanada-En'yo et al. [166] predict a rather large transition rate for this γ-ray branch, $B(E2) = 11.2\text{e}^2\text{fm}^4$, which reflects the fact that both the initial and final states are members of the same deformed rotational band. Finally for the 2^+_3(7.542 MeV) $\rightarrow$ 0^+_2(6.179 MeV) $E_\gamma = 1.363$ MeV, ($E2$), decay in ^{10}Be, which is the band-head of the excited molecular dimer band, a large $B(E2)$-value is expected from the rather large intrinsic deformation of this band as predicted by AMD calculations [171]. These γ-ray decays from the levels with energies above the particle threshold will be very fast and may compete with a retarded particle decay. The 2^+_3 state has a very narrow width ($\Gamma = 6.3 \pm 0.8$ keV, it is situated 700 keV above the threshold for neutron emission [267], and has a measured α+^{6}He decay branch. Itagaki and Okabe [150] predict a huge $B(E2)$ value of $35.72\,\text{e}^2\text{fm}^4$ for this transition, in contrast to its transition to the ground state which is strongly hindered and predicted to have $B(E2) = 0.19\,\text{e}^2\text{fm}^4$.

Transitions in ^{12}Be: As with the molecular states of ^{10}Be and ^{11}Be the large deformations predicted [175] for ^{12}Be should involve very strong γ-ray branches to the ground state or to the first excited 2^+ state. For example, for the 2^+_1(2.10 MeV) $\rightarrow$ 0^+_1 (g.s.), $E_\gamma = 2.10$ MeV, ($E2$)-decay, Kanada-En'yo et al. [175] predict $B(E2) = 14\,\text{e}^2\,\text{fm}^4$. They also predicted a large number of new molecular states at low excitation energies. Descouvemont and Baye [80] calculate a transition rate of 6.6 Wu using microscopic α+^{8}He and ^{6}He+^{6}He wave functions for these levels. They also predict two rotational bands based on the 0^+_2 state and on a 1^-_1 state with large probabilities for intra-band transitions. For example, the $3^-_1 \rightarrow 1^-_1$ transition has a predicted value of $B(E2) = 31.1$ Wu.

7. Models for three-centre systems

7.1. Chain states in nuclei: nuclear polymers

In this section the basic concepts behind the formation of chain states and other three-centre systems in nuclei will be outlined. A more detailed discussion and a comparison with recent data will be given in Section 8.

The first structures which can be built from many α-particles are the linear chain states, since such configurations minimize the Coulomb repulsion between the constituents. These are unique shapes in nuclear physics. We immediately realize when inspecting Fig. 8, that they are obtained by an extension of the two-α-particle structure by placing further nucleons exclusively along the z-axis defined by the axial symmetry of ^{8}Be. With the double degeneracy for spin and isospin these nucleons will condense into an α-particle, and the shapes are hyper-deformed in $^{12-16}$C. We also deduce from Fig. 8, that the next valence nucleons added to such a chain can be placed into orbitals perpendicular to the z-axis. These are the "molecular" π-orbitals with $K = 3/2$, which were discussed before in the case of ^{9}Be. By extending the concept of threshold states we, can propose, as was done in Ref. [283] structures of covalently bound chain states in $^{13-16}$C, as summarised in Fig. 38. This diagram is arranged in such a way, that the different thresholds in the isotopes are aligned to the same level, thus ground states and the excitation energies of the levels are shifted. Binding due to the covalent configurations of the valence neutrons will lower the band heads of the hyper-deformed shapes below the indicated thresholds.

An important aspect, not considered in Fig. 38, will enter in the case of nuclear molecules with two or more valence neutrons, because of the strong short range residual interaction. This effect was already observed in the energy of the ^{10}Be ground state which indicates a two-neutron binding energy of 8.8 MeV. Preserving this configuration leads, in ^{14}C, to the occurrence of intrinsically reflection asymmetric chain states [285,290], based on the ^{10}Be + α structure. The two nucleons remain concentrated just between two of the three α-particles (see Section 8.3.1). Such configurations with their corresponding parity projection are shown schematically in Fig. 39. The discussion of the ^{14}C chain states will either be based on the basic covalent molecular structures defined for single neutrons by the Hückel method, the three centre states identified for ^{13}C in reference [207], or on the sub-structures like ^{10}Be, or ^{6}He and α-particles.

The properties of the symmetric linear structures in $^{14-16}$C have been calculated by Itagaki [152]. The bending modes of the pure 3α-particle chain are predicted to be stabilised in the corresponding covalently bound molecular configurations with extra neutrons, particularly in ^{16}C. Because of the pairing interaction, the concepts of covalent molecular binding must be submitted to close scrutiny for nuclear chains. States with strong clustering but with paired neutrons are expected to be found well below the threshold energies indicated in Figs. 4 and 38.

7.2. Cluster states of triangular shapes

A further possibility for three-body systems is the formation of triangular shapes. The basic concepts for such structures are introduced below and experimental details for the cases of ^{13}C and ^{14}C are given in Section 8. We note that recently these structures have also been discussed in the mean-field approach in heavier nuclei [85,259].

For the present case involving an explicit cluster structure, the symmetries of the 3-body systems are important. To illustrate this point, we revisit the results from Refs. [36,296]. In the algebraic cluster model of Bijker and Iachello [36] the symmetries of an oblate top, consisting of three identical clusters, are treated. The system has a discrete symmetry expressed as D_{3h} which consists of a rotation, D_3 and a parity operation, P with $D_{3h} = D_3\, P$. The parity of the bands is determined by $P = (-)^K$, where K is the projection of the total spin on the symmetry axis. This determines the spin sequence of the bands, they will have the structure, of $J = 0, 2, 4, \ldots$, for $K = 0$ or $J = K, K + 1, K + 2, \ldots$ for $K \neq 0$. Due to this symmetry no states with dipole character and no $L = 1$ transitions should occur. The role of the vibrational excitations is important in such systems, these are the excited states within the cluster–cluster potential. The algebraic model can in particular deal with the coupling of these vibrational states to the rotations. The bands with $K \neq 0$ can be obtained by vibrational excitations, with values $K = 3n + 1, 3n + 2$ and $J = K, K + 1, K + 2$.

The other work on three (non-identical) cluster systems of note is that of Wiebicke and Zhukov [296]. In this work the potential energy of three interacting clusters are calculated. This is a geometric three-cluster model for nuclei consisting of α-particles, ^{12}C and ^{16}O cores. The potentials for the cluster–cluster interaction are of the molecular type as discussed in Section 3, chosen to reproduce features of the binary channels, such as scattering states or bound states. In this work

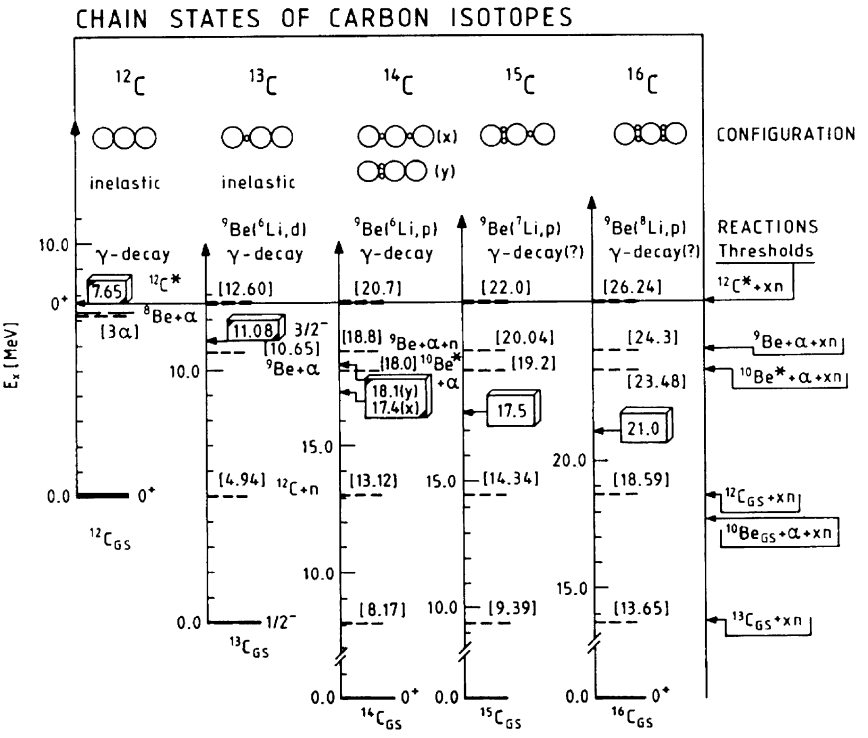

Fig. 38. Schematic diagram (from Ref. [283]) showing the expected energies of chain states in carbon isotopes for the $(3\alpha + X$ neutrons) linear cluster configurations; thresholds for decay into α-particles and neutrons are aligned to the same level.

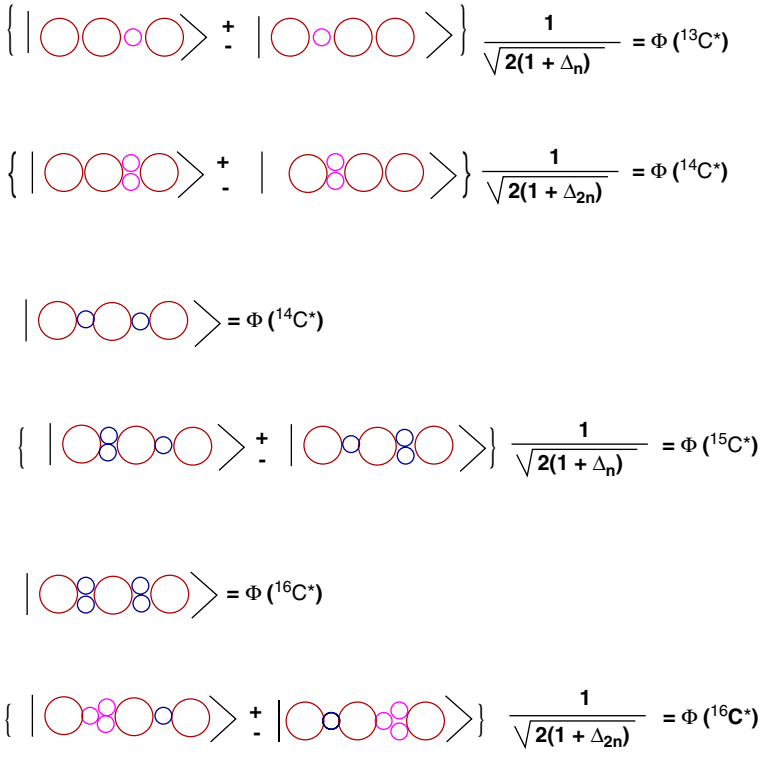

Fig. 39. Schematic illustration of the configurations and their parity projections for linear chains in $^{13-16}$C with different sharing of the neutrons. The parity projection is only needed for intrinsically reflection asymmetric states.

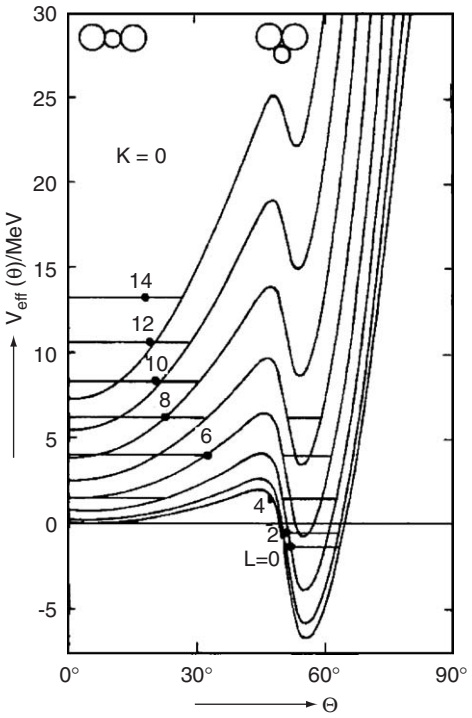

Fig. 40. Illustration of the potential energy corresponding to configurations with different angular orientations of the clusters in the system $^{12}C + \alpha + ^{12}C$, from [296].

the stability of different arrangements (also triangular shapes) as a function of angular momentum are discussed. For the total energy there appears a potential minimum for the most closely packed shapes. The potential energy plotted as a function of the orientation angle of the third particle relative to the axis of two others is shown in Fig. 40. From these results we can also deduce that the cluster decay of the triangular shape at higher angular momentum will generally pass through a stretched (linear) configuration. Actually a barrier in the angular variable appears between the linear and the triangular configurations and a tunnelling process between these shapes becomes important at lower angular momentum.

From physical chemistry [197] we know that in the linear configurations the bending mode is an important degree of freedom. The coupling of the bending mode and the rotation in a three-body molecule is a classical problem of physical chemistry: the vibrations of the binary sub system of clusters in a rotating system introduce, due to the Coriolis forces, a bending mode. The extension of these approaches to multi-centre nuclear molecules with valence particles, is a very appealing subject for future study.

8. Results for three-centre systems

8.1. Oblate and prolate states in carbon isotopes

In order to identify the strongly deformed states in carbon isotopes all spectroscopic information accumulated in the last decades can be used. The carbon isotopes provide excellent examples for testing the concept of complete spectroscopy, since for these nuclei a large variety of reactions have been studied. The first step is to identify the states with single-particle properties. By "removing" these states from the spectrum, multi-particle–multi-hole configurations remain as candidates for cluster states. These deformed states can be selected by their population characteristics and are then grouped into rotational bands.

The discussion of ^{14}C chain states can be based on the symmetric covalent molecular structures for three centres identified in [207] for ^{13}C, or alternatively on the subdivision into the sub-structures such as ^{10}Be, or ^{6}He and the

α-particle (Ref. [290]), and are schematically shown in Fig. 41. The fully symmetric configurations are expected at higher excitation energies as predicted by Itagaki [152] for ^{14}C and ^{16}C. In the latter case the bending modes of the pure three α-particle chain are expected to be stabilised by the extra neutrons.

The oblate cluster states in $^{13-14}$C are connected to the crossing of orbits in the deformed shell model on the oblate side, i.e. above the shell closure with $N = 6$ associated with ^{12}C on the left side of the diagram in Fig. 8. These $^{13-14}$C configurations will be coupled to the 0^+ ground state, to the second 0^+_2 state and the 3^- state of ^{12}C. For the 0^+_2 state no specific orientation of the three α-particles can be defined and the bending mode is expected to be an important part of the wave function [82]. Therefore, this state also serves as a basis for covalently bound three α-particle chains in $^{13-14}$C. However, an important new aspect (in contrast to atomic molecules) enters in the case of nuclear molecules, e.g. in the case of ^{14}C, and that is the strong short range pairing interaction between two neutrons. As noted earlier, this leads to the formation of intrinsically reflection asymmetric chain states [54,285,290], based on the $^{10}\mathrm{Be} + \alpha$ structures. This gives rise to rotational bands as parity inversion doublets.

Itagaki et al. [152,154] have recently performed calculations for the oblate, triangular, shapes [155]. They obtain excitation energies with the band head below the threshold for $^{10}\mathrm{Be} + \alpha$ (12.012 MeV). The oblate cluster states in ^{14}C can also overlap (or mix) with shell model states based on $^{12}\mathrm{C}_{\mathrm{g.s.}}$, or on the $(2^{+*}\ldots)\otimes$ (2n)- configuration, whilst the prolate shapes are expected not to be mixed with such shell-model states. These considerations help to identify the cluster states, as we expect a very different selectivity for the population of these ^{14}C-states in different reactions [290].

Thus, for ^{14}C, three different cluster configurations can be expected:

(i) intrinsically reflection symmetric linear chains corresponding to the α-n-α-n-α configuration with the valence particles equally distributed among the three basis centres ("X-configuration" in Fig. 41). The valence particle density distributions will be concentrated outside the symmetry axis (see [207]) in the π-bonds; for the σ-bonds the neutrons will be concentrated on the axis. Mixed π–σ configurations can be considered as in the case of the 1^- state in ^{10}Be.

(ii) linear, intrinsically reflection asymmetric configurations corresponding to the structure α-2n-α–α with the two valence neutrons in the same covalent π-bond between two centres (with the pairing energy as in the ^{10}Be (g.s.). This is the "Y-configuration" in Fig. 41, giving rise to parity inversion doublets.

(iii) oblate configurations related to a triangular structure, with σ-bonds between two α-particles. As discussed in Refs. [154,155,207], the π-bonds would penetrate the α-particles and should be thus hindered by the Pauli principle. The neutron can alternatively be placed out of the α-particle plane as discussed in [203].

The linear "X" and "Y" chain configurations of ^{14}C represent cases with very different binding energies, because the two neutrons are very strongly bound in ^{10}Be. The band head for the "Y"-configuration is expected below the threshold for $^{10}\mathrm{Be} + \alpha$ (at 12.012 MeV) and thus well below the threshold (20.4 MeV) for the "unbound chain" with the structure α-n-α-n-α. For the asymmetric Y-configuration, the states would be associated with symmetric and antisymmetric wave functions constructed from the two possible ways to share the 2n-covalent bond (see Fig. 45). The rotational bands must appear as parity inversion doublets (see Refs. [46,285]) with quantum numbers $K = 0^+$ and 0^-. The positive parity members should be lower in excitation energy. The splitting of the two bands will be determined by a non-orthogonality term Δ (see Section 8.3).

The symmetric "X" - configuration should exist at an excitation energy not far below the decay threshold of 20.40 MeV. Its energy will be determined by the covalent binding effect of the π-orbitals for the two valence nucleons (approximately 2×1.66 MeV). With an additional effect due to the residual interaction the band head can be expected at a excitation energy around ≈ 17 MeV.

8.2. *Complete spectroscopy in* ^{13}C

The structure of ^{13}C will be reviewed in more detail, it will serve as an illustration of the identification of cluster states, which are mostly particle unstable states. Using a large body of information a complete spectroscopy of the states up to an excitation energy of 20 MeV can be achieved. With a separation of the single-particle states the ordering of the remaining states into $K = 3/2^-$ and $3/2^+$ bands is obtained.

The mass 13 nuclei have been the subject of many shell–model calculations, e.g. [192,207,212,213] and references therein. Generally, normal (negative) parity states in ^{13}C (and ^{13}N) arise from various recouplings of the nine nucleons in the *p*-shell. For the positive parity states with a nucleon in the *sd*-shell, a very satisfactory description is obtained

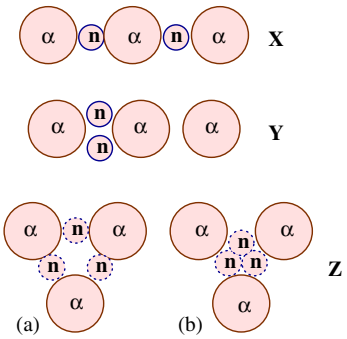

Fig. 41. Schematic illustration of the triangular and the two possible linear chain configurations in ^{14}C. X, is the most symmetric configuration with positive parity; Y, is intrinsically reflection asymmetric forming parity doublets. Z, corresponds to oblate shapes with delocalised neutrons: (a) with a node of the valence particle wave function at the centre, $J^\pi = 3^-$; (b) with a maximum of the valence particle wave functions at the centre $-J^\pi = 0^+$. Dashed lines indicate sharing of the two valence neutrons among the three centres, from [290].

in the weak coupling model, with the lowest two core states ^{12}C [188]. A survey of these states is given in Fig. 42. Experimentally, the level schemes of ^{13}C and ^{13}N are reasonably well determined for excitation energies up to about 9.5 MeV [8], and these are states well described by the shell-model [96,133]).

Problems in the interpretation arise with the states above an excitation energy of 9.50 MeV. In the *p*-shell calculations [66] there are no candidates for several of the observed states such as the 9.90 MeV $3/2^-$, 10.75 MeV $7/2^-$, 10.82 MeV $5/2^-$ and 11.08 MeV $1/2^-$ levels. These are found to be predominantly $p^7(sd)^2$ in character and possibly arise from the coupling of two nucleons in the lowest *sd*-shell Nilsson orbit to the ground state ($K = 3/2$) and the first excited state ($K = 1/2$) bands of an $A = 11$ core [211]. As in the ^{16}O case, one can expect that in ^{13}C there is a significant contribution from multi-particle–multi-hole excitations, namely $p^5(sd)^4$ configurations, which then naturally introduces as an alternative the use of cluster models. In a weak-coupling scheme, the aforementioned states in ^{13}C have to be constructed with the 0_2^+, 0_3^+ and 3_1^- core excitations (see Fig. 42). Since these ^{12}C states are not reproduced even with the largest shell-model calculations [212], but are known to be well described by the cluster models [111], we expect similar cluster structures for the ^{13}C states in this excitation energy region.

8.2.1. Cluster states with $K = 1/2^+$ and $1/2^-$

Apart from the single–particle states in ^{13}C, two conspicuous states appear with spin-parity $1/2^-$, $1/2^+$ at excitation energies of 8.86 MeV and 11.00 MeV, respectively. These states have a rather unusual structure, the $1/2^+$ state at 10.996 MeV is observed as a strong resonance in the α+^{9}Be system but is never observed in "simple" reactions and does not fit into the level scheme of shell-model calculations. The same statements can be made for the $1/2^-$ state at 8.86 MeV, however, this state can not be populated by an α+^{9}Be reaction due to its low excitation energy. The inelastic scattering to these states is found to be weak, but the angular distributions have the same shape as those observed in inelastic scattering for the second 0_2^+-state in ^{12}C, which is known to be a cluster state. It is proposed that the two states are oblate in character and correspond to the $1p_{1/2}$ and $2s_{1/2}$ orbits (the first two states of ^{13}C) but coupled to the second 0_2^+-state, as shown in Fig. 42. The energy spacing between the two states is slightly smaller for the core excited pair, in accordance with an expected larger rms-radius of the 0_2^+-state. These two states may have triangular structure, see also Refs. [207,208]. The valence neutron may stabilize the underlying 3-α-particle structure to a triangular shape as recently discussed for ^{14}C by Itagaki et al. [154,155] and illustrated in Section 8.3.3.

A prolate linear configuration with $K = 1/2$ is expected at even higher excitation energy and the Coriolis decoupling would be rather strong, moreover, the widths of the states are expected to be large and make their identification rather difficult.

8.2.2. Rotational bands of ^{13}C with $K = 3/2^\pm$

Here we provide some information on the members of the two prolate bands, which are candidates for linear chains. They have been identified by their relation to particular reactions. The 9.897 MeV state is a candidate for the $K = 3/2^-$ band–head (the spin assignment is well established [117]). The state appears as a very narrow resonance ($\Gamma = 26$ keV),

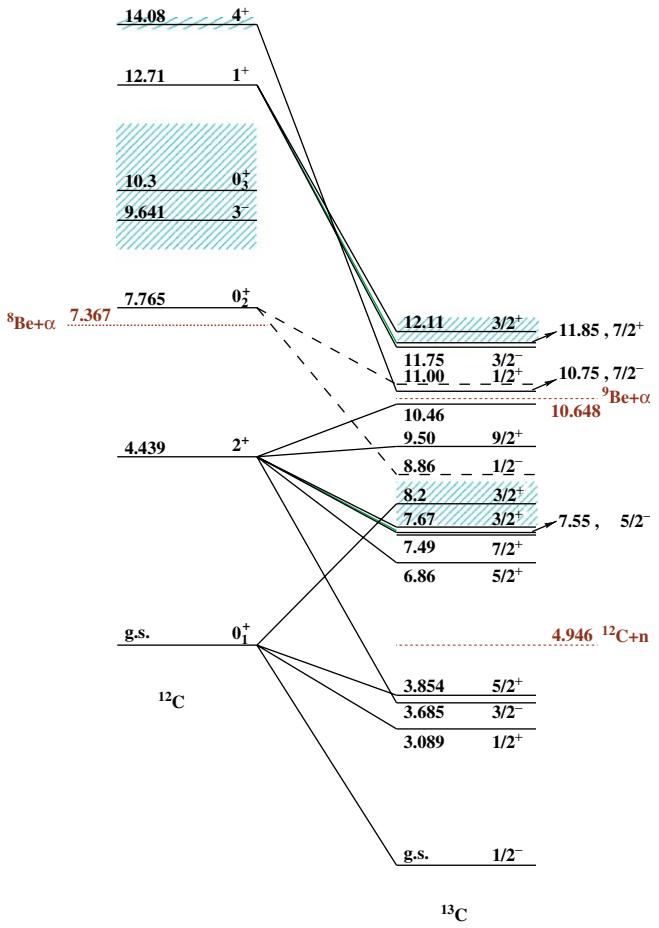

Fig. 42. Energy levels of ^{13}C, grouped into single-particle states coupled to the indicated states of ^{12}C (except for 3^-_1). The remaining states in ^{13}C, ordered into rotational bands are shown in Fig. 43, from [207].

which is quite unusual considering that it is ≈5 MeV above the threshold for neutron emission. This state is barely (or not at all) populated in one-nucleon transfer reactions [207], but it is rather prominent in two- and three-nucleon transfer and also quite strong in α-transfer on ^{9}Be. The candidate for the next state ($5/2^-$) of the rotational band is at 10.818 MeV. As with the $3/2^-$ state, this state is only weakly populated in one-nucleon transfer. It is not seen in proton inelastic scattering (while a closely lying state at 10.753 MeV is excited). Unfortunately, it is rarely cleanly resolved in multi-nucleon transfer reactions, in α-transfer reactions the strongest peak in the spectrum is at $E_x \approx 10.80$ MeV. The 10.818 MeV resonance has, however, been observed in ^{9}Be(α, n)^{12}C measurements [301]. The next $7/2^-$ state at 12.438 MeV is also only weakly (if at all) populated in one-nucleon transfer reactions. Furthermore, it is seen in a number of α+^{9}Be reactions as a rather strong resonance. Based on the above arguments, this state is not a *p*-shell level ($0\,\hbar\omega$) as proposed by Millener et al. [211], but is a member of the $K = 3/2^-$ rotational band. The 14.13 MeV state is the strongest resonance seen in ^{9}Be(α, α)^{9}Be and in ^{9}Be(α, n_2)^{12}C*(7.65 MeV) reactions and is also clearly seen in the ^{9}Be(^{6}Li, d)^{13}C reaction. These facts provide strong arguments to place it as a high spin member of the $K = 3/2^-$ band. The state at 16.08 MeV has been previously tentatively assigned as ($7/2^+$) in [8]. It is seen in the ^{9}Be(α, α)^{9}Be reaction and it is very strong in the ^{9}Be(α, n_0)^{12}C and ^{9}Be(α, n_1)^{12}C*(4.44 MeV) reactions. With these observations a coupling of $L = 4^+ \otimes {}^9\mathrm{Be}(3/2^-)$, and the $11/2^-$ assignment can be proposed.

For the $K = 3/2^+$ band, the state at 11.080 MeV is the only candidate for the band head, as it is extremely narrow ($\Gamma \leqslant 4$ keV). This fact indicates that neutron decay goes through $L = 2$ (implying positive parity). The first excited state of the $K = 3/2^+$ band would be the 11.950 MeV, a ($5/2^+$) state which has an established spin and parity [8]. It is only

Table 3
States for the proposed two rotational bands with $K = 3/2$ in ^{13}C. The widths, Γ, are taken from Refs. [8,187,193]

J^π proposed	E_x (MeV)	J^π assignment in Ref. [8]	Γ (keV)
$K = 3/2^-$			
$3/2^-$	9.897		26
$5/2^-$	10.818		24
$7/2^-$	12.438		336
$9/2^-$	14.13	$3/2^-$	150
$11/2^-$	16.08	$(7/2^+)$	150
$K = 3/2^+$			
$3/2^+$	11.080	$1/2^-$	$\leqslant 4$
$5/2^+$	11.950		150
$7/2^+$	13.41	$(9/2^-)$	35
$9/2^+$	15.28		
$11/2^+$	16.950	none	330

weakly seen in one-nucleon transfer reactions and it is not seen (or only very weakly) in inelastic scattering of protons, of ^{3}He nuclei and of α-particles. It is very strongly populated in various ^{9}Be + α capture reactions implying a large α-strength. In the ^{7}Li(^{9}Be,^{13}C → α+^{9}Be)t reaction, a strong peak is seen at 11.950 MeV. For the 13.41 MeV state a tentative assignment of $9/2^-$ had been given in Ref. [8], however, it is probably the $7/2^+$ member of the $K = 3/2^+$ band. As with all the states in the proposed bands, it is only weakly seen in one-nucleon transfer reactions, but it is always very strong in the α+^{9}Be reactions, and it is strongly populated in the ^{9}Be(^{6}Li, d)^{13}C reaction. Finally, we examine the 15.28 and 16.95 MeV states. For these levels the experimental data are very scarce and little is known about their structure. However, they are rather strong in reactions involving either α-transfer or capture, and thus are strong candidates for the $9/2^+$ and $11/2^+$ members of the band. As seen in Fig. 44 the excitation energies of the states in Table 3 follow the $J(J + 1)$ relation quite well, suggesting the present assignments are correct. However, the new assignments need to be confirmed experimentally. Such measurements are complex and difficult to interpret due to the density of states in this region. For example, a study of the ^{14}C(^{13}C,^{9}Be + α) reaction [233] has been interpreted in terms of the population of oblate states, and that the 14.13 MeV state may have such a character. Clearly, this is an area which demands greater experimental focus.

With the existing experimental data we can identify two molecular parity-split rotational bands (given in Table 3 and illustrated in Figs. 43 & 44), they correspond to a strongly deformed structure with hyper-deformation. As discussed at the beginning of this section the underlying structure (^{9}Be+α or α+α+α+n) can be reflection asymmetric, therefore also the interpretation as a parity doublet [207] appears appropriate. In addition, the states of such a structure should have large α-widths. Indeed, the states are strongly populated in reactions such as ^{9}Be(α,α)^{9}Be, ^{9}Be(α,n)^{9}Be, and ^{9}Be(^{6}Li,d)^{13}C. Also the capture reaction, ^{9}Be(α,n)^{12}C, which is interesting for astrophysical reasons, has been measured several times with excellent resolution [301,187].

8.3. *Cluster states in* ^{14}C

In Section 7.1 the identification of chain states in ^{14}C was mentioned as an important step for establishing the existence of nuclear polymers. To identify the cluster states in ^{14}C we proceed, as in the case of ^{13}C, with the concept of complete spectroscopy. We have to select the single–particle configurations in ^{14}C, then the remaining states are classified through the selectivity of their population in multi–nucleon transfer reactions. In these reactions multi-particle, multi-hole configurations, involving in particular also proton excitations, must be prominent. A number of rotational bands connected to different symmetries of cluster-configurations are expected. The reflection asymmetric states should be grouped into parity doublets with band heads below the energies of the relevant thresholds of asymptotically asymmetric fragmentation. From the data on the level schemes and the excitation energies the rotational bands are constructed and their moments of inertia are derived.

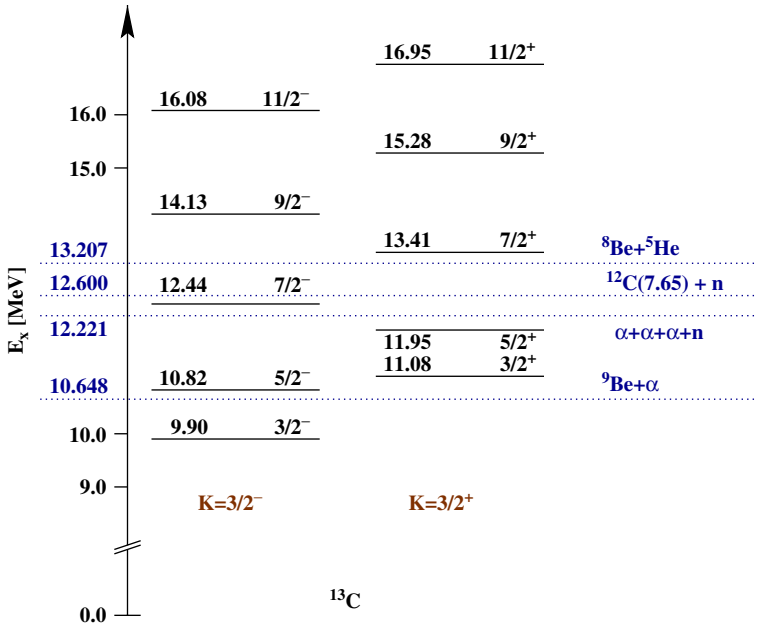

Fig. 43. Plot of energy levels of ^{13}C forming rotational bands with the K-quantum numbers as indicated. The spin assignments are discussed in the text. Thresholds for various structure components in ^{13}C are shown, from [207].

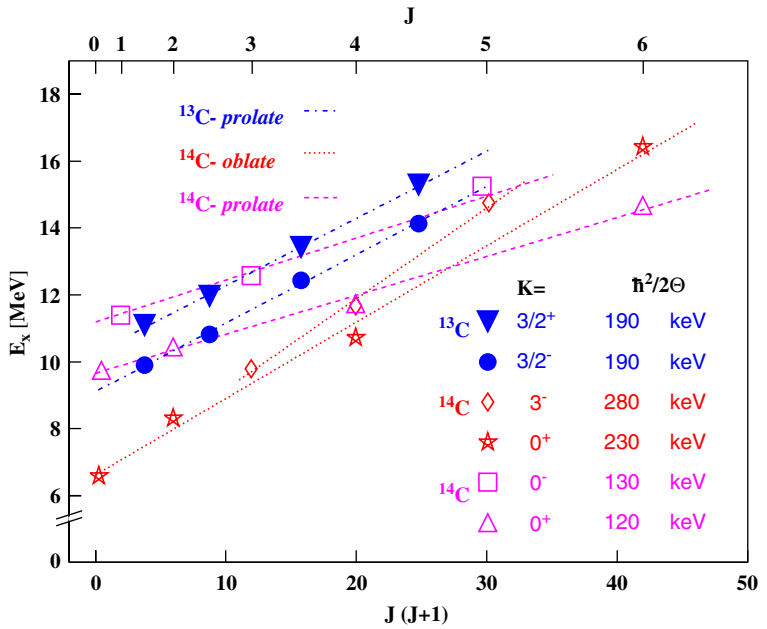

Fig. 44. Excitation energies plotted as a function of spin, $(J(J+1))$ and moments of inertia of oblate and prolate rotational bands in $^{13-14}$C, from [291].

8.3.1. *Configurations in* ^{14}C *based on the* $\alpha+^{10}$Be *system*

The intrinsically symmetric linear molecular orbital configurations based on the three-centre cluster model have been introduced for one neutron using the Hückel Method (Section 2.4) for the ^{13}C-chain states, the molecular LCNO wave functions of the valence neutron are given explicitly in Ref. [207]. Two neutrons can be placed in such basis states,

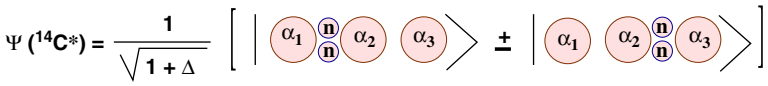

Fig. 45. Schematic illustration of the parity projection for a linear chain configuration in ^{14}C forming a parity inversion doublet with $K = 0^{\pm}$; the bands start close to the ^{10}Be + α threshold, from [290].

however, these states are expected at higher excitation energies. The configurations with the ^{10}Be + α substructure, where two neutrons remain bound due the pairing interaction, will have a higher binding energy. These structures are not directly related to the Hückel wave functions, as described below.

The covalent orbitals responsible for the binding in ^{14}C with two neutrons will be based on the ^{10}Be ground state with the $(\pi)^2$-configuration (the $(\sigma)^2$ is 6 MeV higher in excitation energy). The valence particles then remain concentrated outside of the symmetry axis. Therefore we start with an intrinsically reflection asymmetric configuration consisting of an ^{4}He+^{10}Be structure, then symmetrize the total wave function and project onto good parity as illustrated schematically in Fig. 45.

The final result will reflect the strong pairing in the 2n-configurations, two bands are expected with signature splitting and with their band-head energies close to the (^{4}He+^{10}Be)-threshold. Another, less favourable structure would be based on the decomposition into ^{6}He+^{8}Be, but this configuration has a much higher threshold. The nonorthogonality Δ in Fig. 45 is a function of the distance between the clusters and is given by an overlap of the type:

$$\Delta(R_{ij}) = \langle {}^{10}\mathrm{Be}(\alpha_1\alpha_2) \otimes \alpha_3 | \alpha_1 \otimes {}^{10}\mathrm{Be}(\alpha_2\alpha_3)\rangle. \tag{29}$$

This represents the exchange probability, a process in which the two neutrons and an α-particle are exchanged in either sequence between the two outer α-particles. This will determine the energy splitting of the two parity split bands. In the inversion doublet with $K = 0$ (parities + and −), the negative parity band head is at higher excitation energy. The latter must start with a $J = 1^-$ state, because a cluster state with $J = 0^-$ (unnatural parity) is not allowed, due the spins ($S = 0$) of the constituents. The probability for a transition between the two reflected configurations shown in Fig. 45 should be similar to the ^{13}C case.

As already stated the reflection symmetric states with good (positive) parity, which are built from symmetric three-centre Hückel states are expected at higher excitation energies. However, mixing between these configurations and the presently discussed states of the positive parity band is possible.

8.3.2. Complete spectroscopy for ^{14}C

The total number of "simpler" states with nucleon configurations with a shell model core increases with increasing number of valence particles. Thus, for the two valence particles in ^{14}C, it becomes more difficult to establish a complete spectroscopy with differing classifications for the "normal" states and the more strongly deformed cluster states. This exercise has been performed using information from data compilations and recent multi-nucleon transfer reactions. Many multi-nucleon transfer reaction studies populating ^{14}C may also be found in the literature, for a complete list see Ref. [290].

For the development of a complete spectroscopy the following reactions have been studied recently [290]:

(i) the 2n-stripping on ^{12}C; (ii) 2p-pick-up from ^{16}O; and (iii) the ^{5}He-transfer on ^{9}Be.

(1) *Results from 2-neutron transfer onto* ^{12}C. Several projectiles have been used for the 2n-transfer, including ^{14}N, ^{15}N and ^{16}O, all at $E_{\mathrm{lab}} \approx 15$ MeV/nucleon (Fig. 46). The transferred angular momentum at this energy is $\approx 2.3\,\hbar$ per nucleon. In these stripping processes there is no population of the *s*-shell, but the population of the $p_{1/2}$-shell, and dominantly of the $d_{5/2}$ and $d_{3/2}$-shells is expected, with a good probability to reach also the $f_{7/2}$-shell. Usually the differential cross section is proportional to the angular momentum transfer and to the final spin value, and high spin values are particularly enhanced for very negative *Q*-values. The strongly populated states in the two-neutron stripping reactions shown in Fig. 46 are predominantly connected to stretched two neutron configurations. The combinations of two orbits coupled to a maximum spin which are observed for the two neutron configurations, are the following:

(a) A weak population of configurations consisting of combinations with one nucleon in the 2*s*-orbital.
(b) The states consisting of combinations of the *p*- and *f*-orbitals are expected to be strongly populated.
(c) The strongest transitions observed must correspond to two neutrons in the *d*- and *f*-orbitals.

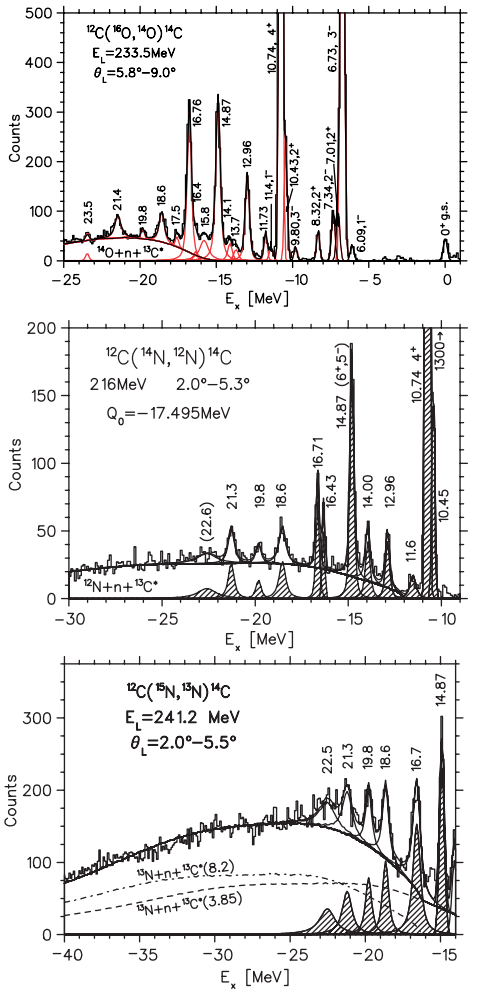

Fig. 46. Spectra for 2n–transfer reactions on ^{12}C, obtained with the Q3D-spectrometer at the ISL-accelerator facility, with three different projectiles ^{16}O, ^{14}N, and ^{15}N, respectively, at an incident energy of approximately 15 MeV/nucleon. The angular range of the Q3D-opening is indicated, from [290].

For the stretched configurations the simple shell model approach of Tsan Ung Chan [56,57] can be used to obtain predictions for the excitation energy of the two-nucleon high spin configurations [290]. The excitation energy is obtained as the sum of the energies of the neutron orbitals in ^{13}C, plus a pairing energy. For the spectra shown in Fig. 46 the measured energy positions of the states agree with the predicted energies of stretched configurations, which are compiled in Table 4. We list the many states of ^{14}C populated in the 2n-transfer reactions (sometimes not resolved) which are also populated in the high resolution ^{9}Be(^{7}Li, d)^{14}C reaction shown in Fig. 47. It is interesting to note that for many of these states no analog states are observed in the 2p-stripping reaction leading to the mirror nucleus ^{14}O studied in Ref. [186]. The "new" states at higher excitation energies are the candidates for strongly clustered molecular states. Only with neutrons can these structures be stabilised due to covalent binding.

The weaker lines at higher excitation energy observed in the 2n-transfer in Fig. 46 are expected to be related to core excitations ($^{12}C^{*}_{2+}$ and $12C^{*}_{3-}$), or to the population of the $d_{3/2}$- and $f_{7/2}$-shells. In the first case structures with multi-particle, multi-hole excitations which lead to configurations like $(p_{3/2})^{-1} \otimes p_{1/2} \otimes (sd)^2$ are expected, which can be mixed with other configurations. The states built on a core excitation, such as the $^{12}C_{2+}$ or $^{12}C_{3-}$ states are populated in a two-step process with a collective excitation as a first step, a process well established in two-nucleon transfer [287]. In these cases, the states will attain a smaller decay width, because of the increased energy thresholds for the particle decay and the higher angular momentum barriers due to the larger spins.

Table 4
Excitation energies (E_x), configurations and relative yields of states in ^{14}C observed in the (^{7}Li, d) reaction. The proposed spins and configurations are used to interpret the rotational bands of the deformed states, marked in column 3 as oblate or prolate, (and parity *par*). The relative yields (divided by $2J+1$) are normalized to the 2^+-state at 7.012 MeV, given as 200. For the states with unassigned spin, the values are normalized with a spin value of 2, sometimes indicated as (2+). The population strength in 2n-transfer is indicated in the 4th column by the following code: (+)-strong in 2n; (∗)-average or weak in 2n; (−)-not seen in 2n. (ex)-the extra lines not used in the compilation for rotational bands. The levels without parentheses are assigned in [8]

J^π	E_x [MeV] This work	conf/par Proposed	$N/(2J+1)$ Relative	Width; τ or Γ [keV]
0^+	0.0	mixed		0.0
1^-	6.09	$p_{1/2}s_{1/2}$	$179^{(*)}$	<7 fs
0^+	6.59	obl (+)	$338^{(*)}$	3 ps
3^-	6.73	$p_{1/2}d_{5/2}$	$65^{(+)}$	66 ps
0^-	6.906	$p_{1/2}\,s_{1/2}$	$180^{(-)}$	25 ps
2^+	7.012	$\pi p^{-1}_{3/2}p^{-1}_{1/2}$	$200^{(-)}$	9 fs
2^-	7.348	$p_{1/2}d_{5/2}$	$101^{(*)}$	111 fs
2^+	8.318	obl (+)	$97^{(+)}$	3.4
0^+	9.74	prol (+)	$50^{(*)}$	–
3^-	9.80	obl (−)	$183^{(*)}$	45
2^+	10.43	prol (+)	$263^{(+)}$	25
(3^-)	10.498	ex	$131^{(-)}$	12
4^+	10.736	obl (+)	$158^{(+)}$	10
1^+	11.306	ex	$174^{(+)}$	40
1^-	11.39	prol (−)	$220^{(*)}$	25
4^-	11.66	obl (−)	$95^{(-)}$	20
4^+	11.73	prol (+)	$100^{(*)}$	30
(3^-)	12.58	prol (−)	$470^{(-)}$	Two peaks
	12.86	ex	$163^{(+)}$	25
	12.96	ex	$126^{(-)}$	25
	14.03	ex	$(*)$	100
6^+	14.67	prol (+)	$185^{(-)}$	
5^-	14.87	obl (−)	$158^{(+)}$	Two peaks
(5^-)	15.18	prol (−)	$80^{(-)}$	50
(2^+)	15.40	ex	$116^{(-)}$	40
6^+	16.43	obl (+)	$179^{(*)}$	35
(2^+)	16.53	ex	$^{(-)}$	50
(1^+)	16.72	ex	$90^{(+)}$	60
4^-	17.30	ex	$^{(-)}$	80
(2^+)	17.52	ex	$125^{(*)}$	100
(2^+)	17.91	ex	$98^{(-)}$	50
(7^-)	18.03	prol (−)	$114^{(-)}$	70
	18.39	ex	$147^{(-)}$	170
	18.60	ex	$87^{(*)}$	100
	19.14	ex	–	900
(2^+)	19.73	$d_{3/2}d_{3/2}$	$491^{(*)}$	250
	20.02	ex	–	200
	20.75	ex	–	40
	21.00	ex	–	220
	21.41	ex	–	550

(2) *Results for 2p-pick up*. The reaction ^{16}O(^{15}N, ^{17}F)^{14}C at 240 MeV, shows very different states [290] compared with the 2n-stripping reaction. Many of the strongly excited states seen in the cluster transfer reaction, (^{7}Li, d), are observed, a fact which supports assignment of the particle–hole structure of the cluster states in ^{14}C. The higher lying states in ^{14}C, which are excited in 2n-stripping, are not seen in the 2p-pick-up reaction, since these involve the collective particle–hole structure of the core states with neutrons in the (*sd*)-shell, and therefore cannot be populated in a pick-up reaction, unless strong (4p–4h) correlations in the ground state of ^{16}O are involved.

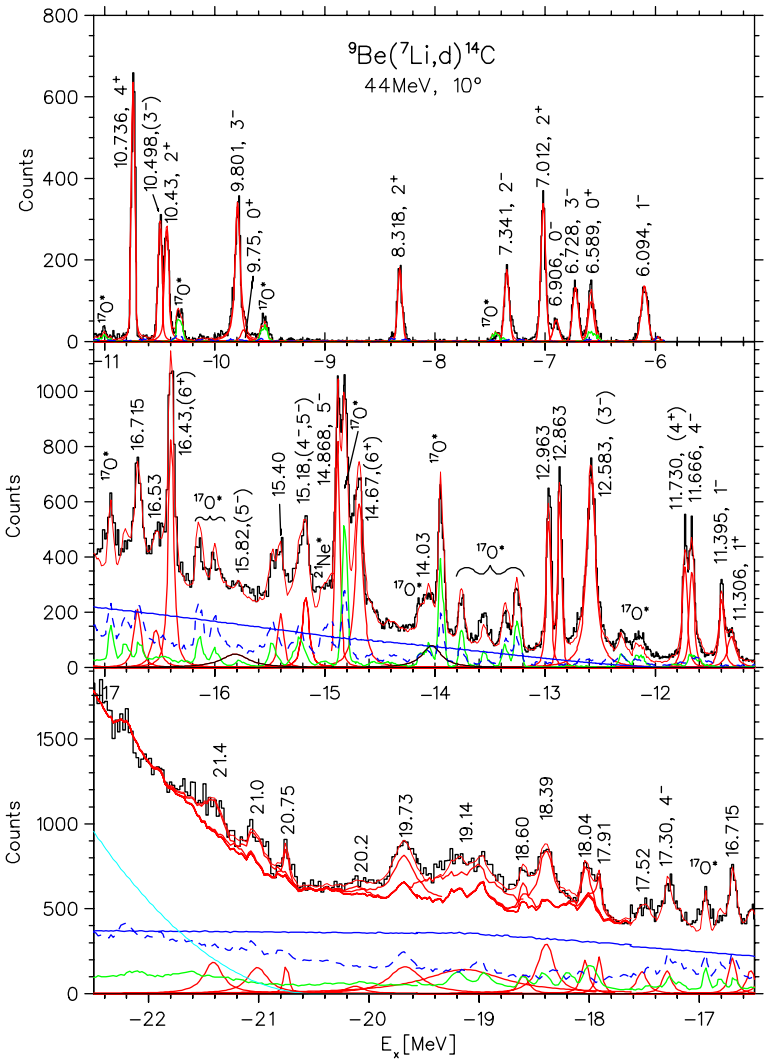

Fig. 47. Deuterium spectrum from ^{5}He-transfer on ^{9}Be obtained with a ^{7}Li beam of $E_{\mathrm{lab}} = 44$ MeV at the Q3D-spectrometer of the accelerator laboratory in Munich [290]. The structured backgrounds shown are 3- and 4-body continua, or measured backgrounds with ^{12}C and ^{16}O targets (full and dashed lines, indicated as ^{17}O* and ^{21}Ne*, respectively).

(3) *The single-particle configurations of* ^{14}C. Although experimentally there are many levels with uncertain structure or spin assignments, we may try, using the selectivity in the population of states, to summarize with some general statements the different structures in ^{14}C. Many states are seen in the 2n-transfer on ^{12}C, because the reaction can strongly populate oblate states, due to their parentage to the ^{12}C-core. These strongly populated oblate states are listed in Table 4. Some of the states associated with core excitations are seen with the 2p-pick-up from ^{16}O. To achieve the complete spectroscopy of this nucleus, the states in ^{14}C can be ordered into a sequence of increasing complexity (and rising excitation energy). The low lying states with positive parity are based on the $^{12}C_{0^+}$ and $^{12}C^{*}_{0^+}$-cores and the neutrons can occupy three different shells ($p_{1/2}$, $s_{1/2}$, $d_{5/2}$), these configurations will mix to form, for example, three 0^+-states in ^{14}C (at 0.0, 6.589 and 9.746 MeV). The lowest shell-model states have overlap with oblate cluster states. These are also expected to form rotational bands. The configurations for the lowest negative parity states will be due to (1p–1h) configurations, namely one $p_{1/2}$ neutron promoted to the (sd)-shell. Creating a hole in the $p_{3/2}$-shell for a proton (π) or neutron (ν) will also give rise to negative parity states, such as the $(p_{3/2})^{-1}(sd)^{1}$ configuration, located at higher excitation energy. These states can alternatively be identified as single particle states built on the ^{13}C*(3/2$^-$) state. The

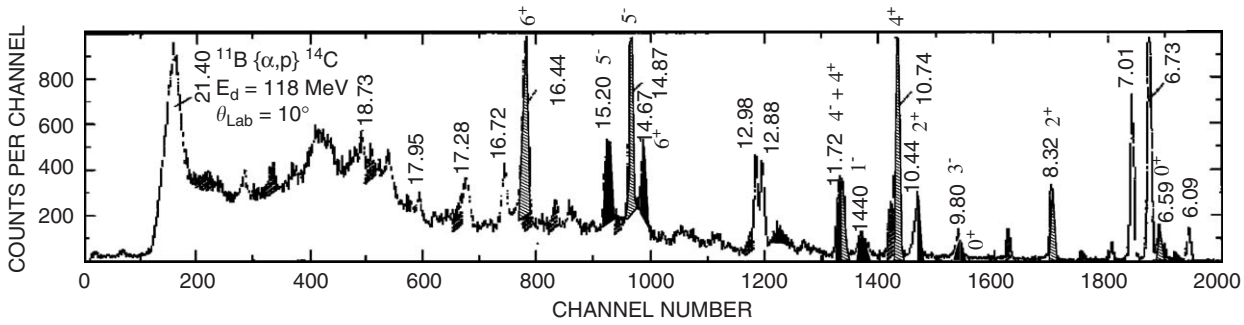

Fig. 48. Spectrum for the triton-transfer reaction ^{11}B(α, p) (adapted from Ref. [13]). The proposed band structure is indicated by black for prolate and by shaded (inclined \\) for oblate bands. Shading is also used to indicate contaminant lines.

resulting levels with positive parity will have (multi particle - multi hole) structure such as $(p_{3/2})^{-1}(p_{1/2})^{-1} \otimes (sd)^2$ for either the proton or the neutron configurations. With the proton excitation we can than have three 2^+ states based on different mixing of the configurations $(p_{1/2})^2$, $(s_{1/2})^2$, and $(d_{5/2})^2$, as for the case of the 0^+ states.

In order to proceed further we may assume that very few states of single-particle character are missing. The guideline is than that the "remaining" states are related to multi-particle excitations and to clustering and larger deformations. Such states should fall into classes of prolate and oblate rotational bands, their band-heads being close to the different cluster decay thresholds.

(4) *Cluster structures*: *results from multi–nucleon transfer.* For the states with cluster structure the selectivity of the various multi-nucleon transfers is most important. A spectrum of the reaction ^{9}Be(^{7}Li, d)^{14}C has been measured [290] with high resolution using a Q3D magnetic spectrometer at an ^{7}Li energy of 44 MeV (Fig. 47). For the reaction mechanism we expect the sequential transfer of an α-particle and a neutron or vice versa. In view of this, the reaction on ^{9}Be turns out not to be very selective relative to prolate or oblate states, because with the alpha-particle transfer both cluster states can be populated. The extra neutron will populate all orbits, the $p_{3/2}$, the $p_{1/2}$, the $s_{1/2}$, as well as the $d_{5/2}$ and $d_{3/2}$-shells.

The spectrum shown in Fig. 47 shows more states than observed in Fig. 46, due to the high resolution, but also due to a different selectivity of the reaction. There is again the preference for high spin states due to the large angular momentum mismatch between the mass 7 projectile and the ejectile of mass 2. Actually, the spectrum shown in Fig. 47 is similar to the spectrum observed in the ^{9}Be(^{6}Li, p) reaction in [6] obtained at a much lower energy, $E_{lab} = 17$ MeV. However, at this energy the compound nuclear process is dominating.

Another very useful reaction is the triton transfer reaction, which has been studied with good resolution via the ^{11}B(^{6}Li,^{3}He)^{14}C in [65] and also with the ^{11}B(α, p)^{14}C reaction in Ref. [13] (Fig. 48). These reactions show remarkable selectivity with an enhancement of the "oblate" cluster states. This observation can be directly related to the structure of the target, ^{11}B, which represents a $p_{3/2}$-hole in the oblate ^{12}C nucleus. Due to the large negative Q-values in the region of high excitation energy (10–18 MeV), these reactions also show a marked selectivity to high spin states. The (α, p) reaction spectrum in Fig. 48 shows as the strongest peaks those states which we later assign to the $K = 0^+$ oblate rotational band (see also Fig. 50). Similarly the states of the oblate $K = 3^-$ band are strongly populated, whereas the proposed prolate states are rather weak, consistent with our interpretation, that the parentage between target configuration and final state determines the probability of the reactions (Fig. 49).

The differential cross-section predominantly depend on the angular momentum transfer, and on the spin multiplicity of the final states, given by $(2J + 1)$. In order to classify the states their relative strength is compared in Table 4 after division by $(2J + 1)$. For a comparison of structural effects all yields are normalized to the value (200) of the first 2^+-state at 7.017 MeV. Note that the states, connected to the "oblate" and "prolate" bands are all equally well populated in (^{7}Li, d), with a tendency for a cut-off at the highest excitation energies.

8.3.3. The proposed oblate rotational bands

The cluster states with oblate shapes are identified using the selectivity of different reactions on targets with oblate shapes and cluster character, these are then grouped into individual bands [290].

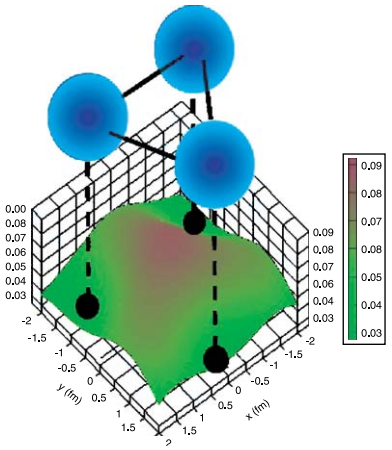

Fig. 49. The triangular shape of the cluster state in ^{14}C. The three α-particles are marked by black dots in a coordinate system as indicated. The density distribution of the valence neutrons is shown as a three-dimensional surface, for the 0_2^+-state (6.589 MeV) and the 3_2^--state (9.801 MeV), from [155].

The 0_2^+ state at 6.59 MeV of ^{14}C may be obtained with the same configurational components [99] as the ground state 0_1^+. The two states are mixed due to the pairing interaction with the configurations in the *p*-, and *sd*-shells, $^{12}C(0_1^+) \otimes [a(p_{1/2})^2 + b(s_{1/2})^2 + c(d_{5/2})^2]$. This gives three 0^+ states. Actually Itagaki et al. [154,155] predicted the oblate "triangular" state in ^{14}C with a spin/parity of 0^+ at 7.85 MeV, very close to the observed energy of the 0_2^+-state at 6.589 MeV. This result also indicates that this state is strongly related to the 0_2^+ in ^{12}C and to the special states in ^{13}C, with spins/parities of $1/2^-$ and $1/2^+$ at excitation energies of 8–10 MeV discussed before, see also Refs. [207,208]. The intrinsic density distribution of this unique configuration [155] is shown in Fig. 49. The figure shows the density of the valence neutrons in a triangular three centre structure, the positions of the α-particles are indicated.

Configurations with an intrinsically fixed "triangular" geometry, in ^{12}C and ^{14}C are expected to form states with a spin of 3^-. For ^{14}C it is most likely the 3_2^- state at 9.801 MeV, predicted by Itagaki et al. at 9.45 MeV. In the spectrum of the ^{5}He-transfer this 3_2^--state is strongly populated, as well as the oblate state at 8.32 MeV (2_2^+), and both are only weakly seen in the 2n-transfer spectrum. The proposed two oblate rotational bands in ^{14}C with $K = 0^+$ and 3^- are shown in Fig. 50. The moments of inertia as obtained from the fits to the excitation energies for these bands, with the parameters ($\hbar/2\Theta$) are $\hbar/2\Theta = 250$ and 290 keV for the $K = 0^+$ and 3^- bands, respectively.

8.3.4. The proposed prolate rotational bands

After the preceding compilation, there are many more states at the higher excitation energy in ^{14}C, which we expect to be cluster states, but with prolate deformations. The linear structure with the reflection asymmetric $^{10}\text{Be} + \alpha$ configuration, illustrated with the parity projection in Fig. 45, gives two rotational bands with $K = 0^\pm$ with a distinct energy splitting. The energies are plotted in Figs. 44 and 50, and the agreement with the rotational model is quite good. The energy splitting between the positive and the negative parity bands in ^{14}C is similar to that of the $K = 3/2$ parity doublet in ^{13}C.

8.3.5. ^{14}C decay studies

In addition to the classification of the ^{14}C states via their population characteristics and their potential rotational properties, it is also possible to deduce their structure via their particle decay, that is if they reside above the α-decay threshold. Such an approach was used by Soić et al. [253], in a study of the $^9\text{Be}(^7\text{Li}, ^{10}\text{Be} + \alpha)$ reaction, illustrated in Fig. 51.

This figure shows the α-decay of ^{14}C excited states to different final states in ^{10}Be. We see a close correspondence with the states populated in the $^{11}\text{B}(\alpha, \text{p})$ reaction (shown in Fig. 48) and the $^9\text{Be}(^7\text{Li}, \text{d})$ (Fig. 47) reactions. Most prominent are the so far unassigned states at 16.44, 18.7, 19.8 and 21.3 MeV. These states are observed in the decay study of the $^{12}\text{C}(^6\text{He}, \alpha, ^{10}\text{Be})\alpha$ reaction [209]. The highest excitation energy states seem to be associated with the

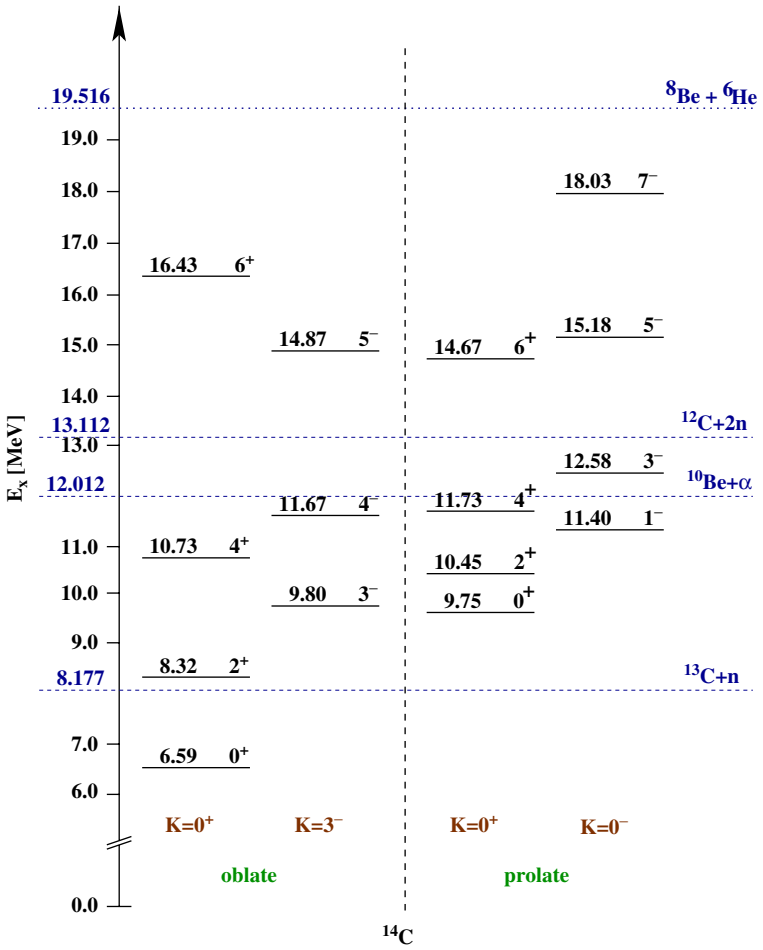

Fig. 50. Energy levels in ^{14}C, with their proposed spins selected from the population characteristics to form rotational bands. The states are used to build four bands with K-quantum numbers as indicated. Thresholds for structures related to the asymptotic fragmentation are shown, from [290].

decay into the 6 MeV states in ^{10}Be, associated with σ configurations of the valence neutrons. It would appear that the decay systematics show that there are indeed two kinds of states in ^{14}C corresponding to the overlap with the ^{10}Be ground or with the ~ 6 MeV excited state configurations. Such experiments provide a powerful structural link between the sub-components of different structure of the longer chain molecules. A recent measurement of the ^{14}C(^{13}C, ^{10}Be+α) reaction [233] finds a similar spectrum of states decaying to the $^{10}\mathrm{Be}_{gs} + \alpha$ final state. In this latter work, this decay channel was linked to the decay of oblate states in ^{14}C. The connection between the break-up states and either their oblate or prolate character requires a determination of their spins.

8.4. *Chain states in* $^{15-16}$C

For the heavier carbon isotopes $^{15-16}$C the isomeric chain states can be formed by adding one or two neutrons, respectively, to the configurations of ^{14}C discussed before. The role of the pairing interaction, however, is still an open question.

For ^{15}C, the chain states could be constructed based on the resonant sharing of a neutron between ^{10}Be and ^{4}He, namely between the lowest states of ^{11}Be and the ^{5}He resonance, a case where the resonant sharing of the neutron can be quite strong leading to a parity splitting in $K = 1/2$ states of similar size as in ^{13}C. In the results of the AMD calculations for states of ^{15}C, it is suggested that a linear-like structure may appear in the high-spin region for the spin and parities $19/2^-$ and $23/2^-$ at 25 MeV $\sim$ 30 MeV region of excitation energy. As shown in Fig. 52, the $19/2^-_1$ state

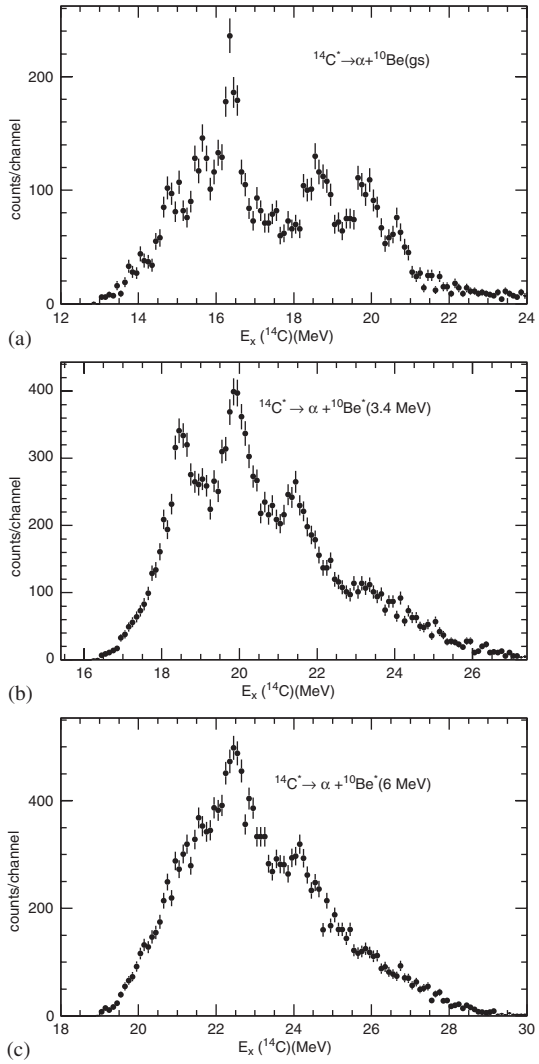

Fig. 51. Resonances in ^{14}C populated in the ^{9}Be(^{7}Li, ^{10}Be + α) reaction, and their decay into different states of ^{10}Be. Top frame: (a) decay to the ground; middle frame; (b) to the 2^{+}_{1} state and lower frame; (c) to the 6 MeV states. Different excited states in ^{14}C are observed to possess differing decay characteristics [253].

of ^{15}C has a largely deformed shape with a linear 3α-chain. It is found that one neutron occupies an *f*-like orbit, which has three nodes along the longitudinal direction as seen in Fig. 52(d). This neutron orbit is regarded as a molecular orbit around the 3α core. It should be noted that the presence of the large centrifugal barrier for this state means that even at high excitation the state would remain narrow and thus the bound state approximation employed in the calculations is reasonable. In the total matter density (Fig. 52(a)), one can see a two cluster-like structure, which corresponds to ^{11}Be+^{4}He.

The ^{11}Be+^{4}He clustering in the linear-chain structure is not the so-called weak-coupling clustering but is the strong-coupling one, where the paired two neutrons remain bound in the Be-core. In this case the spin of the ^{11}Be cluster is strongly coupled with the spin of the relative motion. As a result, the $19/2^{-}$ state contains various rotational states from the $K^{\pi}=1/2^{+}_{1}$ band of ^{11}Be. The $19/2^{-}$ states with linear chain structure are suggested to exist ∼ 15 MeV above the ^{11}Be+^{4}He threshold energy and ∼ 20 MeV above the neutron-decay threshold. The energy relative to the α-decay threshold is compatible to those for the known high-spin α-cluster states in ^{16}O and ^{20}Ne [138,202,257], and that relative to the neutron-decay threshold is almost the same as the one for the 8^{+} state in ^{12}Be. Therefore, it is considered

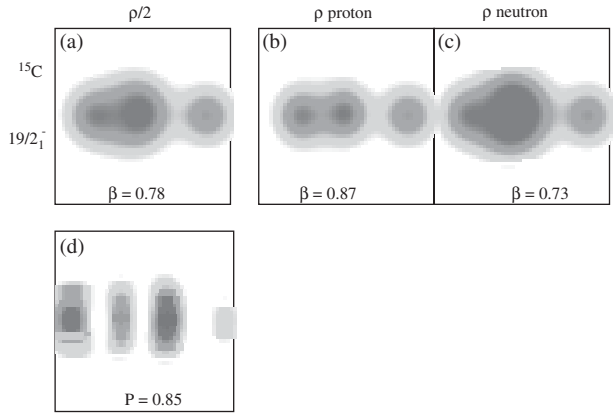

Fig. 52. Density distributions for the intrinsic states of the $J^{\pm} = 19/2^-_1$ state in ^{15}C, as obtained in the theoretical framework of AMD [169], the deformation parameter β_2 is indicated. The matter, as well as the proton and neutron densities are presented in frames (a), (b) and (c), respectively. The bottom frame, (d), presents the density of the highest single-particle neutron orbits, here P indicates the probability of the negative parity component in the single-particle orbit. The box size is 10 fm.

that these cluster states with high spins in ^{15}C might exist as resonant states. For the more qualitative prediction, further theoretical investigations are necessary and the stability against the particle decay should be investigated in more detail.

The most interesting carbon isotope is ^{16}C, which can have as the lowest energy chain state, a highly symmetric configuration with positive parity. As discussed by Itagaki [152], we can use different configurations for the individual valence neutrons located between the individual α-particles: (i) $(\pi)^2$; (ii) $(\sigma)^2$; and (iii) $(\sigma \times \pi)$. If the neutrons are in different orbitals, hybridized configurations [152] are expected. It was suggested that the linear-chain state with the 3α core can be stabilised in ^{16}C against the bending mode if such a mixed $(\pi)^2 \times (\sigma)^2$ configuration is formed, giving rise to mixed configurations reminiscent of hybridisation. The first steps in the quest for complete spectroscopy, with a study of the excited states of ^{16}C, have been started [44,45]. The states with molecular character are not expected at energies close to the ground state, but in excess of 20 MeV, as illustrated in Fig. 38. They are also not expected to be populated in multi-neutron transfer reactions. However, it is known that the structure of ^{16}C close to the ground state is a little unusual in that the $E2$ strength for the excitation of the first 2^+ appears to be hindered [145,129]. This suppression has been explained theoretically using a $^{14}\mathrm{C} + 2\mathrm{n}$ basis [141,258]. There appears to be a decoupling of the valence neutrons from the ^{14}C core [89], an effect also observed in ^{17}B [83]. This type of clustering is not associated with molecule formation, but may be linked to a new form of clustering which is predicted close to the neutron drip-line, see Section 9.1.

9. Future perspectives

The evidence for real (not "quasi") covalently bound nuclear cluster states is well established for dimers in the beryllium isotopes and partially for the carbon isotopes ^{13}C–^{14}C. We feel that the study of nuclear states built from clusters bound by valence neutrons in their molecular configurations is a field with a much larger scope. The most important cluster structures to consider are based on α-particles and ^{16}O, as was summarised in Fig. 4. Experimentally, this research will rely on a combination of charged-particle and γ-ray spectroscopy. While the unbound states will still be characterised by their charged particle decay modes, particle-γ coincidences will be an essential tool. For some cases of very narrow resonances the γ- and particle-decay branches may be established simultaneously. The recent developments in detection techniques and in theoretical models also promise that more complicated multi-cluster systems can be studied in the near future.

Although it is difficult to find many particle stable states for electromagnetic transitions, we can already draw some conclusions from the systematics of the energies of the bands and deduce their moments of inertia. These turn out to be consistent with the model descriptions. The moments of inertia of some cases shown in the present review are summarised in Table 5.

Table 5
Moments of inertia given as the factor $\hbar^2/2\Theta$ for rotational cluster bands in nuclei with $A \approx 10$–16, from experimental work and theoretical predictions

Nucleus	Band head	$\hbar^2/2\Theta$ (keV)	References
^{10}Be	$0^+_2, 1^-_1$	250	Dimer [282]
^{11}Be	$3/2^-_3$	230	Dimer [40]
^{12}Be	0^+_3	210	[40,107]
^{12}C	g.s.	740	[8]
^{13}C	$3/2^-_2, 3/2^+_3$	190	Chain [207]
^{14}C	$0^+_2, 3^-_2$	230,280	Oblate [290]
^{14}C	$0^+_3, 1^-_2$	120,130	Chain [290]
^{14}C	$0^+_2, 3^-_2$	300	Oblate [154,155]
^{16}C	0^+	150	Chain, pred. in [152]

Clearly these moments of inertia are very large, on the other hand the molecular states in light nuclei are only a small sample of the super- and hyper-deformed states in nuclei discussed already 30 years ago by Ragnarsson et al. [239].

9.1. Clustering at the drip line

Clustering will become important at the drip-line, because weakly bound systems will prevail. In the case of very light nuclei at the neutron drip-line, Horiuchi recently speculated [140] that clustering might actually be the preferred structural mode. Indeed in this way a nuclear system overcomes the problem of maximizing the interaction for the excess neutrons with protons. For a large neutron excess around an isospin zero core, the effective surface area of the core is increased by clusterisation. This allows the neutrons to be more widely distributed over the surface of the clusters. This effect is observed in the AMD calculations of the odd-A boron isotopes, (see Fig. 53), where an increased clustering into two separated cores appears with increasing neutron number.

For ^{17}B and for the drip-line nucleus ^{19}B a clusterisation into lithium and helium-like components surrounded by valence neutrons is observed. Molecular-like structure then plays an important role. Presently these structures remain the providence of theory and must be tested at the new generation of radioactive beam facilities. A very recent experimental study [83] of ^{17}B shows a decoupling of the valence neutrons from the core, similar to the case of ^{16}C in Ref. [89].

9.2. Longer chain states, rings and flowers

In order to find nuclear states with clustering and large deformations we may follow the predictions of the Nilsson–Strutinski method for deformation parameters beyond super-deformation ($\beta = 0.6$). Hyper-deformation is expected to be observed in many nuclei at excitation energies and angular momenta close to the fission (ternary) thresholds. The map of shell corrections from references [239,240] extends beyond values of deformation parameters of $\beta = 1.0$. The continuation to even more extended structures, is suggested by the concept of sums of magic clusters (see Table 1). The use of cluster model approaches which are partially discussed in this review will be needed to describe such nuclear states.

Another type of original nuclear structure can be observed with the predicted densities of the very neutron-rich carbon isotopes. The oblate shape of the structure with three α-particles remains, but in addition to the triangular shapes discussed in Section 7.2 for ^{14}C, the extra neutrons (see Fig. 54 from the AMD calculations in Ref. [172]), we observe oblate densities with higher order deformations (“flowers”).

The discussion of the multi α-cluster systems leads us immediately to the question of the stability of longer chain states. Their stability relative to a bending mode has to be considered. A stabilisation due to the covalent orbits is expected to be connected to the height of the potential barrier as function of the bending angle. In any case a folded chain, in the form of a ring of a regular oblate arrangement of clusters with symmetries due to rotations by an integer number (N) divisions of 360° is expected to have the lowest energy. The formation of such structures in the normal nuclear reactions considered in this review, seems to be impossible. However, the condensation into such clustered configurations from highly excited (and rotating) neutron-rich nuclear matter is a possibility. This picture of exotic

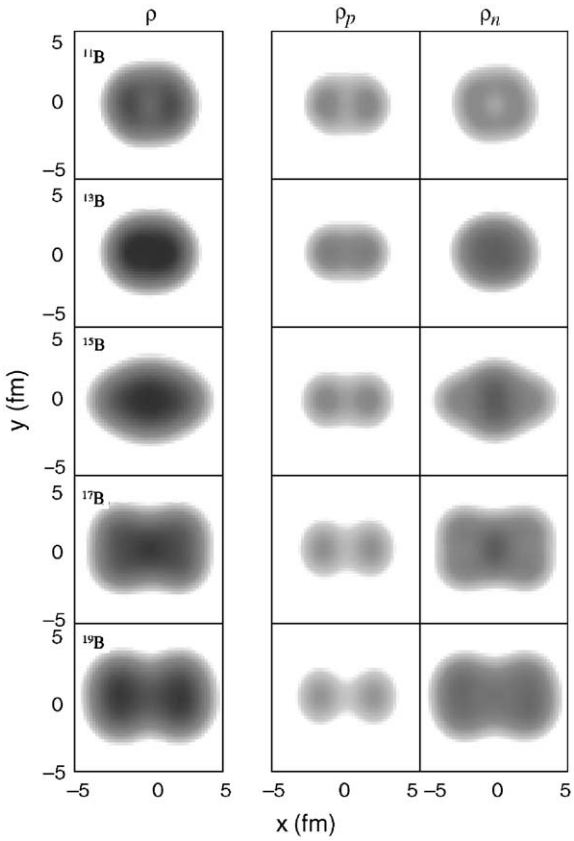

Fig. 53. Density distributions of boron isotopes, $^{11-19}$B, with parity projection from AMD calculations. The densities of the protons and neutrons as well as their sum, ρ, are shown, from [172].

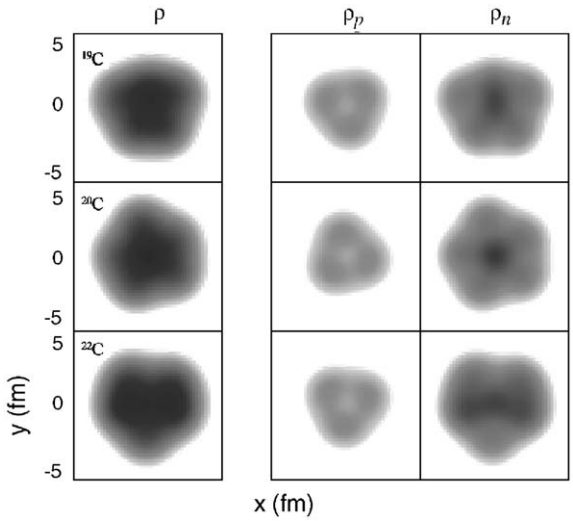

Fig. 54. Density distributions of in very neutron-rich isotopes of carbon, $^{19-22}$C, the intrinsic wave functions without parity projection are shown. The plot of the densities of the protons and neutrons as well as their sum illustrate the distinctly different deformations for neutrons and protons.

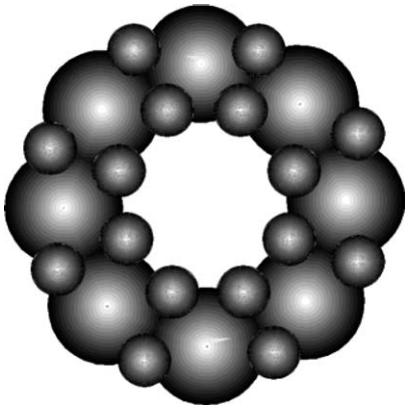

Fig. 55. Schematic visualization of the density distributions of a ring of alpha-particles (large balls), bound by valence neutrons (smaller balls), as envisaged by Wilkinson [299]. The valence neutrons have to be considered to be strongly delocalised so as to create the quantal molecular binding effect.

nuclei being formed from α-particles and neutrons, can be found in the ideas of Wilkinson [299]. Wilkinson discussed hot nuclear matter rotating with significant angular momenta, conditions which may be encountered in intermediate energy heavy-ion collisions. Such conditions, it was argued, would give rise to nuclear rings, composed of "touching" α-particles with intervening pairs of neutrons such as shown in Fig. 55. The search for such structures is obviously a considerable challenge.

9.3. Molecular structures in heavier nuclei

In the experimental search for nuclear cluster structure the systems in the mass 18–36 region have been a popular subject at the time of the detailed studies of the α-particle transfer reactions [19]. In even heavier nuclei a strong decrease of the α-spectroscopic factor in the ground states with increasing mass number and with increasing neutron excess is observed. For such nuclei close to the valley of stability the thresholds for the decomposition into clusters (according to the Ikeda diagram) are high. Excited states in these nuclei have a large width, because they are embedded in the continuum with a high density of compound nuclear states. However, clustering aspects for "exotic" heavy nuclei with $N = Z$, nuclei consisting of $N = Z$ clusters with a few extra valence nucleons on the "proton-rich" side of the valley of stability, will appear at lower excitation energies. For these systems a new field of cluster structure awaits exploration. It must be studied with proton-rich projectiles at the future facilities: the rare isotope accelerators planned in many laboratories.

Acknowledgments

It is a pleasure to thank many colleagues, who were involved and helped to revive the work on molecular structure in nuclei. For contributions to this review and for checking many details, we thank, in particular, M. Milin and H.G. Bohlen, and referees for their detailed criticism and suggestions. M. Freer thanks the A.v. Humboldt foundation for their support.

References

[1] Y. Abe, J. Hiura, H. Tanaka, Prog. Theor. Phys. 49 (1973) 800.
[2] Y. Abe, Nuclear Molecular Phenomena, in: N. Cindro (Ed.), Proceedings of the International Conference on Resonances in Heavy Ion Reactions, North-Holland, Amsterdam, 1978, p. 211.
[3] S. Aberg, L.-O. Jönsson, Z. Phys. A 349 (1994) 205.
[4] A. Adahchour, D. Baye, P. Descouvemont, Nucl. Phys. A 579 (1994) 305.
[5] S. Ahmed, et al., Phys. Rev. C 69 (2004) 024303.
[6] F. Ajzenberg-Selove, et al., Phys. Lett. B 40 (1972) 205.
[7] F. Ajzenberg-Selove, Nucl. Phys. A 506 (1990) 1.

[8] F. Ajzenberg-Selove, Nucl. Phys. A 523 (1991) 1.
[9] D.E. Alburger, S. Mordechai, H.T. Fortune, R. Middleton, Phys. Rev. C 18 (1978) 2727.
[10] S. Ali, A.R. Bodmer, Nucl. Phys. 80 (1966) 99.
[11] E. Almqvist, D.A. Bromley, J.A. Kuehner, Phys. Rev. Lett. 4 (1960) 515.
[12] T. Ando, K. Ikeda, A. Tohsaki, Prog. Theor. Phys. 64 (1980) 1608.
[13] R. Andrews, et al., Nucl. Phys. A 468 (1987) 43.
[14] S. Aoyama, S. Mukai, K. Kato, K. Ikeda, Prog. Theor. Phys. 93 (1995) 99.
[15] S. Aoyama, K. Kato, K. Ikeda, Prog. Theor. Phys. 142 (Suppl.) (2001) 35.
[16] K. Arai, Y. Ogawa, Y. Suzuki, K. Varga, Phys. Rev. C 54 (1996) 132.
[17] K. Arai, P. Descouvemont, D. Baye, W.N. Catford, Phys. Rev. C 68 (2003) 014310.
[18] K. Arai, Phys. Rev. C 69 (2004) 014309.
[19] A. Arima, S. Kubono, in: D.A. Bromley (Ed.), Treatise in Heavy Ion Science, vol. 1, Plenum Press, NY, 1985, p. 617 and refs. therein.
[20] N.I. Ashwood, et al., Phys. Rev. C 63 (2001) 034315.
[21] N.I. Ashwood, et al., Phys. Rev. C 68 (2003) 017603.
[22] U. Atzrott, P. Mohr, H. Abele, C. Hillenmayer, G. Staudt, Phys. Rev. C 53 (1996) 1336.
[23] D.A. Auton, Nucl. Phys. A 157 (1970) 305.
[24] W. Bauhoff, H. Schultheis, R. Schultheis, Phys. Rev. C 22 (1980) 861.
[25] W. Bauhoff, H. Schultheis, R. Schultheis, Phys. Rev. C 26 (1982) 1725.
[26] D. Baye, J. Deenen, Y. Salmon, Nucl. Phys. A 289 (1977) 511.
[27] D. Baye, Nucl. Phys. A 460 (1986) 581.
[28] D. Baye, Phys. Rev. Lett. 58 (1987) 2738.
[29] D. Baye, P. Descouvemont, in: K. Ikeda (Ed.), Proceedings of the Fifth International Conference on Clustering Aspects in Nuclear and Subnuclear Systems (1988), Kyoto, Japan, Phys. Society of Japan, 1989, p. 103.
[30] C.W. Beausang, J. Simpson, J. Phys. G 22 (1996) 527.
[31] C. Beck, Y. Abe, N. Aissoaui, B. Djerroud, F. Haas, Phys. Rev. C 49 (1994) 2618.
[32] C. Beck, Y. Abe, N. Aissoaui, B. Djerroud, F. Haas, Nucl. Phys. A 534 (1995) 445.
[33] A.V. Belozyorov, R. Kalpakchieva, Yu.E. Penionzhkevich, Z. Dlouhy, S. Pisko, J. Vincour, H.G. Bohlen, M. von Lucke-Petsch, A.N. Ostrowski, D.V. Alexandrov, E.Yu. Nikolskii, B.G. Novatskii, D.N. Stepanov, Nucl. Phys. A 636 (1998) 419.
[34] S.J. Bennett, M. Freer, B.R. Fulton, J.T. Murgatroyd, P.J. Woods, S.C. Allcock, W.D.M. Rae, A.E. Smith, J.S. Lilley, R.R. Betts, Nucl. Phys. A 534 (1991) 445.
[35] H.A. Bethe, R.F. Bacher, Rev. Mod. Phys. 8 (1936) 82–229;
H.A. Bethe, Rev. Mod. Phys. 9 (1937) 69.
[36] R. Bijker, F. Iachello, Annals of Physics 298 (2003) 334.
[37] R. Bilwes, B. Bilwes, L. Stuttge, et al., Phys. Rev. Lett. 70 (1993) 259.
[38] H.G. Bohlen, W. von Oertzen, Phys. Lett. B 37 (1971) 451.
[39] H.G. Bohlen, et al., Nuovo Cimento A 111 (1998) 841.
[40] H.G. Bohlen, et al., Prog. Part. Nucl. Phys. A 42 (1999) 17.
[41] H.G. Bohlen, W. von Oertzen, A. Blazevic, B. Gebauer, M. Milin, T. Kokalova, Ch. Schulz, S. Thummerer, A. Tumino, in: Yu.E. Penionzhkevich, E.A. Cherepanov (Eds.), in: Proceedings of the International Symposium on Exotic Nuclei, Lake Baikal, Russia, 2001, World Scientific, Singapore, 2002, p. 453.
[42] H.G. Bohlen, et al., in: R. Jolos, W. Scheid (Eds.), Proceedings of the Symposium on Nuclear Clusters, Rauischholzhausen, 2002, EP Systema, Debrecen, Hungary, 2003, p. 53.
[44] H.G. Bohlen, et al., Phys. Rev. C 68 (2003) 054606.
[45] H.G. Bohlen, R. Kalpakchieva, W. von Oertzen, T.N. Massey, A.A. Ogloblin, G. de Angelis, Ch. Schulz, Tz. Kokalova, C. Wheldon, J. Phys. G 31 (2005) 1461.
[46] A. Bohr, B. Mottelson, Nuclear Structure, vol. II, Benjamin, Inc., Reading MA, 1975.
[47] M. Brack, J. Damgard, A.S. Jensen, H.C. Pauli, V.M. Strutinski, C.Y. Wong, Rev. Mod. Phys. 44 (1972) 320.
[48] M.E. Brandan, G.R. Satchler, Phys. Rep. 285 (1997) 143.
[49] P. Braun-Munzinger, J. Barrette, Phys. Rep. 87 (1982) 209.
[50] C.A. Bremner, S.P.G. Chappell, W.D.M. Rae, I. Boztosun, M. Freer, M.P. Nicoli, S.M. Singer, B.R. Fulton, D.L. Watson, B.J. Greenhalgh, G.K. Dillon, R.L. Cowin, Phys. Rev. C 66 (2002) 034605.
[51] D.M. Brink, in: C. Bloch (Ed.), Proceedings of the International School of Physics “Enrico Fermi”, Varenna, 1965, Course, 36, Academic Press, New York, 1966, p. 247.
[52] D.A. Bromley, J.A. Kuehner, E. Almqvist, 1960, Phys. Rev. Lett 4 (1960) 365.
[53] D.A. Bromley, J.A. Kuehner, E. Almqvist, Phys. Rev. 123 (1961) 878.
[54] P.A. Butler, W. Nazarewicz, Rev. Mod. Phys. 68 (1996) 350.
[55] J. Carlson, Phys. Rev. C 38 (1988) 1879.
[56] T.U. Chan, M. Agard, J.F. Bruandet, C. Morand, Phys. Rev. C 19 (1979) 244.
[57] T.U. Chan, Phys. Rev. C 36 (1987) 838.
[58] S.P.G. Chappell, D.L. Watson, S.P. Fox, C.D. Jones, W.D.M. Rae, P.M. Simmons, M. Freer, B.R. Fulton, N.M. Clarke, N. Curtis, M.J. Leddy, J.S. Pople, S.J. Hall, R.P. Ward, G. Tungate, W.N. Catford, G.J. Gyapong, S.M. Singer, P.H. Regan, Phys. Rev. C 51 (1995) 695.
[59] S.P.G. Chappell, W.D.M. Rae, Phys. Rev. C 53 (1996) 2879.

[60] S.P.G. Chappell, W.D.M. Rae, C.A. Bremner, G.K. Dillon, D.L. Watson, B. Greenhalgh, R.L. Cowin, M. Freer, S.M. Singer, Phys. Lett. B 444 (1998) 260.
[61] P. Chevallier, F. Scheibling, G. Goldring, I. Plessar, M.W. Sachs, Phys. Rev. 160 (1967) 827.
[62] N. Cindro, Rivista del Nuovo Cimento 4 (1981) 1.
[63] N. Cindro, Ann. Phys. Fr. 13 (1988) 289.
[64] N. Cindro, R.M. Freeman, F. Haas, Phys. Rev. C 33 (1986) 1280.
[65] M.E. Clark, K.W. Kemper, Nucl. Phys. A 425 (1984) 185.
[66] S. Cohen, D. Kurath, Nucl. Phys. 73 (1965) 1.
[67] T.M. Cormier, J. Applegate, G.M. Berkowitz, P. Braun-Munzinger, P.M. Cormier, J.W. Harris, C.M. Jachcinski, L.L. Lee Jr., J. Barrette, H.E. Wegner, Phys. Rev. Lett. 38 (1977) 940;
T.M. Cormier, C.M. Jachcinski, G.M. Berkowitz, P. Braun-Munzinger, P.M. Cormier, M. Gai, J.W. Harris, J. Barrette, H.E. Wegner, 1978, Phys. Rev. Lett. 40 (1978) 924.
[68] E. Costanzo, M. Lattuada, S. Romano, D. Vinciguerra, N. Cindro, M. Zadro, M. Freer, B.R. Fulton, W.D.M. Rae, Phys. Rev. C 44 (1991) 111.
[69] E. Costanzo, et al., Eur. Phys. J. A 5 (1999) 69.
[70] A. Csótó, Phys. Rev. C 48 (1993) 165.
[71] A. Csótó, Phys. Rev. C 49 (1994) 3035.
[72] N. Curtis, A.St.J. Murphy, N.M. Clarke, M. Freer, B.R. Fulton, S.J. Hall, M.J. Leddy, J.S. Pople, G. Tungate, R.P. Ward, W.N. Catford, G.J. Gyapong, S.M. Singer, S.P.G. Chappell, S.P. Fox, C.D. Jones, D.L. Watson, W.D.M. Rae, P.M. Simmons, P.H. Regan, Phys. Rev. C 53 (1996) 1804.
[73] N. Curtis, M. Shawcross, W.N. Catford, B.R. Fulton, N.M. Clarke, S.J. Hall, J.T. Murgatroyd, S.P.G. Chappell, R.L. Cowin, G. Dillon, D.L. Watson, Phys. Rev. C 62 (2000) 034603.
[74] N. Curtis, D.D. Caussyn, N.R. Fletcher, F. Maréchal, N. Fay, D. Robson, Phys. Rev. C 64 (2001) 044604.
[75] N. Curtis, et al., Phys. Rev. C 70 (2004) 014305.
[76] N. Curtis, et al., Phys. Rev. C 73 (2006) 057301.
[77] P. Descouvemont, Phys. Rev. C 52 (1995) 704.
[78] P. Descouvemont, Nucl. Phys. A 626 (1997) 647.
[79] P. Descouvemont, Eur. Phys. J. A 12 (2001) 413.
[80] P. Descouvemont, D. Baye, Phys. Lett. B 505 (2001) 71.
[81] P. Descouvemont, Nucl. Phys. A 699 (2002) 463.
[82] N. de Takacsy, S. Das Gupta, Phys. Lett. B 33 (1970) 556.
[83] Zs. Dombrádi, et al., Phys. Lett. B 621 (2005) 81.
[84] A.H. Dóte, Horiuchi, Y. Kanada-En'yo, Phys. Rev. C 56 (2001) 1844.
[85] J. Dudek, A. Gozdz, N. Schunck, M. Mikiewicz, Phys. Rev. Lett. 88 (2002) 252502.
[86] M. Dufour, P. Descouvemont, Nucl. Phys. A 672 (2000) 153.
[87] M. Dufour, P. Descouvemont, Nucl. Phys. A 726 (2003) 53.
[88] J.M. Eisenberg, W. Greiner, Microscopic Theory of the Nucleus, vol. 3, North-Holland Publishing, Amsterdam, 1972 p. 426.
[89] Z. Elekes, et al., Phys. Lett. B 586 (2004) 34.
[90] O. Endō, I. Shimodaya, J. Hiura, Prog. Theor. Phys. 31 (1964) 1157.
[91] K.A. Erb, D.A. Bromley, in: D.A. Bromley (Ed.), Treatise in Heavy Ion Science, vol. 3, Plenum Press, NY, 1985.
[92] D.V. Fedorov, A.S. Jensen, Phys. Lett. B 389 (1996) 631.
[93] H. Feldmeier, K. Bieler, J. Schnack, Nucl. Phys. A 586 (1995) 493.
[94] H. Feshbach, J. Phys. Colloq. 11-C5-37 (Fr. Suppl.) (1976) 177.
[95] R. Feynman, The Feynman Lectures in Physics, vol. III.
[96] D. Fleming, et al., Phys. Rev. 166 (1968) 1012.
[97] H. Flocard, P.H. Heenen, S.J. Krieger, M.S. Weiss, Prog. Theor. Phys. 72 (1984) 1000.
[98] A. Fonseca, J. Revai, A. Matveenko, Nucl. Phys. A 326 (1979) 182;
A. Fonseca, J. Revai, A. Matveenko, Nucl. Phys. A 339 (1980) 465
[99] H.T. Fortune, G.S. Stephans, Phys. Rev. C 25 (1982) 1.
[100] H.T. Fortune, et al., Phys. Rev. C 50 (1994) 1355.
[101] R.M. Freeman, et al., Phys. Rev. C 38 (1988) 1081.
[102] R.M. Freeman, F. Haas, A. Elanique, A. Morsad, C. Beck, Phys. Rev. C 51 (1995) 3504.
[103] M. Freer, R.R. Betts, A.H. Wuosmaa, Nucl. Phys. A 587 (1995) 36.
[104] M. Freer, N.M. Clarke, R.A. Le Marechal, G. Tungate, R.P. Ward, W.D.M. Rae, Phys. Rev. C 51 (1995) 3174.
[105] M. Freer, A.C. Merchant, J. Phys. G 23 (1997) 261.
[106] M. Freer, N.M. Clarke, B.R. Fulton, J.T. Murgatroyd, A.St.J. Murphy, S.P.G. Chappell, R.L. Cowin, G. Dillon, D.L. Watson, W.N. Catford, N. Curtis, M. Shawcross, V.F.E. Pucknell, Phys. Rev. C 57 (1998) 1277.
[107] M. Freer, et al., Phys. Rev. Lett. 82 (1999) 295.
[108] M. Freer, J.T. Murgatroyd, S.M. Singer, N. Curtis, D.J. Henderson, D.J. Hofman, A.H. Wuosmaa, Phys. Rev. C 63 (2001) 034317.
[109] M. Freer, C. R. Physique 4 (2003) 475.
[110] M. Freer, et al., Phys. Rev. Lett. 96 (2006) 042501.
[111] Y. Fujiwara, et al., Prog. Theor. Phys. 68 (Suppl.) (1980) 29.

[112] Y. Fukushima, M. Kamimura, in: T. Marumori (Ed.), Proceedings of the International Conference on Nuclear Structure, Tokyo, 1977;
Y. Fukushima, M. Kamimura, J. Phys. Soc. Jpn. 44 (1978) 225;
M. Kamimura, Nucl. Phys. A 351 (1981) 456.
[113] B.R. Fulton, W.D.M. Rae, J. Phys. G 16 (1990) 333.
[114] B.R. Fulton, in: M. Korolija, Z. Basrak, R. Caplar (Eds.), Proceedings of the Seventh International Conference on Clustering Aspects of Nuclear Structure and Dynamics, Island of Rab, Croatia, 1999, World Scientific, Singapore, River Edge, NJ, 2000, p. 122.
[115] Y. Funaki, A. Tohsaki, H. Horiuchi, P. Schuck, G. Röpke, Phys. Rev. C 67 (2003) 051306.
[116] H.O.U. Fynbo, Y. Prezado, J. Äysto, U.C. Bergmann, M.J.G. Borge, P. Dendooven, W. Huang, J. Huikari, H. Jeppesen, P. Jones, B. Jonson, M. Meister, G. Nyman, M. Oinonen, K. Riisager, O. Tengblad, I.S. Vogelius, Y. Wang, L. Weissman, K.W. Rolander, Eur. Phys. J. A 15 (2002) 135.
[117] W. Galati, J.D. Brandenberger, J.L. Weil, Phys. Rev. C 5 (1972) 1508.
[118] G. Gamow, Proc. Roy. Soc. A 126 (1930) 632.
[119] V.Z. Goldberg, W.H. Traska, G.V. Rogachev, et al., in: R. Jolos, W. Scheid (Eds.), Proceedings of the Symposium on Nuclear Clusters, Rauischholzhausen, EP Systema, Debrecen, Hungary, 2003, p. 89.
[120] W. Greiner, J.Y. Park, W. Scheid, Nuclear Molecules, World Scientific, Singapore, 1995 p. 48 and p.91.
[121] J.J. Griffin, J.A. Wheeler, Phys. Rev. 108 (1957) 311.
[122] F. Haas, Y. Abe, Phys. Rev. Lett. 46 (1981) 1667.
[123] L.R. Hafstad, E. Teller, Phys. Rev. 54 (1938) 681.
[124] M.N. Harakeh, et al., Nucl. Phys. A 344 (1980) 15.
[125] M. Harvey, Proceedings of the Second International Conference on Clustering Phenomena in Nuclei, College Park, USDERA Report ORO-4856-26, 1975, p. 549.
[126] W. Heisenberg, Z. Physik 96 (1935) 473.
[127] L. Hernandez de la Pena, P.O. Hess, G. Levai, A. Algora, J. Phys. G 27 (2001) 2019.
[128] G. Herzberg, Molecular Spectra and Molecular Structure, vol. I, Spectra of Diatomic Molecules, van Nostrand Comp. Inc., Princeton, 1950.
[129] K. Heyde, L. Fortunato, J.L. Wood, Phys. Rev. Lett. 94 (2005) 199201.
[130] D.L. Hill, J.A. Wheeler, Phys. Rev. 89 (1953) 1102.
[131] Y. Hirabayashi, Y. Sakuragi, Y. Abe, Phys. Rev. Lett. 74 (1994) 4141.
[132] J. Hiura, I. Shimodaya, Prog. Theor. Phys. 30 (1963) 585;
J. Hiura, I. Shimodaya, Prog. Theor. Phys. 36 (1966) 977.
[133] C.H. Holbrow, et al., Phys. Rev. C 9 (1974) 902.
[134] H. Horiuchi, K. Ikeda, Prog. Theor. Phys. A 40 (1968) 277.
[135] H. Horiuchi, Prog. Theor. Phys. 43 (1970) 375.
[136] H. Horiuchi, K. Ikeda, Y. Suzuki, Prog. Theor. Phys. 52 (Suppl.) (1972) Chapt. 3.
[137] H. Horiuchi, Prog. Theor. Phys. 51 (1974) 1266;
H. Horiuchi, Prog. Theor. Phys. 53 (1975) 447.
[138] H. Horiuchi, K. Ikeda, Cluster model of the nucleus, International Review of Nuclear Physics, vol. 4, World Scientific, Singapore, 1986, p. 1, and references therein.
[139] H. Horiuchi, Y. Kanada-En'yo, Nucl. Phys. A 616 (1997) 394c.
[140] H. Horiuchi, in: M. Korolija, Z. Basrak, R. Caplar (Eds.), Proceedings of the Seventh International Conference on Clustering Aspects of Nuclear Structure and Dynamics, Island of Rab, Croatia, 1999, World Scientific, Singapore, River Edge, NJ, 2000, p. 405.
[141] W. Horiuchi, Y. Suzuki, Phys. Rev. C 73 (2006) 037304.
[142] F. Hoyle, The Astrophys. J. Suppl. Ser. 1 (1954) 12.
[143] F. Iachello, in: J.S. Lilley, M.A. Nagarajan (Eds.), Proceedings of the International Conference Clustering Aspects of Nuclear Structure, Daresbury, Reidel Publ. Company, 1985, p. 101.
[144] K. Ikeda, N. Tagikawa, H. Horiuchi, Prog. Theor. Phys. 464 (Suppl.) (1968).
[145] N. Imai, et al., Phys. Rev. Lett. 92 (2004) 062501.
[147] B. Imanishi, W. von Oertzen, Phys. Lett. B 87 (1979) 188.
[148] B. Imanishi, W. von Oertzen, Phys. Rep. 155 (1987) 29.
[149] B. Imanishi, W. von Oertzen, H. Voit, Phys. Rev. C 35 (1987) 359.
[150] N. Itagaki, S. Okabe, Phys. Rev. C 61 (2000) 044306.
[151] N. Itagaki, S. Okabe, K. Ikeda, Phys. Rev. C 62 (2000) 034301.
[152] N. Itagaki, S. Okabe, K. Ikeda, I. Tanihata, Phys. Rev. C 64 (2001) 014301.
[153] N. Itagaki, S. Hirose, T. Otsuka, S. Okabe, K. Ikeda, Phys. Rev. C 65 (2002) 044302.
[154] N. Itagaki, T. Otsuka, S. Okabe, K. Ikeda, in: R. Jolos, W. Scheid (Eds.), Proceedings of the Symposium on Nuclear Clusters, Rauischholzhausen, EP Systema, Debrecen, Hungary, 2003, p. 47.
[155] N. Itagaki, T. Otsuka, K. Ikeda, S. Okabe, Phys. Rev. Lett. 92 (2004) 014301.
[156] M. Ito, Y. Sakuragi, Phys. Rev. C 62 (2000) 064310.
[157] M. Ito, Y. Sakuragi, Y. Hirabayashi, Phys. Rev. C 63 (2001) 064303.
[159] M. Ito, Y. Hirabayashi, Y. Sakuragi, Phys. Rev. C 66 (2002) 034307.
[160] M. Ito, K. Kato, K. Ikeda, Phys. Lett. B 588 (2004) 43.
[161] M. Ito, Phys. Lett. B 636 (2006) 293.
[162] M. Itoh, et al., Nucl. Phys. A 738 (2004) 268.

[163] H. Iwasaki, et al., Phys. Lett. B 491 (2000) 8.
[164] J.D. Jackson, Phys. Rep. 320 (1999) 27.
[165] A.S. Jensen, K. Riisager, D.V. Fedorov, E. Garrido, Rev. Mod. Phys. 76 (2004) 215.
[166] Y. Kanada-En'yo, H. Horiuchi, Phys. Rev. C 52 (1995) 628.
[167] Y. Kanada-En'yo, H. Horiuchi, A. Ono, Phys. Rev. C 52 (1995) 647.
[168] Y. Kanada-En'yo, H. Horiuchi, Phys. Rev. C 55 (1997) 2860.
[169] Y. Kanada-En'yo, Phys. Rev. Lett. 81 (1998) 5291.
[170] Y. Kanada-En'yo, H. Horiuchi, A. Dóte, J. Phys. G 24 (1998) 1499.
[171] Y. Kanada-En'yo, H. Horiuchi, A. Dóte, Phys. Rev. C 64 (1999) 064304.
[172] Y. Kanada-En'yo, H. Horiuchi, Prog. Theor. Phys. 142 (Suppl) (2001) 205.
[173] Y. Kanada-En'yo, H. Horiuchi, Phys. Rev. C 66 (2002) 024305.
[174] Y. Kanada-En'yo, Phys. Rev. C 66 (2002) 011303(R).
[175] Y. Kanada-En'yo, H. Horiuchi, Phys. Rev. C 68 (2003) 014319.
[176] Y. Kanada-En'yo, M. Kimura, H. Horiuchi, C. R. Physique 4 (2003) 497.
[177] D.T. Khoa, W. von Oertzen, Phys. Lett. B 304 (1993) 8.
[178] D.T. Khoa, W. von Oertzen, H.G. Bohlen, Phys. Rev. C 49 (1994) 1652.
[179] D.T. Khoa, W. von Oertzen, Phys. Lett. 342B (1995) 6.
[180] D.T. Khoa, G.R. Satchler, W. von Oertzen, Phys. Rev. C 56 (1997) 954.
[181] D.T. Khoa, W. von Oertzen, H.G. Bohlen, F. Nuoffer, Nucl. Phys. A 672 (2000) 387.
[182] M. Kimura, H. Horiuchi, Phys. Rev. C 69 (2004) 051304(R).
[183] Y. Kondo, Y. Abe, T. Matsuse, Phys. Rev. C 19 (1979) 1356.
[184] Y. Kondo, F. Michel, G. Reidemeister, Phys. Lett. B 242 (1990) 340.
[185] A.A. Korsheninnikov, et al., Phys. Lett. B 343 (1995) 53.
[186] L. Kraus, et al., Phys. Rev. C 37 (1988) 2529.
[187] R. Kunz, et al., Phys. Rev. C 53 (1996) 2486.
[188] A.M. Lane, Rev. Mod. Phys. 32 (1960) 519.
[189] M. Labiche, et al., Phys. Rev. C 60 (1999) 027303.
[190] L. Landau, Phys. Z. Sov. 2 (1932) 46;
C. Zener, Proc. Roy. Soc. London A 147 (1932) 696.
[191] G. Leander, S.E. Larsson, Nucl. Phys. A 239 (1975) 93.
[192] T.-S.H. Lee, D. Kurath, Phys. Rev. C 22 (1980) 1670.
[193] C. Lee, et al., Phys. Rev. C 58 (1998) 1005.
[194] R.A. Le Marechal, N.M. Clarke, M. Freer, B.R. Fulton, S.J. Hall, S.J. Hoad, G.R. Kelly, R.P. Ward, C.D. Jones, P. Lee, D.L. Watson, Phys. Rev. C 55 (1997) 1881.
[195] E. Liatard, et al., Europhys. Lett. 13 (1990) 401.
[196] J.A. Liendo, N. Curtis, D.D. Caussyn, N.R. Fletcher, T. Kurtukian-Nieto, Phys. Rev. C 65 (2002) 034317.
[197] J.P. Lowe, Quantum Chemistry, second ed., Academic Press, New York, 1997.
[198] R. Machleidt, K. Holinde, Ch. Elster, Phys. Rep. 149 (1987) 1.
[199] F.M. Marques, et al., Phys. Lett. B 476 (2000) 219.
[200] S. Marsh, W.D.M. Rae, Phys. Lett. B 153 (1985) 21.
[201] S. Marsh, W.D.M. Rae, Phys. Lett. B 180 (1986) 185.
[202] T. Matsuse, M Kamimura, Y. Fukushima, Prog. Theor. Phys. 53 (1975) 706.
[203] P. McEwan, M. Freer, J. Phys. G 30 (2004) 1.
[204] A.C. Merchant, W.D.M. Rae, Nucl. Phys. A 549 (1992) 431.
[205] C.J. Metelko, M. Freer, N.I. Ashwood, N. Curtis, N.M. Clarke, N. Soic, V.A. Ziman, R.J. Woolliscroft, S.D. Pain, V.F.E. Pucknell, R.C. Lemmon, B.R. Fulton, D.L. Watson, R.P. Ward, D. Varley, Phys. Rev. C 68 (2003) 054321.
[206] F. Michel, S. Ohkubo, G. Reidemeister, Progr. Theor. Phys. 132 (Suppl.) (1998) 7.
[207] M. Milin, W. von Oertzen, Eur. Phys. J. A 14 (2002) 295.
[208] M. Milin, W. von Oertzen, Fizika B 12 (2003) 61.
[209] M. Milin, et al., Nucl. Phys. A 730 (2004) 285.
[210] M. Milin, et al., Nucl. Phys. A 763 (2005) 623.
[211] D.J. Millener, et al., Phys. Rev. C 39 (1989) 14.
[212] P. Navrátil, J.P. Vary, B.R. Barrett, Phys. Rev. Lett. 84 (2000) 5728;
P. Navrátil, J.P. Vary, B.R. Barrett, Phys. Rev. C 62 (2000) 054311.
[213] P. Navrátil, W. Erich Ormand, Phys. Rev. C 68 (2003) 034305.
[214] W. Nazarewicz, in: Proceedings of the International Conference on Nuclear Shapes and Nuclear Structure at Low Excitation Energie, Cargese, Plenum, New York, 1991.
[215] W. Nazarewicz, J. Dobaczewski, Phys. Rev. Lett. 68 (1992) 154.
[216] T. Neff, H. Feldmeier, Nucl. Phys. A 713 (2003) 311 and ⟨http://theory.gsi.de⟩.
[217] M.P. Nicoli, F. Haas, R.M. Freeman, et al., Phys. Rev. C 60 (1999) 064608.
[218] S.G. Nilsson, Mat. Fys. Medd. Dan. Vid. Selsk. 29 (16) (1955).
[219] R. Nouicer, et al., Phys. Rev. C 60 (1999) 4.

[220] Y. Ogawa, K. Arai, Y. Suzuki, K. Varga, Nucl. Phys. A 673 (2000) 122.
[221] S. Ohkubo, Phys. Rev. Lett. 74 (1995) 2176.
[222] S. Ohkubo, K. Yamashita, Phys. Rev. C 66 (2002) 021301.
[223] S. Okabe, Y. Abe, H. Tanaka, Prog. Theor. Phys. 57 (1979) 866;
S. Okabe, Y. Abe, Prog. Theor. Phys. 61 (1979) 1049.
[224] A. Ono, H. Horiuchi, T. Maruyama, A. Ohnishi, Prog. Theor. Phys. 87 (1992) 1185.
[225] A. Ono, H. Horiuchi, Phys. Rev. C 51 (1995) 299.
[226] A. Ono, H. Horiuchi, T. Maruyama, A. Ohnishi, Phys. Rev. C 47 (1993) 2652.
[227] A.N. Ostrowski, H.G. Bohlen, A.S. Demianova, et al., Z. Physik A 343 (1992) 489.
[228] V.R. Pandharipande, Nucl. Phys. A 738 (2004) 66.
[229] J.Y. Park, W. Greiner, W. Scheid, Phys. Rev. C 21 (1980) 958;
J.Y. Park, W. Greiner, W. Scheid, Phys. Rev C 25 (1982) 1902.
[230] L. Pauling, The Nature of the Chemical Bond, Cornell University Press, Ithaca, 1960.
[231] R.J. Peterson, Nucl. Phys. A 377 (1982) 41.
[232] S.C. Pieper, R.B. Wiringa, J. Carlson, Phys. Rev. C 70 (2004) 054325.
[233] D.L. Price, et al., Nucl. Phys. A 765 (2006) 263.
[235] W.D.M. Rae, S. Marsh, Phys. Lett. B 161 (1985) 251.
[236] W.D.M. Rae, A.C. Merchant, B. Buck, Phys. Rev. Lett. 69 (1992) 3709.
[237] W.D.M. Rae, A.C. Merchant, Phys. Rev. Lett. 74 (1995) 4145.
[238] W.D.M. Rae, in: K. Ikeda (Ed.), Proceedings of the Fifth International Conference on Clustering Aspects in Nuclear and Subnuclear Systems, Kyoto, Japan, Phys. Society of Japan, 1989, p. 80.
[239] I. Ragnarsson, S.G. Nilsson, R.K. Sheline, Phys. Rep. 45 (1978) 1.
[240] I. Ragnarsson, S. Aberg, R.K. Sheline, Phys. Script. 24 (1981) 215.
[241] G.V. Rogachev, et al., Phys. Rev. C 64 (2001) 051302.
[242] S. Roy, et al., Phys. Rev. C 52 (1995) 1524.
[243] S. Saito, Prog. Theor. Phys. 40 (1968) 893.
[244] S. Saito, Prog. Theor. Phys. 41 (1969) 705.
[245] S. Saito, S. Okai, R. Tamagaki, M. Yasuno, Prog. Theor. Phys. 50 (1973) 1561.
[246] A. Saito, et al, in: A. Ohnishi, N. Itagaki, Y. Kanada-En'yo, K. Kato (Eds.), Proceedings of the International Symposium on Clustering Aspects of Quantum Many-body Systems (2001), Kyoto, World Scientific, Singapore, 2002, p. 39.and RIKEN Accelerator Progress Report 2001, p. 55; also A. Saito, et al., Prog. Theor. Phys. 146(Suppl.) (2002), 615; ibid, Nucl. Phys. A 738 (2004) 337.
[247] D. Scharnweber, W. Greiner, U. Mosel, Nucl. Phys. A 164 (1971) 257.
[248] M. Seya, M. Kohno, S. Nagata, Prog. Theor. Phys. 65 (1981) 204.
[249] M. Shawcross, N. Curtis, W.N. Catford, N.M. Clarke, B.R. Fulton, S.J. Hall, J.T. Murgatroyd, S.P.G. Chappell, R.L. Cowin, G. Dillon, D.L. Watson, Phys. Rev. C 63 (2001) 034311.
[250] S. Shimoura, et al., Phys. Lett. B 560 (2003) 31.
[251] I. Shimodaya, R. Tamagaki, H. Tanaka, Prog. Theor. Phys. 27 (1962) 793.
[252] N. Soić, S. Blagus, M. Bogovac, S. Fazinić, M. Lattuada, M. Milin, D. Miljanić, D. Rendić, C. Spitaleri, T. Tadić, M. Zadro, Europhys. Lett. 34 (1996) 7.
[253] N. Soić, et al., Phys. Rev. C 68 (2003) 014321.
[254] R.G. Stokstad, Statistical Models of Heavy Ion Resonances, in: D.A. Bromley (Ed.), Treatise on Heavy Ion Collisions, vol. 3, Plenum Press, New York, 1985.
[255] V. Subotin, W. von Oertzen, et al., Phys. Rev. C 64 (2001) 014601.
[256] Y. Sugiyama, Y. Tomita, H. Ikezoe, Y. Yamanouchi, K. Ideno, S. Hamada, T. Sugimitsu, M. Hijiya, Y. Kondo, Phys. Lett. B 312 (1993) 35.
[257] Y. Suzuki, Prog. Theor. Phys. 55 (1976) 1751.
[258] Y. Suzuki, H. Matsumura, B. Abu-Ibrahim, Phys. Rev. C 70 (2004) 051302.
[259] S. Takami, K. Yabana, M. Matsuo, Phys. Lett. B 431 (1998) 242.
[260] M. Takashina, M. Ito, Y. Kudo, S. Okabe, Y. Sakuragi, Phys. Rev. C 67 (2003) 014609.
[261] N. Takigawa, A. Arima, Nucl. Phys. A 168 (1971) 593.
[262] R. Tamagaki, H. Tanaka, Prog. Theor. Phys. 34 (1965) 191.
[263] I. Tanihata, T. Kobayashi, O. Yamakawa, S. Smimoura, K. Ekuni, K. Sugimoto, N. Takahashi, T. Shimoda, H. Sato, Phys. Lett. B 206 (1988) 592.
[264] T. Tarutina, I.J. Thompson, J.A. Tostevin, Nucl. Phys. A 733 (2004) 53.
[265] A. Thiel, J. Phys. G 16 (1990) 867.
[266] S. Thummerer, et al., J. Phys. G 11 (2003) 509.
[267] R.R. Tilley, et al., Nucl. Phys. A 745 (2004) 155.
[268] A. Tohsaki, H. Horiuchi, P. Schuck, G. Ropke, Phys. Rev. Lett. 87 (2001) 192501.
[269] Y. Tosaka, Y. Suzuki, K. Ikeda, Prog. Theor. Phys. 83 (1990) 1140.
[270] A. Tumino, et al., Eur. Phys. J. A 12 (2001) 327.
[271] E. Uegaki, S. Okabe, Y. Abe, H. Tanaka, Prog. Theor. Phys. 57 (1977) 1262;
E. Uegaki, Y. Abe, S. Okabe, H. Tanaka, Prog. Theor. Phys. 59 (1978) 1031;
E. Uegaki, Y. Abe, S. Okabe, H. Tanaka, Prog. Theor. Phys. 62 (1979) 1621.

[272] E. Uegaki, Prog. Theor. Phys. 132 (Suppl.) (1998) 135 and references therein.
[273] E. Uegaki, Y. Abe, Phys. Lett. B 231 (1989) 28.
[274] K. Varga, Y. Suzuki, R.G. Lovas, Nucl. Phys. A 571 (1994) 447.
[275] K. Varga, Y. Suzuki, I. Tanihata, Nucl. Phys. A 588 (1995) 157c.
[276] K. Varga, Y. Suzuki, R.G. Lovas, Phys. Rev. C 66 (2002) 041302.
[277] W. von Oertzen, Nucl. Phys. A 148 (1970) 529.
[278] W. von Oertzen, W. Nörenberg, Nucl. Phys. A 207 (1973) 529.
[279] W. von Oertzen, H.G. Bohlen, Phys. Rep. C 19 (1975) 1.
[280] W. von Oertzen, B. Imanishi, H.G. Bohlen, W. Treu, H. Voit, Phys. Lett. B 93 (1980) 21.
[281] W. von Oertzen, et al., Z. Physik A 353 (1996) 373.
[282] W. von Oertzen, Z. Physik A 354 (1996) 37.
[283] W. von Oertzen, Z. Physik A 357 (1997) 355;
W. von Oertzen, Il Nuovo Cimento A 110 (1997) 895.
[285] W. von Oertzen, Eur. Phys. J. A 11 (2001) 403.
[286] W. von Oertzen, D. T. Khoa, H. G. Bohlen, Europhysics News, vols. 31/2, and 31/3 (2000).
[287] W. von Oertzen, A. Vitturi, Rep. Prog. Phys. 64 (2001) 1247.
[288] W. von Oertzen, H.G. Bohlen, C. R. Phys. 4 (2003) 465.
[289] W. von Oertzen, D.T. Khoa, H.G. Bohlen, Nucl. Phys. A 722 (2003) 202.
[290] W. von Oertzen, et al., Eur. Phys. J. A 21 (2004) 193.
[291] W. von Oertzen, Nucl. Phys. A 738 (2004) 264.
[292] C.F. von Weizsäcker, Die Atomkerne, Akadem. Verlagsanstalt, Leipzig, 1937.
[293] C.F. von Weizsäcker, Naturwiss. 26 (1938) 209.
[294] W. Wefelmeier, Zeit. f. Phys. 107 (1937) 332.
[295] J.A. Wheeler, Phys. Rev. 52 (1937) 1107.
[296] H.J. Wiebicke, M.V. Zhukov, Nucl. Phys. A 351 (1981) 321.
[297] K. Wildermuth, Th. Kanellopoulos, Nucl. Phys. 7 (1958) 150.
[298] K. Wildermuth, W. McClure, Springer Tracts in Modern Physics, vol. 41, Springer, Berlin, Vienna, 1966;
K. Wildermuth, Y.C. Tang, Unified Theory of the Nucleus, Clustering Phenomena in Nuclei, Vieweg, Brauschweig, 1977.
[299] D.H. Wilkinson, Nucl. Phys. A 452 (1986) 296.
[300] R.B. Wiringa, S.C. Pieper, J. Carlson, V.R. Pandharipande, Phys. Rev. C 62 (2000) 014001.
[301] P.R. Wrean, C.R. Brune, R.W. Kavanagh, Phys. Rev. C 49 (1994) 1205.
[302] A.H. Wuosmaa, et al., Phys. Rev. Lett. 58 (1987) 1312.
[303] A.H. Wuosmaa, R.R. Betts, M. Freer, B.G. Glagola, Th. Happ, D.J. Henderson, P. Wilt, I.G. Beardon, Phys. Rev. Lett. 68 (1992) 1295.
[304] A.H. Wuosmaa, Z. Phys. A 349 (1994) 249;
A.H. Wuosmaa, M. Freer, B.B. Back, R.R. Betts, J.C. Gehring, B.G. Glagola, Th. Happ, D.J. Henderson, P. Wilt, I.G. Bearden, Phys. Rev. C 50 (1994) 2909.
[305] A.H. Wuosmaa, R.R. Betts, M. Freer, B.R. Fulton, Ann. Rev. Nucl. Part. Sci. 45 (1995) 89.
[306] A.H. Wuosmaa, et al., Phys. Rev. C 65 (2002) 024609.
[307] T. Yamada, P. Schuck, Phys. Phys. C 69 (2004) 024309.
[308] J. Zhang, W.D.M. Rae, Nucl. Phys. A 564 (1993) 252.
[309] J. Zhang, W.D.M. Rae, A.C. Merchant, Nucl. Phys. A 575 (1994) 61.